INVESTIGATION OF THE MICROSTRUCTURAL AND MECHANICAL PROPERTIES OF ZK60/15% SILICON CARBIDE AND 0.2 - 0.5% NANO ALUMINUM NITRIDE REINFORCED COMPOSITES

2023
PhD THESIS
MCHANICAL ENGINEERING

Abdulmuaen M. M. SAGER

Thesis Advisor
Prof. Dr. İsmail ESEN

INVESTIGATION OF THE MICROSTRUCTURAL AND MECHANICAL PROPERTIES OF ZK60/15% SILICON CARBIDE AND 0.2 - 0.5% NANO ALUMINUM NITRIDE REINFORCED COMPOSITES

Abdulmuaen M. M. SAGER

Thesis Advisor
Assoc. Prof. Dr. İsmail ESEN

T.C.
Karabuk University
Institute of Graduate Programs
Department of Mechanical Engineering

Prepared as
PhD Thesis

KARABUK
November 2023

I certify that in my opinion the thesis submitted by Abdulmuaen M. M. SAGER titled "INVESTIGATION OF THE MICROSTRUCTURAL AND MECHANICAL PROPERTIES OF ZK60/15% SILICON CARBIDE AND 0.2 - 0.5% NANO ALUMINUM NITRIDE REINFORCED COMPOSITES " is fully adequate in scope and in quality as a thesis for the degree of Doctor of Science.

Prof. Dr. İsmail ESEN .....

Thesis Advisor, Department of Mechanical Engineering

This thesis is accepted by the examining committee with a unanimous vote in the Department of Mechanical Engineering as a Doctor of Science thesis. 17/11/2023.

Examining Committee Members (Institutions)	Signature
Chairman : Prof. Dr. İsmail ESEN (KBU)	.....
Member : Assoc. Prof. Dr. Yunus TÜREN (NEU)	.....
Member : Assoc. Prof. Dr. Mehmet Akif KOC (SUBU)	.....
Member : Assoc. Prof. Dr. Recep KILIC (SUBU)	.....
Member : Prof. Dr. Selami SAGIROGLU (KBU)	.....

The degree of Doctor of Science by the thesis submitted is approved by the Administrative Board of the Institute of Graduate Programs, Karabuk University.

Assoc. Prof. Dr. Zeynep ÖZCAN .....

Director of the Institute of Graduate Programs

“I declare that all the information within this thesis has been gathered and presented in accordance with academic regulations and ethical principles and I have according to the requirements of these regulations and principles cited all those which do not originate in this work as well.”

Abdulmuaen M. M. SAGER

ABSTRACT

Ph. D. Thesis

INVESTIGATION OF THE MICROSTRUCTURAL AND MECHANICAL PROPERTIES OF ZK60/15% SILICON CARBIDE AND 0.2 - 0.5% NANO ALUMINUM NITRIDE REINFORCED COMPOSITES

Abdulmuaen M. M. SAGER

Karabük University
Institute of Graduate Programs
Department of Mechanical Engineering

Thesis Advisor:
Prof. Dr. İsmail ESEN
November 2023, 137 pages

In this study, the microstructure, hardness, compression, wear, thermal properties, im mersion, and potentiodynamic corrosion behaviors of extruded ZK60 matrix composi tes reinforced with forty-five μm 15% silicon carbide (SiC) particles and aluminium nitride nanoparticle (AIN) reinforcement (0.2-0.5% 760nm) were examined. The manufacturing procedure includes preparing, pressing, and sintering powder mixtures; alloying and casting with melt-based induction mixing; homogenizing and extruding; and, as a last step, checking the microstructure, hardness, compression, wear, corrosion, and thermal properties. a unique technique known as liquid-based mixing was used to prevent the agglomeration of nanoparticle powders and to guarantee their homogeneous distribution while creating powder blends. It was made up of a mixture of 15% SiC,15% SiC with 0.2% AlN, and 15% SiC with 0.5% AlN nanoparticles. The composites' reinforcing materials, SiC and AlN mixes, were first

combined with magnesium powder as the primary alloy, crushed under 450 MPa of pressure, and sintered at 420°C. Second, the melt is mechanically mixed after the sintered compacts are added to the ZK60 alloy matrix at the semi-solid melting temperature. The melts are combined for 30 minutes to create a homogenous mixture. The homogeneous mixture is then poured into metal molds to create composite samples. The composite samples were extruded at 300°C with an extrusion ratio of 16:1 and a piston speed of 0.3 mm/s after being homogenized for 24 hours at 400°C. Microstructure studies of the produced samples were done for cast, homogenized, and extruded samples. Microstructure studies revealed that SiC and AlN additions were distributed uniformly across the matrix. Agglomerations in the structure were seen as the reinforcement ratio grew to 0.5%. The number of secondary phases has significantly decreased, but the size of the α-Mg grains has not changed significantly, according to the microstructure images of the homogenized samples. The dynamic recrystallization (DYK) that occurs during hot extrusion causes all alloys to noticeably reduce their grain size in the post-extrusion microstructure pictures. After microstructure characterization the hardness analysis, the compressive strength, and the dry friction behaviour of all composite samples was investigated. Depending on the percentage ratios of SIC and AlN reinforcement elements in the matrix, it was seen that the compressive strength and hardness of the composites increased, and the friction coefficient decreased. While the wear rate of the unreinforced ZK60 alloy was 4.5e-5 g/m, this value decreased by 37.5 percent to 2.5e-5 g/m in the 0.5% AlN +15% SiC reinforced ZK 60 alloy. In addition, according to the percentages of SiC and AlN reinforcing elements in the matrix, the corrosion resistance increased. It was discovered that the reinforced ZK60+ 15% SiC (ZK60I), ZK60+ 15% SiC+ 0.2% AIN (ZK60II), and ZK60+ 15% SiC+ 0.5% AIN (ZK60III) compounds had potentiodynamic corrosion resistance that was 1.6, 1.8, and 3.5 times higher than that of the unreinforced ZK60 alloy. The calculated immersion corrosion rates for the unreinforced ZK60, ZK60I , ZK60II, and ZK60III reinforcements were 2090.73, 1748.19, 1479.84, and 1397.79 (mg/year), respectively. The presence of a layer rich in Si-O elements on the surface of the AlN+SiC reinforced composites boosted corrosion resistance, according to the results of the SEM and elemental spectrum response analysis of the corrosion surfaces.

According to the XRD results, the creation of Mg_2Si intermetallics in the structure of the SiC reinforced composites increased corrosion resistance.

Keywords **:** ZK60, SiC, AIN, Hybrid composite materials, magnesium, nanoparticle, liquid-based mixing method, wear, corrosion,

Science Code : 91501

ÖZET

Doktora Tezi

ZK60/%15 SİLİSYUM KARBÜR VE %0.2 - 0.5 NANO ALÜMİNYUM NİTRÜR TAKVİYELİ KOMPOZİTLERİN MİKROYAPI VE MEKANİK ÖZELLİKLERİNİN ARAŞTIRILMASI

Abdulmuaen M. M. SAGER

Karabük Üniversitesi
Lisansüstü Eğitim Enstitüsü
Makine Mühendisliği Anabilim Dalı

Tez Danışmanı:
Prof. Dr. Ismail ESEN
Kasım 2023, 137 sayfa

Bu çalışmada, kırk beş µm %15 silisyum karbür (SiC) parçacıkları ve alüminyum nitrür nanoparçacık (AIN) ile güçlendirilmiş ekstrüde ZK60 matris kompozitlerin hibrit kompozitlerin mikro yapısı, sertliği, sıkıştırma, aşınma, termal özellikleri, daldırma ve potansiyodinamik korozyon davranışları takviye (%0.2-0.5 760nm) incelenmiştir. Üretim prosedürü, toz karışımlarının hazırlanmasını, preslenmesini ve sinterlenmesini içerir; eriyik bazlı indüksiyon karışımı ile alaşımlama ve döküm; homojenleştirme ve ekstrüzyon; ve son adım olarak mikro yapı, sertlik, sıkıştırma, aşınma, korozyon ve termal özelliklerin kontrol edilmesi. Toz karışımları oluşturulurken nanopartikül tozların topaklanmasını önlemek ve homojen dağılımlarını garanti altına almak için sıvı bazlı karıştırma olarak bilinen benzersiz bir teknik kullanıldı. %15 SiC(p), %15 SiC(p) ve %0,2 AlN karışımından yapılmıştır,

ve %15 SiC(p) ve %0,5 AlN nanoparçacıkları. Kompozitlerin takviye elemanları olan SiC ve AlN karışımları önce ana alaşım olarak magnezyum tozu ile karıştırıldıktan sonra 450 MPa basınç altında preslenmiş ve 420°C'de sinterlenmiştir. İkinci olarak, sinterlenmiş parçalar yarı katı erime sıcaklığında ZK60 alaşım matrisine yerleştirilir ve eriyik mekanik olarak karıştırılır. Eriyikler 30 dakika karıştırılıp homojen bir karışım oluştuktan sonra karışımlar metal kalıplara dökülerek kompozit numuneler elde edilir. 400°C'de 24 saat homojenizasyondan sonra kompozit numuneler 300°C'de 16:1 ekstrüzyon oranı ve 0,3 mm/s piston hızı ile ekstrüde edildi. Döküm, homojenize ve ekstrüde edilmiş numuneler için üretilen numunelerin mikroyapı analizleri yapılmıştır. Mikro yapı çalışmaları, SiC ve AlN ilavelerinin matris boyunca düzgün bir şekilde dağıldığını ortaya çıkardı. Donatı oranı büyüdükçe yapıdaki yığılmalar görüldü. %0,5 Homojenleştirilmiş numunelerin mikro yapı görüntülerine göre, ikincil fazların sayısı önemli ölçüde azaldı, ancak α-Mg taneciklerinin boyutu önemli ölçüde değişmedi. Sıcak ekstrüzyon sırasında meydana gelen dinamik yeniden kristalleşme (DYK), tüm alaşımların ekstrüzyon sonrası mikroyapı resimlerinde tane boyutlarını belirgin şekilde küçültmesine neden olur. SiC ve AlN takviyesi genel olarak sertliği ve basınç dayanımını arttırmıştır. Mikroyapı karakterizasyonu ve sertlik analizinden sonra, tüm kompozit numunelerin kuru sürtünme davranışları incelenmiştir. Matris içerisindeki SIC ve AlN takviye elemanlarının yüzde oranlarına bağlı olarak kompozitlerin basınç dayanımı ve sertliğinin arttığı, sürtünme katsayısının ise azaldığı görülmüştür. Takviyesiz ZK60 alaşımının aşınma oranı 4,5e-5 g/m iken, %0,5 AlN + %15 SiC takviyeli ZK 60 alaşımında bu değer yüzde 37,5 azalarak 2,5e-5 g/m oldu. Ayrıca matristeki SiC ve AlN takviye elemanlarının yüzdelerine bağlı olarak korozyon direncinin arttığı görülmüştür. Sonuç olarak, güçlendirilmiş ZK60+ %15 SiC (ZK60SiC15), ZK60+ %15 SiC+02AIN (ZK60SiC15AlN0.2) ve ZK60+ %15 SiC+ %0,5 AIN (ZK60SiC15AlN0.5) bileşiklerinin potansiyodinamik korozyon direncinin 1,6 kat arttığı görüldü. , takviyesiz ZK60 alaşımına kıyasla 1,8 ve 3,5 kat. Daldırma korozyon oranları takviyesiz ZK60, ZK60SiC15, ZK60SiC15AlN0.2 ve ZK60SiC15AlN0.5 donatılar için sırasıyla 2090.73, 1748.19, 1479.84 ve 1397.79 (mg/yıl) olarak hesaplanmıştır. Korozyon yüzeylerinin SEM ve elementel spektrum tepki analizleri sonucunda, AlN+SiC takviyeli kompozitlerin yüzeyinde Si-O elementlerice zengin bir tabakanın varlığı korozyon direncini artırmıştır. Ek olarak,

XRD sonuçlarına göre SiC takviyeli kompozitlerin yapısında Mg2Si intermetaliklerin oluşumu korozyon direncini iyileştirmiştir.

Anahtar Kelimeler: Hibrit kompozit malzemeler, magnezyum, nanopartikül, sıvı bazlı karıştırma yöntemi, aşınma, korozyon, termal iletkenlik.

Bilim Kodu **:** 91501

ACKNOWLEDGMENT

First, I would like to give thanks to my advisor, Prof. Dr. Ismail ESEN, for his great interest and guidance in my graduate study. I would like to extend my sincere thanks to the Government of Libya and the Libyan Embassy in Turkey for providing me with financial support and all the expenses of accommodation, tuition and living expenses to obtain my Master of Science program.

And I want to express my profound gratitude to Bengo for his assistance in completing the requirements of the thesis.

Finally, I would especially want to thank my family for their endless love and understanding over the years. This accomplishment would not have been possible without them. Thank you.

This study has been supported by Karabuk University under the project number KBU BAB-22-DR-023, and the authors thanks for the valuable support.

CONTENTS

Page

Page

Page

Page

LIST OF FIGURES

Page

Page

Page

LIST OF TABLES

Page

SYMBOLS AND ABBREVIATIONS INDEX

ABBREVIATIONS

SiC : silicon carbide

Al_2O_3 : alumina

B_4C : boron carbide

CNT : carbon nano tube

AlN : aluminum nitride

Mg : magnesium

MgO : magnesium oxide

Si : silicon

Al : aluminum

Fe : iron

Zn : zinc

Zr : zirconium

Cu : copper

MMK : metal matrix composites

TiC : titanium carbide

PART 1

INTRODUCTION

Magnesium is the metal with the lowest density, is a prominent substance today Because of its great mechanical qualities, remarkable decomposition potential, and exceptional compatibility with biological systems. [1–4]. Nonetheless, Magnesium alloys' poor absolute strength, weak ductility, and low corrosion and wear performances prevent them from employed across various applications. Significant efforts have been made to improve these features thus far. [5–8]. Commercial magnesium alloys from the ZK family have excelled because they provide a superb blend of durability, ductility, and the ability to be extruded [9,10]. The composition of the alloy also affects its capacity to be extruded. Despite increasing Mg's strength Zn decreases alloy solidus temperature, increasing hot cracking risk.. [11]. Conversely, the inclusion of 0.8 wt % Zr raises the Mg-Zn alloys' solidus temperature, improving their extrudability. Due to the zirconium enrichment of the Mg-Zn alloy system, ZK60 was produced. [12]. Additionally, it has been shown in literature research that Zn and Zr are the main elements in sediments generated during aging. [13]. An examination of the consequences of precipitation, dislocation, and the strengthening of fine grains were used to determine the increase in strength. Together, the aforementioned information allows one to conclude that the microstructure improvement procedures improve the ZK60 magnesium alloy [14]. Furthermore, based on the literature [15], as compared to pure ZK60 alloy, the 1% Ce with ZK60 alloy has a reduced volume fraction of uncrystallized grains, which boosts compressive yield strength. Particularly brittle Mg-Zn-Ce particles reduced the length at the break, but the inclusion of Ce also boosted yield and tensile strength. The addition of 1.0 wt% Ce was reported to enhance the hot workability, however it deteriorated at high Ce ratios [16]. The major intermetallic precipitate for the ZK60 alloy, Mg7Zn3, has a 20% greater hardness than MgZn2Ce intermetallic, which the formation of this compound occurs due to an unintentional introduction of metal, leading to the partial

removal of solute from the magnesium solid solution.. [17]. Utilizing the formation of a protective layer of oxide on the surface that is susceptible to wear, the addition of Ce to alloys considerably increases their dry wear resistance. [18]. According to Wu et al [19], Yb "Ytterbium reinforcement of ZK60 results in a 17% improvement in tensile strength. The ZK60-1Sm "Samarium" alloy, on the other hand, showed better strength and ductility when compared to ZK60 alloy [20].

According to Abbas et al [21], 12 passes of equal channel angular extrusion (ECAP) boosted ZK60's ability to absorb hydrogen by 5.3 wt. Huang et al.'s [22] Conducting research on the impact that Bi has on the microstructure and mechanical characteristics of extruded ZK60 showed a notable 15% enhancement in tensile strength. According to Liang et al. [10], the rod-shaped β_1^'-MgZn precipitated phase brought about a considerable improvement in the mechanical properties of the LPBF ZK60 Mg alloy thanks to its appearance. Wear resistance and elongation-to-fracture were both improved by fifty percent when 0.2 weight percent of Nd was added. According to studies by Zengin et al. [8]. In a recent study by Labib et al [23], The impact of incorporating SiC at levels of 5%, 10%, and 15% into pure magnesium was studied. The findings indicated that Mg with a 15% SiC content demonstrated increased wear resistance at all temperatures. The shear punch test's deformability remained unaffected after extrusion, while the wrought ZK60 alloy's tensile, ultimate, shear, and tensile elongation to failure characteristics increased [24]. In a recent study conducted by Banijamali et al [25], it was discovered that the inclusion of Y-containing precipitates enhances the hardness and wear resistance of the ZK60 alloy when 3 wt percent Y is introduced. Behnamian et al. [26] shown that increasing the concentration of multi-walled carbon nanotubes to 0.5 wt% led to a decrease in wear rates and an enhancement in hardness. Conversely, the hardness increased while the rate of wear escalated as the concentration of boron carbide was boosted to higher levels. YIN et al [11] conducted a study on the mechanical and corrosion characteristics of an extruded Mg-Zn-Mn alloy. The addition of Zn to Mg enhances the alloy's strength while simultaneously improving it has qualities that prevent rusting. The optimal anti-corrosion property may be achieved at a Zn concentration of 1%. Consequently, zirconium was introduced into the Mg-Zn alloy system, resulting in the development of ZK60. Zinc enhances corrosion resistance by neutralizing the harmful impact of

nickel and iron impurities [27]. Due to the amalgamation of these beneficial components, ZK60 alloys have improved mechanical properties. ZK60 alloys may also be produced readily at high temperatures and have a minimal propensity for cracking [13,16]. In other words, dynamic recrystallization (DRX) takes place during the hot forming processes, which can enhance the mechanical properties. However, several ZK60 alloy characteristics, including, high temperature strength, , and corrosion resistance, continue to be inferior to those of its rivals. As a result, numerous attempts to enhance these features have been tried thus far. The incorporation of various elements into magnesium alloys of the ZK series, aiming to leverage the benefits of their thermal stability.. When the ZK60 alloy was created utilizing the selective laser melting SLM process, according to Wu CL et al. [28], the rate of hydrogen generation was reduced by 30%, and their corrosion current density ware decreased by 50%. The mechanical characteristics and microstructure of the hot rolled ZK60 alloy with the addition of Ce base metal were assessed by Silva et al. [29], while Liu et al. al [30] It was observed that the ZK60 alloy, when subjected to hot rolling, displayed greater strength and elongation at the point of fracture in comparison to its cast counterpart. Similarly, the Mg-2Zn-0.2Mn alloy showcased enhanced corrosion resistance post extrusion and aging, attributed to its finer average grain size, more evenly distributed phases, and reduced porosity in comparison to the cast alloy. As indicated in a study published in existing literature [31], hydrothermal methods were employed to fabricate ZK60 magnesium alloys, which were subsequently coated with a composite layer and hydroxyapatite (HA). The outcomes indicated that treatment solutions with a pH of 9 yielded hydroxyapatite coatings with the most significant enhancement in corrosion resistance. There is also Tang et al. [32]'s investigation into porthole die extrusion using ZK60 Mg alloy. High extrusion speed raised the temperature and eliminated the precipitate in β1'," which resulted in the formation of transparent grains. Localized pitting increased the pace of corrosion, which later slowed down due to the formation of a denser, more protective layer. In addition, Z. Li et al.[33]. Heat treatment was tested on ZK60 magnesium microstructure and corrosion. Heat-treated ZK60 alloys (T4 and T6) were exhibited superior resistance against corrosion compared to the untreated ZK60 alloys, which underwent processes of water quenching at 515°C for 2 hours and water quenching at 515°C for 2 hours followed by air cooling at 160°C for 24 hours. Notably, the ZK60 alloy subjected to

T4 treatment demonstrated the most optimal corrosion resistance. Enhanced corrosion resistance in magnesium alloys correlates with a reduced rate of hydrogen release. Conversely, a higher rate of hydrogen evolution leads to flaws in the coatings and diminishes their effectiveness as protective layers. In a recent investigation conducted by Song et al.[34], the influence of hydrogen on the corrosion performance of the Mg-2Zn and Mg-5Zn alloy compositions was examined. The microstructure of the Mg substrate also exerts a significant influence on the charging hydrogen effect. insertion methods for organic functional groups. In their investigation into the creation of biodegradable magnesium alloys, Wei et al. [5] showed that Ion implantation treatment has the dual effect of reducing the rate of corrosion and improving the biocompatibility of the alloy. Furthermore, other investigations focused on investigating the impact of biodegradation on magnesium and ZK60 alloy behavior in both rat models and simulated urine environments. The estimated corrosion rates, based on current densities, were found to be 1.36 mm/y for pure Mg and 0.96 mm/y for the ZK60 alloy. Correspondingly, the corrosion current densities were measured at 59.66 ± 6.41 A/cm² and 41.94 ± 0.53 A/cm², respectively. These findings indicate the suitability of ZK60 alloy for use in biodegradable stents designed for urinary applications [35]. Gao et al. [36] Performed a research investigation on the ability of biodegradable magnesium alloys, created by selective laser melting, to resist corrosion. The researchers discovered that the surface layers exhibited enhanced defensive characteristics, facilitated by phases enriched in Mn and/or Sn, played a crucial role in impeding the penetration of the surrounding medium. This resulted in decreased current exchange with the matrix and contributed to improved corrosion behavior. Furthermore, the presence of solute Mn and/or Sn induced alterations in the corrosion potential that further bolstered the alloy's corrosion resistance.

Shuai et al. [37] conducted an investigation into the mechanical characteristics and resistance to corrosion of magnesium alloys enclosed within a 3D honeycomb nanostructure. The research highlighted the benefits of a finely grained ZK60 magnesium alloy, which was manufactured using a sequence of upsetting procedures. This alloy demonstrated a favourable combination of strength, corrosion resistance, and ductility, as described in existing literature [3]. Additionally, Wang et al. [38] explored the degradation of composite bio-coatings on ZK60 alloy utilized a

combination of electrophoresis deposition and microarc oxidation. In their research, Yang et al. [39] employed an in-situ apatite deposition method to provide protection for a laser-produced magnesium-based composite. Their findings indicated that magnesium had a corrosion-inhibiting effect. Furthermore, Youwen et al. [40], discovered that magnesium improved the degradation of a laser-additive manufactured magnesium-based composite. According to literature [3], repeated upsetting (RU) decreased corrosion in fine-grained ZK60 magnesium alloy. This was due to the alloy's reduced grain size and higher corrosive solution exposure of non-basal planes. However, the three-pass sample has good strength, ductility, and corrosion resistance, making it a promising biodegradable magnesium alloy. Research on the electrochemical and immersion corrosion of ZK60 magnesium alloy before and after hydroxyl ion implantation reveals that a less-toxic functional ion implantation method might prevent Mg alloy implant corrosion [6]. Zengin et al. [41] examined how adding Y affected extrude Mg-Zn-Nd-Zr alloy corrosion and microstructure. Based on their investigation, they discovered that Y-free extruded alloys had a low resistance to corrosion. As a result of micro galvanic contact, Y at a weight percentage of one enhanced the corrosion resistance. This table provides a list of the standard mechanical features of the ZK60.

Table 0.1. Presents the mechanical characteristics of ZK60 alloy [42].

Alloy	Nominal composition	Elongation at fracture (%)	Tensile strength (MPa)	Yield strength (MPa)
ZK 60	Mg-6Zn-0.6Zr	8	315	235

1.1. ZK60 MAGNESIUM ALLOY

ZK60 magnesium alloy is a widely studied material with various applications in different industries. It has high strength-to-weight ratio, good mechanical properties, damping capacity, easy machinability, and corrosion resistance [43]. However, ZK60 alloy also has some limitations, such as its high degradation rate and poor room temperature ductility compared to commercial aluminium alloys [44].

One of the key characteristics of ZK60 alloy is its grain size, which can significantly affect its properties. Superplastic metals, including magnesium alloys, generally have grain sizes in the range of 3-5 μm [45]. Nevertheless, methods such as equal-channel angular pressing (ECAP) and high-pressure torsion (HPT) have the capability to generate submicron-sized grain structures within the alloy.[45,46]. These refined grains, if stable at elevated temperatures, can contribute to the excellent superplastic behaviour of the material [45].

The microstructure of ZK60 alloy can be further modified through various methods. For example, homogenization treatment can refine the grain structure of the casting ZK60 alloy [47]. Heat treatment processes, such as T5 and T6 treatments, can also affect the mechanical properties and microstructure of the alloy [48,49]. Additionally, the addition of alloying elements like yttrium (Y) and can lead to microstructural refinement and enhance the mechanical characteristics of the ZK60 alloy [22].

The corrosion behaviour of ZK60 alloy is an important aspect to consider for its applications. The alloy has been found to be prone to localized corrosion, which can lead to the creation of deep cracks on the surface [50]. To improve the corrosion resistance of ZK60 alloy, different surface modifications and coatings have been investigated. For example, microarc oxidation (MAO) coatings and hydroxyapatite (HA) coatings have been applied to the alloy to enhance its corrosion resistance [51,52]. Other methods, such as Fe ion implantation and coating, have also been explored to modify the surface properties and corrosion resistance of ZK60 alloy [53].

In terms of specific applications, extensive research has been conducted on the ZK60 alloy for its potential use in biomedical implants. Its biocompatibility and biodegradability make it a promising material for orthopaedic applications [54,55]. However, the rapid degradation rate of the alloy might pose a challenge, and researchers have been investigating methods to control and optimize its degradation behaviour [56,57]. Coatings, such as chitosan and polycaprolactone (PCL), have been used for ZK60 alloy to improve their corrosion resistance and biocompatibility [58,59].

ZK60 alloy has also been explored for hydrogen storage applications. Studies have shown that the utilization of severe plastic deformation techniques like ECAP and HPT on the ZK60 alloy presents substantial benefits as a hydrogen storage material.[60]. The stability of hydrogenation properties in ZK60 alloy has been investigated in long-term studies [60].

Furthermore, ZK60 alloy has been used in the development of composites and coatings to enhance its mechanical and wear properties. For example, silicon carbide (SiC) and aluminum nitride (AlN) particles have been added to the alloy matrix to strengthen it and improve its wear resistance [61]. Friction stir processing (FSP) has been utilized to enhance the microstructure and elevate the superplastic characteristics of the ZK60 alloy. [62].

In conclusion, ZK60 magnesium alloy is a versatile material with a wide range of applications. Its properties can be modified through various processing techniques, heat treatments, and alloying element additions. The alloy's grain size, microstructure, corrosion resistance, and mechanical properties can be tailored to suit specific application requirements. Ongoing research aims to further optimize the properties of ZK60 alloy and explore its potential in various industries, including aerospace, biomedical, and hydrogen storage.

1.2.THE EFFECT OF SIC ADDITION TO MAGNESIUM

The addition of SiC (silicon carbide) to magnesium alloys has been studied extensively in the literature. SiC is a ceramic reinforcement that is known for its high strength, hardness, and compatibility with metallic matrices [63]. When SiC particles are added to magnesium alloys, they can improve various properties of the composite material. One of the key benefits of SiC addition to magnesium is the enhancement of mechanical properties. SiC reinforcement can increase the stiffness, specific strength, and dimensional stability of magnesium alloys[64]. It has been reported that even a small amount of nano-sized SiC can lead to similar or even better creep resistance compared to creep-resistant magnesium alloys [65]. SiC particles can also improve the wear resistance of magnesium composites [66]. The addition of SiC particles causes a

considerable change in the microstructure of the composite, resulting in improved mechanical properties [67].

SiC addition to magnesium can also have a positive effect on the corrosion resistance of the composite material. Several studies have shown that Mg composites with incorporated SiC particles exhibit enhanced anti-corrosion properties [63]. SiC can form a protective layer on the surface of the composite, reducing the corrosion rate [68]. Additionally, SiC can improve the wettability of magnesium, leading to better interfacial bonding between the matrix and the reinforcement [69]. The microstructure of SiC-reinforced magnesium composites is influenced by the addition of SiC particles. SiC particles can refine the grain structure of magnesium alloys, resulting in finer grain sizes [70]. The inclusion of SiC particles can result in the creation of a structured pattern comprising areas with a higher concentration of particles alongside regions devoid of particles. The size and dispersion of SiC particles within the composite material can significantly impact its microstructure and mechanical properties [71].

The processing techniques used to fabricate SiC-reinforced magnesium composites can also impact the properties of the material. Various techniques, such as stir casting, powder metallurgy, and friction stir welding, have been employed to produce SiC-reinforced magnesium composites [72–74]. The choice of processing technique can affect the distribution and dispersion of SiC particles in the composite, which in turn can influence the physical properties and mechanical of the material [75].

In summary, incorporating SiC into magnesium alloys can enhance mechanical characteristics, including resistance to creep, stiffness, and wear.SiC can also enhance the corrosion resistance of magnesium composites. The microstructure of SiC-reinforced magnesium composites is influenced by the addition of SiC particles and the processing technique used. Further research is needed to optimize the SiC content, particle size, and processing parameters to achieve the desired properties in SiC-reinforced magnesium composites.

1.3.THE EFFECT OF ALN NANO PARTICLE ADDITION TO MAGNESIUM

The addition of aluminium nitride (AlN) nanoparticles to magnesium alloys has been studied extensively to investigate its effects on the structure, phase composition, and

mechanical properties of the resulting composites. In a study by [76], it was shown that increasing the proportion of AlN particles from 5 to 15 wt.% led to a decrease in the density and strength of the samples. The size of the AlN particles used in this study ranged from 1 to 3 μm. Similarly, Meignanamoorthy et al.(2022) [77] found that the addition of nano AlN particles to an Al-Si-Mg alloy matrix composite resulted in a decrease in the amount of magnesium. This suggests that the addition of AlN nanoparticles to magnesium alloys can have a negative effect on the density and strength of the composites. On the other hand, Sankaranarayanan et al. (2014) [78] investigated the effect of varying the volume fraction of nano-AlN addition on the microstructural and mechanical properties of pure magnesium. They found that the addition of nano-AlN particles improved the microstructural and mechanical properties of the pure magnesium matrix. Similarly, Garrido et al. (2020) [79] reported that the dispersion of AlN nanoparticles into nanocrystalline aluminium enhanced its hardness and elastic modulus. These findings suggest that the addition of AlN nanoparticles can have a positive effect on the microstructural and mechanical properties of magnesium alloys. Incorporation of nanoparticles in magnesium and its alloys has also been shown to result in the formation of more stable secondary phases and a reduction in ductility [63]. This suggests that the addition of nanoparticles, including AlN nanoparticles, to magnesium alloys can affect the formation of secondary phases and the ductility of the composites. The addition of AlN nanoparticles to magnesium alloys has been found to have multiple beneficial effects. Paramsothy et al. (2012) [80] investigated the effects of Al2O3 nanoparticle addition to cast magnesium-based systems and found that it enhanced the strength and ductility of the corresponding magnesium alloys. Similarly, Paramsothy et al. (2012) [81] studied the effects of TiC nanoparticle addition to a hybrid magnesium alloy and found that it enhanced the mechanical response of the alloy. These findings suggest that the addition of nanoparticles, including AlN nanoparticles, can have positive effects on the mechanical properties of magnesium alloys. The dispersion of nanoparticles, including AlN nanoparticles, in magnesium alloy matrices has been shown to be important for achieving good reinforcing effects. Shimizu et al. (2008) [82] found that the dispersibility of carbon nanotubes in a magnesium alloy matrix was important for achieving a good reinforcing effect. Similarly, Lakavat (2021) [83] reported that the addition of nano Al2O3 enhanced the deposition of Ni-P on an AZ91 magnesium

composite. These findings suggest that the dispersion of nanoparticles, including AlN nanoparticles, in magnesium alloy matrices is crucial for achieving the desired reinforcing effects. The crystal structure and lattice parameters of AlN nanoparticles and magnesium have similarities, which makes the growth of magnesium on an AlN particle relatively easy [84]. This suggests that the addition of AlN nanoparticles to magnesium alloys can facilitate the growth of magnesium on the nanoparticles. In summary, the addition of AlN nanoparticles to magnesium alloys can have both positive and negative effects on the properties of the resulting composites. The specific effects depend on factors such as the proportion and size of the nanoparticles, the processing techniques used, and the specific alloy composition. The dispersion of the nanoparticles in the magnesium alloy matrix is crucial for achieving the desired reinforcing effects. Further research is needed to optimize the addition of AlN nanoparticles to magnesium alloys and to understand the underlying mechanisms of their effects.

1.4. CORROSION AND WEAR BEHAVIOUR OF ZK60 MAGNESIUM ALLOY

The corrosion and wear behaviour of ZK60 magnesium alloy has been extensively studied in various research articles. These studies have investigated the corrosion resistance, wear properties, and surface modifications of ZK60 magnesium alloy to understand its performance in different environments and applications. One study by Baril et al. (2001) [85] investigated the corrosion behaviour of as-cast magnesium alloys, including ZK60, in a sodium sulfate solution using electrochemical impedance spectroscopy. The study analysed the corrosion product layer using transmission electron microscopy. The results provided insights into the time-dependent corrosion behaviour of ZK60 magnesium alloy. Another study by Ishizaki et al. (2011) [86] concentrated on examining the corrosion resistance and endurance of a superhydrophobic surface applied to a magnesium alloy. This surface was coated with a nanostructured cerium oxide film and fluoroalkyl silane molecules. Electrochemical tests and contact angle measurements were employed to assess the coating's ability to resist corrosion in a corrosive NaCl aqueous solution. Bagherifard et al. (2018) [87] Explored were the impacts of nanofeatures resulting from severe shot peening on the

mechanical, corrosion, and cytocompatibility properties of the magnesium alloy AZ31, akin to ZK60. The research findings indicated that severe shot peening mitigated localized corrosion by reducing the size of secondary phase particles and encouraging microstructural uniformity. Mostaed et al. (2014) [88] Investigated was the impact of the equal channel angular pressing (ECAP) process on the mechanical and corrosion attributes of pure magnesium and ZK60 magnesium alloy, particularly for potential use in biodegradable stent applications. The findings highlighted that ECAP had a marginal effect on the overall corrosion resistance of the ZK60 alloy. Silva et al. (2019) [46] Researched was the impact of high-pressure torsion (HPT) on the microstructure, hardness, and corrosion behavior of various magnesium alloys, including pure magnesium and ZK60. The study employed transmission electron microscopy to scrutinize the microstructure and concluded that HPT resulted in the refinement of the grain structure of the ZK60 alloy. Zhang et al. (2017) [35] Examined was the biodegradation performance of both pure magnesium and the ZK60 alloy in artificial urine and rat models. The investigation involved analyzing the corrosion mechanism through methods such as electrochemical impedance spectroscopy and potentiodynamic polarization tests. Furthermore, the corrosion potential of the ZK60 alloy was assessed across various environments. Kumar et al. (2021) [66] studied the wear behaviour of SiC reinforced magnesium alloy composites, including AZ91, which is similar to ZK60. The study evaluated the extensive wear behaviour of the composites with different SiC particulate variations. Lee et al. (2017) [89]

The primary focus was to enhance the corrosion resistance of a biodegradable magnesium alloy by creating a defensive ceramic coating through a micro-arc oxidation (MAO) process. This study aimed to elevate the corrosion resistance of the underlying material, specifically targeting its suitability for orthopedic implant applications. Trang et al. (2023) [90] Explored in this study was the in vitro cellular biocompatibility and in vivo degradation behaviour of a calcium phosphate-coated ZK60 magnesium alloy. The research aimed to assess the impact of various calcium phosphate layers on both the corrosion resistance and biocompatibility of the ZK60 alloy. Sager et al. (2022) [61] the study examined ZK60 matrix composites reinforced with silicon carbide and aluminium nitride nanoparticles' microstructure, mechanical, and wear characteristic. The primary objective was to enhance the mechanical strength and wear resistance of the ZK60 alloy. Myagkikh (2023) [91] Explored in the study

was the strain rate sensitivity concerning the mechanical properties of the ZK60 alloy, particularly under conditions involving significant corrosion damage. The research delved into investigating the role of diffusible hydrogen in the fracture mechanism of metals and its influence on the degree of embrittlement in the ZK60 alloy. Li et al. (2020) [92]

Explored were the impacts of microstructure and phase composition on the corrosion characteristics of cast magnesium alloy ZK60 when exposed to NaCl solution. The study involved analyzing the corrosion tendencies of the ZK60 alloy through weight loss measurements. Dou et al. (2022) [93] Researched was the enhancement of surface friction and corrosion resistance in the AZ31 magnesium alloy through ion implantation and ultrasonic rolling. The study's findings indicated a decrease in the wear rate of the magnesium alloy subsequent to ion implantation. Gao et al. (2010) [94] studied the effect of Mg2+ concentration on the biocompatibility of pure magnesium. The study investigated the corrosion behavior of different magnesium alloys, including AZ91, in Hank's solution and found that the corrosion resistance of AZ91 was the best. Xue et al. (2022) [95] investigated the corrosion behaviour of ZK60 wrought magnesium alloys with micro-arc oxidation (MAO) coatings exposed to salt spray and constant stress corrosion conditions. The study evaluated the influence of forging process and MAO coating on the corrosion behavior of ZK60 alloy. Banijamali et al. (2020) [18] examined ZK60 magnesium alloy tribology with cerium. The research examined ZK60 alloy mechanical characteristics and wear resistance with varied cerium adding rates. Zhao et al. (2021) [96] examined cold-sprayed NiCrAl coating on AZ91D magnesium alloy microstructure and characteristics. The wear mechanism of AZ91D alloy was studied, showing parallel furrows, fractures, and debris. Rodrigues et al. (2021) [97] examined plasma electrolytic oxidation-coated ZK30 magnesium alloy corrosion resistance and tribology. The research used PEO coatings to enhance ZK30 alloy corrosion and wear resistance. Merson et al. (2017) [98] examined ZK60 magnesium alloy corrosion following significant plastic deformation. The research examined ZK60 alloy mechanical characteristics, biocompatibility, and biodegradability. Chen et al. (2017) [56] examined the impact of heat treatment on the mechanical and biodegradable characteristics of extruded ZK60 alloy. The research assessed the microstructure and mechanical characteristics of the ZK60 alloy after various heat treatment procedures.

Jian et al. (2023) [99] The objective was to develop a surface modification technique for ZK60 magnesium alloy implants that could gradually degrade while stimulating bone healing. The study suggested employing micro-arc oxidation (MAO) treatment on the ZK60 alloy to improve its corrosion resistance and biological activity.. Su et al. (2020) [54] researched was the corrosion-wear performance of a biocompatible magnesium matrix composite in simulated body fluid. The study incorporated hydroxyapatite within a magnesium matrix composite to assess its corrosion resistance and wear properties. Xue et al. (2019) [51] characterized the corrosion performances of micro-arc oxidation (MAO) coatings on AZ31B, AZ80, and ZK60 cast magnesium alloys. The study investigated the corrosion behaviour of the coated and uncoated alloys using electrochemical measurements. Fahad & Bavanish (2021) [100] Examined was a wear and corrosion investigation on AZ91D magnesium alloy reinforced with nano lanthanum and nanoceria via the stir casting method. The study scrutinized various wear mechanisms, encompassing abrasive, oxidation, adhesion, and delamination, involved in the research. Zheng et al. (2014) [53] investigated the surface corrosion resistance and characteristics of ZK60 magnesium alloy modified by Fe ion implantation and deposition. The study analysed the surface microstructures and corrosion behavior of the modified alloy. These studies provide valuable insights into the corrosion and wear behaviour of ZK60 magnesium alloy and offer potential strategies for improving its performance in various applications. The research findings contribute to the understanding of the factors influencing the corrosion resistance, wear properties, and surface modifications of ZK60 alloy.

1.5. MECHANICAL AND CHEMICAL PROPERTIES OF ZK60 MAGNESIUM ALLOY

ZK60 is a magnesium alloy that is composed of 5 wt% Zn, 0.8 wt% Zr, and the remaining balance being magnesium [101]. It is known for its excellent mechanical properties, with high specific stiffness/strength, good damping capacity, and die-castability [102]. The alloy has been extensively studied for different applications, such as bone repair materials, orthopedic implants, and automotive components [89,103,104].

One of the most factors that affect the mechanical properties of ZK60 is the grain size. Superplastic metals, including ZK60, typically have grain sizes in the range of 3-5 μm [45]. However, processing techniques like equal-channel angular pressing (ECAP) and high-pressure torsion (HPT) can produce submicrometric grain sizes in the alloy [45,46]. These refined grains can enhance the superplastic behaviour of ZK60 at elevated temperatures [45]. Severe plastic deformation methods, including equal-channel angular pressing (ECAP) and high-pressure torsion (HPT), have been applied to refine the grain structure of the ZK60 magnesium alloy. [46]. These techniques can lead to the formation of a submicrometric grain size, which can enhance the superplastic behaviour of the alloy [45]. The refined grain structure obtained through severe plastic deformation can also improve the mechanical properties of ZK60, such as strength and ductility [105].

ZK60 magnesium alloy can also be processed through submerged friction stir processing (SFSP) [106]. This technique involves severe plastic deformation with enhanced cooling rates, which promotes dynamic recrystallization and retards grain growth [106]. As a result, the as-cast microstructure of ZK60 is refined, leading to improved mechanical properties.

The mechanical properties of ZK60 can be further enhanced by the addition of alloying elements. For example, the addition of holmium (Ho) to ZK60 magnesium alloy has been shown to improve its microstructure and mechanical properties [102]. The presence of Ho can refine the grain structure and enhance the strength and ductility of the alloy [102].

In terms of corrosion resistance, ZK60 magnesium alloy has been found to exhibit good in vivo and in vitro degradation rates, as well as excellent biocompatibility [35]. The alloy has been investigated for its potential use in biodegradable implants, where it gradually dissolves in the human body and is replaced by bone tissue [35]. Different surface modification methods, such as micro-arc oxidation (MAO) and plasma electrolytic oxidation (PEO), have been utilized to enhance the corrosion resistance of ZK60.[89,97]. Coating ZK60 magnesium alloy with hydroxyapatite has also been explored to enhance its biocompatibility and corrosion resistance [103].

Hydroxyapatite (HA), possessing a chemical composition akin to bone mineral, finds extensive application in coating magnesium alloys for bone repair purposes. The HA coating can provide a protective barrier against corrosion and promote bone integration [103].

In terms of tribological properties, the exploration involved studying ZK60 matrix composites that were reinforced with silicon carbide (SiC) particles and aluminum nitride (AlN) nanoparticles.[61]. The addition of these reinforcements can improve the wear resistance of ZK60 alloy.

In summary, ZK60 magnesium alloy is a promising material with excellent mechanical properties and biocompatibility. It can be processed through various techniques to refine its grain structure and enhance its superplastic behaviour. The addition of alloying elements and the use of surface modification techniques can further improve its mechanical properties and corrosion resistance. The alloy has potential applications in bone repair materials, orthopedic implants, and automotive components.

1.6. BIOCOMPATIBILITY OF ZK60 MAGNESIUM ALLOY

Biocompatibility is a crucial factor to consider when evaluating the suitability of magnesium alloys for biomedical applications. Magnesium alloys have gained significant attention in the field of biomedicine due to their low density, good castability, high damping capacity, and good biocompatibility [107]. Among the various magnesium alloys, ZK60 magnesium alloy, which is composed of magnesium, zinc, and zirconium, has been extensively studied for its biocompatibility and degradation behavior [42,54,99,108–110]. Zinc and zirconium are chosen as alloying constituents in biodegradable magnesium alloys, such as ZK60, because of their capability to enhance strength and exhibit favorable biocompatibility.[111]. Incorporating zinc and zirconium into magnesium alloys can enhance their mechanical characteristics and corrosion resistance, rendering them suitable for biomedical applications [46,108,109]. ZK60 magnesium alloy has been reported to exhibit good mechanical properties and is considered a potential biodegradable material [54,56].

The degradation behaviour of ZK60 magnesium alloy is an important aspect to consider for its biocompatibility. Studies conducted in vitro aimed to assess the degradation rate, hydrogen evolution, ion release, surface characteristics, and cytotoxicity of ZK60 magnesium alloy [111]. The degradation rate of ZK60 alloy can be influenced by factors such as the microstructure, heat treatment, and surface coatings [35,48,56,97,104,112,113]. Surface modifications, such as microarc oxidation (MAO) coatings and hydroxyapatite (HA) coatings, have been investigated to improve the corrosion resistance and biocompatibility of ZK60 magnesium alloy [52,114,115].

In addition to degradation behaviour, the cytocompatibility of ZK60 magnesium alloy has also been studied. In vitro cytocompatibility tests have been conducted to evaluate the biocompatibility of ZK60 alloy with different cell types [90,111,116–118]. The effects of surface coatings, such as calcium phosphate (Ca-P) coatings and HA coatings, on the cytocompatibility of ZK60 alloy have been investigated Trang et al. (2023)Yang et al., 2015)[90,118]. It has been reported that surface modifications, such as Ca-P coatings and HA coatings, can enhance the corrosion resistance and biocompatibility of ZK60 magnesium alloy. Furthermore, the mechanical properties of ZK60 magnesium alloy, such as hardness and corrosion behaviour, have been studied [46,56,97,114,119]. Severe plastic deformation techniques, such as high-pressure torsion (HPT) and equal-channel angular pressing (ECAP), have been used to process and refine the grain structure of ZK60 magnesium alloy, resulting in improved mechanical properties [46,120,121]. Heat treatment processes, such as solution heat treatment and aging treatment, have also been investigated to improve the mechanical and biodegradable properties of ZK60 alloy [48,56].

In summary, the biocompatibility of ZK60 magnesium alloy has been extensively studied, considering its low density, good castability, high damping capacity, and good biocompatibility. The degradation behavior, cytocompatibility, mechanical properties, and surface modifications of ZK60 alloy have been investigated to evaluate its suitability for biomedical applications. Surface coatings, such as microarc oxidation (MAO) coatings and hydroxyapatite (HA) coatings, have been explored to improve the corrosion resistance and biocompatibility of ZK60 magnesium alloy. Severe plastic

deformation techniques and heat treatment processes have been used to refine the grain structure and improve the mechanical properties of ZK60 alloy. Overall, the research on ZK60 magnesium alloy provides valuable insights into its biocompatibility and potential applications in the biomedical field.

.

While several studies have focused on enhancing the corrosion resistance of magnesium ZK60/SiC composites [122], there has also been research conducted on the impact of incorporating nano-diamond content on the characteristics of magnesium alloys [123]. Nevertheless, there have been no studies undertaken on the impact of SiC and AlN additions on the characteristics of ZK60 alloy. The aim of this work was to improve the mechanical characteristics and corrosion resistance of the ZK60 alloy by using micro SiC and nano AlN particles. In addition, the corrosion performance of the extrudates was evaluated on both the paralleel and traansverse surfaces throughout the extrusion process. Consequently, our research is partitioned into two segments: a comprehensive examination of existing literature and practical investigations. However, literature review and experimental studies were examined separately. In the "Introduction" section, which is the first part of these studies, a general view of the study is given. The general properties of magnesium and magnesium alloys are discussed in detail in the second chapter. In addition, the effects of Mg alloys on alloying elements and their application areas in various industries are given. In the third chapter, metal matrix composite materials and the reinforcement elements used are explained. Wear and corrosion behaviour of magnesium-based materials are discussed in detail in the fourth chapter. The devices used in the experimental research and the experiments performed are explained in the five chapter. The sixth chapter of the study contains a detailed analysis of the results as well as the experimental find and the discussion section. The general results of the research are presented in the seventh chapter, which is the last chapter.

PART 2

MAGNESIUM AND MAGNESIUM ALLOYS

2.1. MAGNESIUM

Magnesium, symbolized as Mg with atomic number 12, is a silvery-white metal recognized for its lightweight, ductile, and notably reactive properties. It ranks as the eighth most abundant element in the Earth's crust and possesses a density of 1.74 g/cm^3. This characteristic distinguishes it prominently when juxtaposed with the densities of commonly utilized commercial metals like steel (7.8 g/cm^3) and aluminum (2.7 g/cm^3). Magnesium is sourced from minerals such as dolomite, magnesite, and carnallite.[127]. Magnesium ranks as the sixth most abundant metal and the eighth most abundant element on Earth. Table 2.1 exhibits additional crucial physical properties of magnesium. Its low density, coupled with a commendable strength-to-weight ratio, renders it especially fitting for components necessitating reduced weight. The low melting temperature and latent heat of melting improve the castability properties of magnesium, and thus the production of cast parts can be done effectively. In addition, magnesium has very good machinability, good damping ability, and good weldability. On the other hand, the exceptionally low oxidation potential of magnesium, such as -2.37 V, increases its susceptibility to galvanic corrosion and reduces its corrosion resistance. In addition, magnesium has low creep strength.

Table 2.1. Some important physical properties of magnesiu[127,128].

Density	**1.74 g/cm3**
The atomic number	12
The melting point	650 °C (1,202 °F)
The Boiling point	1,090 °C (1,994 °F)
Conductivity	Magnesium is a good conductor of both electricity and heat.
Hardness	Magnesium is a relatively soft metal and can be easily scratched or dented about 30-47 HB.

Flammability	Magnesium is highly flammable and can ignite easily, which makes it a potential fire hazard if not handled properly.
modulus of elasticity	45 GPa
Corrosion resistance	Magnesium is prone to corrosion, but it can be protected from corrosion by anodizing or other surface treatments.

Magnesium has a hexagonal close-packed (HCP) crystal structure, which can be described as a stack of close-packed layers of atoms arranged in a hexagonal pattern. The HCP crystal structure is characterized by two lattice parameters, a and c, where a represents the distance between the centres of two adjacent atoms in the same plane and c represents the distance between two adjacent planes. Under atmospheric pressure, pure magnesium crystallizes in a hexagonal, tightly packed structure. Figure 2.1 shows the atomic arrangements and fundamental planes and directions in the magnesium unit cell. The fundamental directions in the magnesium unit cell are the [0001] direction, which is perpendicular to the basal plane and parallel to the c-axis, and the <11-20> directions, which are parallel to the basal plane. The <11-20> directions can be identified by the notation [uvw], where u, v, and w are integers that represent the direction vector relative to the crystal axes.

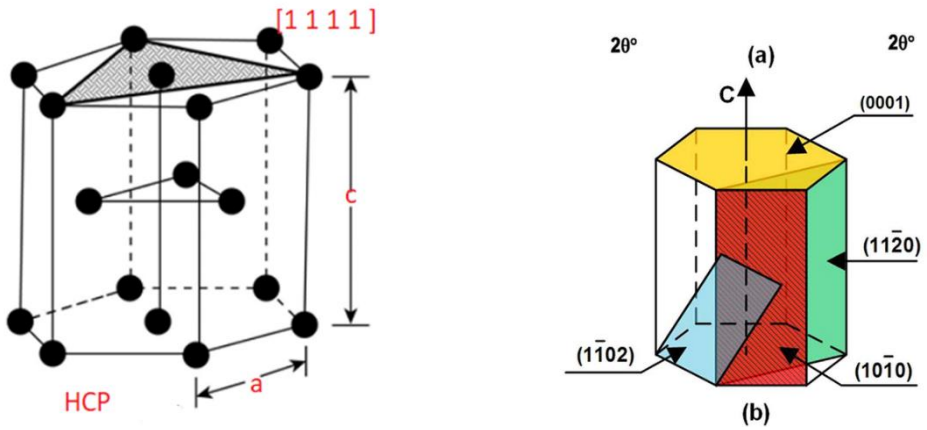

(a) (b)

Figure 2.1. Schematic representation of magnesium unit cell crystal structures a) atomic positions; b) base plane and fundamental planes in the region [129].

2.2. MAGNESIUM ALLOYS

For engineering applications, pure magnesium is frequently used with the alloy. magnesium's formability is improved through alloying for both wrought and cast products. The most popular alloying components are zin and aluminium. Other alloying components that significantly affect an alloy's characteristics include manganese, silicon, and rare earth metals [130]. The addition of an alloying element can also affect other important properties of the melt, such as reactivity, castability, and corrosion properties. It is possible to give desired properties to magnesium alloys through the careful selection of alloying elements. For example, it is typical to add alloy elements to Mg to develop mechanical qualities. Aluminium (Al) improves castability, tensile strength, and hardness[131]. Zinc (Zn) Increases tensile strength and hardness Refine grain structure [132]. Manganese (Mn) increases yield strength and reduces the effect of iron on corrosion resistance [133]. Silicon (Si) addition to molten metal generally enhances viscosity, improves creep resistance by forming Mg2Si particles, but may reduce corrosion resistance in certain magnesium alloys.[134], Rare earth metals, when added to alloys, tend to reduce the freezing range while increasing hardness [135]. There are many magnesium alloys that have been produced until now and have been accepted because they have certain properties. Some of these and their prominent features are shown in Table 2.2.

Table 2.2. Some magnesium alloys and their distinctive properties[127].

Alloy	**Typically contains**	**Characteristics and commonly used**
AZ31B	3% Al and 1% Zn.	It has excellent combination of strength, ductility, and formability. It is commonly used in sheet and plate forms for aerospace, automotive, and consumer electronics applications.
AZ91D	9% Al and 1% Zn.	It has excellent strength, but is also highly resistant to corrosion, making it a popular choice for automotive parts, such as steering wheels, frames, and wheels.
AM60B	6% Al and 0.27% Mn.	It has highly resistant to corrosion and has good castability, making it a popular choice for cast automotive components, such as transmission cases and housings.
ZK60A	5.5%Zn and 0.45%k	It has excellent tensile strength and is highly resistant to impact and vibration, making it a popular choice for aerospace and defence applications.

WE43	4% Y and 3% Nd.	It is known for its high strength, excellent corrosion resistance, and good high-temperature performance, making it a popular choice for aerospace and defence applications.
AZ31	3% Al and 1% Zn	It has good strength and excellent corrosion resistance. It is often used in aerospace and automotive applications.
AZ91	9% Al and 1% Zn.	It has good strength, excellent castability, and good corrosion resistance. It is often used in automotive and electronic components.
ZK60	6% Zn and 0.5% k.	It has good strength, excellent castability, and good creep resistance. It is often used in aircraft and aerospace applications.
WE43	4% Y and 3% E.	It has excellent high-temperature strength and good creep resistance. It is often used in aerospace and defence applications.
ZK30	3% Zn and 0.5% k.	It has good strength, corrosion resistance, and castability, making it suitable for use in a wide range of applications. It is commonly used in aerospace, automotive, and sporting equipment industries.
AZ63	6% Al and 3% Zn.	It has a good balance of strength, corrosion resistance, and castability. It is commonly used in aerospace, automotive, and other high-performance applications.

2.2.1. Commonly Used Alloying Elements and Their Effects on Mg Alloys

1. Zinc (Zn): Zinc is frequently incorporated into magnesium alloys to enhance their strength, hardness, and resistance to creep. Additionally, the addition of zinc improves the castability of magnesium alloys, elevates their corrosion resistance, and decreases the overall density of the alloy.
2. Manganese (Mn): Manganese is used to improve the strength and ductility of magnesium alloys. It also enhances the castability and improves the resistance to corrosion and wear.
3. Rare earth elements (REEs): Rare earth elements such as cerium, lanthanum, and neodymium are added to magnesium alloys to improve their high-temperature performance, creep resistance, and corrosion resistance. REEs also improve the mechanical properties of magnesium alloys, including their strength and ductility.

4. Copper (Cu): Copper is added to magnesium alloys to improve their strength and hardness. The addition of copper also enhances the corrosion resistance and improves the castability of magnesium alloys.
5. Nickel (Ni): Nickel is added to magnesium alloys to improve their mechanical properties, such as strength and ductility. The addition of nickel also improves the corrosion resistance of magnesium alloys.
6. Silicon (Si): Silicon is added to magnesium alloys to improve their castability and reduce the risk of hot cracking during casting. The addition of silicon also improves the strength and wear resistance of magnesium alloys.
7. Titanium (Ti): Titanium is added to magnesium alloys to improve their strength, creep resistance, and high-temperature performance. The addition of titanium also enhances the corrosion resistance of magnesium alloys.

Magnesium alloys are commonly used in various applications due to their high strength-to-weight ratio, excellent corrosion resistance, and good heat dissipation properties. Alloying elements are added to magnesium to improve its mechanical, physical, and chemical properties for specific applications[136].

It is important to note that the effects of alloying elements on magnesium alloys can vary depending on the type and amount of the element added, as well as the specific application of the alloy. Here are some commonly used alloying elements and their effects on magnesium alloys:

2.2.1.1. Aluminum

Aluminum (Al): Aluminum is the most common alloying element used in magnesium alloys. It increases the strength and hardness of magnesium alloys, improves corrosion resistance, and enhances castability. The addition of aluminum also increases the solid solution strength of magnesium alloys, which improves the high-temperature performance of the material. The binary phase diagram formed by magnesium and aluminium is shown in Figure 2.2. The Mg-Al binary phase diagram shows the phases that are formed when magnesium and aluminum are combined in different ratios and heated to various temperatures. The diagram is a useful tool for understanding the

behavior of magnesium-aluminum alloys. At low aluminum concentrations (less than 5% by weight) [129], the binary alloy forms a single phase known as the alpha phase, which is a solid solution of magnesium in aluminum. As the aluminum concentration increases, the alpha phase becomes richer in aluminum, until it reaches a maximum solubility of around 12% aluminum at the eutectic point (around 470°C) [129,137]. At concentrations above 12% aluminum, the binary alloy forms an intermetallic compound known as Mg2Al3, which is also called the beta phase. This phase has a complex crystal structure and is much harder and more brittle than the alpha phase. The beta phase can exist in different stoichiometries, with the Mg2Al3 compound being stable from around 12% to 24% aluminum, and other related compounds such as Mg17Al12 and Mg41Al24 forming at higher aluminum concentrations. The Mg-Al binary phase diagram also shows the temperatures at which the distinct phases form, which can be useful for designing processing and heat treatment schedules for magnesium-aluminum alloys. The diagram can also be used to predict the microstructure and properties of magnesium-aluminum alloys based on their composition and processing history[129,137].

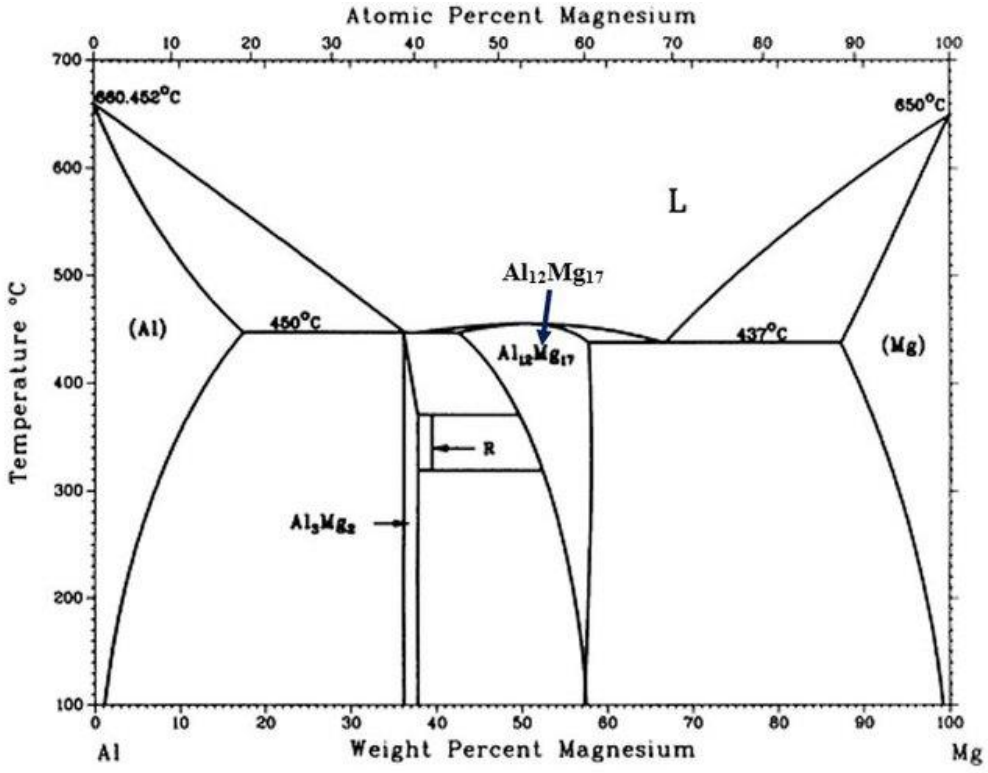

Figure 2.2. Mg-Al binary phase diagram [127].

2.2.1.2. Zinc

Zinc is the second-most-used alloying element in magnesium after aluminium. Zinc is not commonly used as an alloying element in magnesium. The most common alloying elements used with magnesium are aluminum, zinc, and manganese. Aluminum is typically the primary alloying element used in magnesium alloys, with zinc and manganese added in smaller amounts. These alloying elements can improve the mechanical properties of magnesium, such as strength, stiffness, and corrosion resistance. Zinc improves fluidity during melting and casting, but it can also cause microporosity in castings. Zinc is also a good grain size reducer [138]and increases strength because of the Hall-Petch effect [139]. Zinc also enhances corrosion resistance by mitigating the adverse impact of iron and nickel impurities on the corrosion process.[127,140]. Zinc is often used in combination with aluminum in magnesium alloys, as the two elements can form a stable intermetallic compound that can improve the strength and creep resistance of the alloy. However, zinc is not typically used as the primary alloying element in magnesium alloys.

The binary phase diagram of magnesium and zinc is shown in Figure 2.3. The maximum solubility of zinc in magnesium solid solution is about 6.2% wt. Similar to aluminum, since its solubility at room temperature is about 1% wt., the degradation of supersaturated solid solution can be controlled by heat treatment, aging can be realized, and the strength of the alloy can be increased [141,142]. On the other hand, with the addition of Zn to polycrystalline magnesium, the strength at room temperature can be significantly increased by solid solution hardening. Caceres and Blake have shown that the ductility of magnesium can be increased up to 1.0% (2.6% wt) by zinc addition[143]. The reason for this increase is the softening of the prismatic planes because of the addition of zinc. It was observed that the rate of strain hardening increased with increasing Zn addition, and the softening caused by these secondary slips was balanced by solid solution hardening, and the ductility decreased [144].

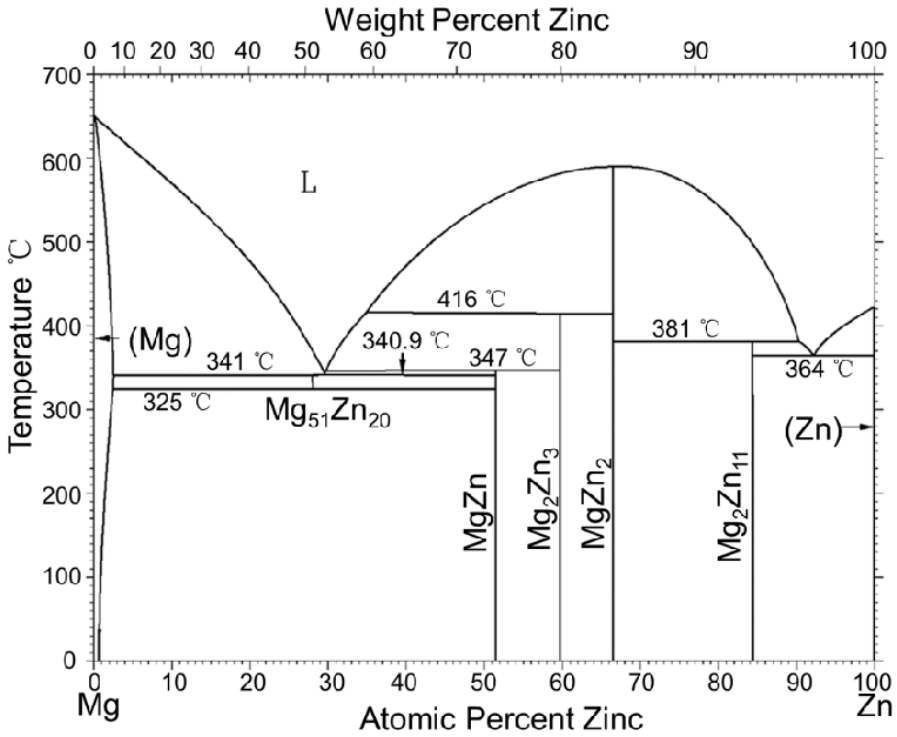

Figure 2.3. Mg-Zn binary phase diagram [127].

2.2.1.3. Zirconium

Zirconium is an extraordinarily strong grain reducer in magnesium alloys, but this effect is valid in the absence of Al, Mn, Si, and Fe elements in the structure because it's forms stable compounds with these elements and its grain reducer effect is lost [127]. For this reason, only magnesium alloys based on zinc and rare earth elements can be grain reduced with zirconium. which is effective as a grain refiner in magnesium alloys because it has a strong affinity for oxygen, and can scavenge oxygen from the melt, forming zirconium oxide particles that act as nucleation sites for the growth of fine grains. However, the strength of the resulting alloy will depend on other factors such as the specific composition of the alloy, the processing conditions used, and the final heat treatment [137,145]. In addition, the addition of the Zr element to the Mg-Zn binary system increases the solidus temperature of the alloy and provides an extra benefit to the hot deformation process [146]. These properties have led to the development of some important commercial Mg-Zn-Zr wrought magnesium alloys (ZK40 and ZK60).

The Mg-Zn-Zr system, owing to the advantageous combination of zinc (Zn) and zirconium (Zr) elements, is acknowledged as one of the most widely utilized and well-suited magnesium alloy systems, following the Mg-Al-Zn system, in commercial applications. In the investigations made so far in the Mg-Zn-Zr system, no triple phase formed by these three elements has been found[145,147]. The intermetallics formed in this system are mostly Zn-Zr and Mg-Zn binary phases. The low solubility of Zn and Zr elements in Mg solid solution at room temperature and the low formation enthalpy between Zn and Zr can be shown as the main reasons for the formation of these compounds. As can be seen from the Zn-Zr binary phase diagram in Figure 2.4, ZnZr and Zn2Zr intermetallics are intermetallics with high thermal stability, and these intermetallics were frequently observed in previous studies examining the Mg-Zn-Zr system[145,148,149]. The phase relationships between zinc (Zn) and zirconium (Zr) at different compositions and temperatures. At low temperatures and low concentrations of Zr, the diagram shows a single-phase region of pure zinc (α-Zn). As the concentration of Zr increases, a new intermetallic compound ZnZr is formed, which has a hexagonal crystal structure and exists in a limited compositional range. At higher temperatures, a second intermetallic compound, Zn5Zr, is formed which has a cubic crystal structure and a wider compositional range. The diagram also shows a eutectic point at around 5% Zr and 420°C, where the liquid phase transforms into a mixture of α-Zn and Zn5Zr upon cooling. Overall, the Zn-Zr binary phase diagram illustrates the phase transformations that occur when zinc and zirconium are combined and can be useful for understanding the behavior of alloys that contain these elements.

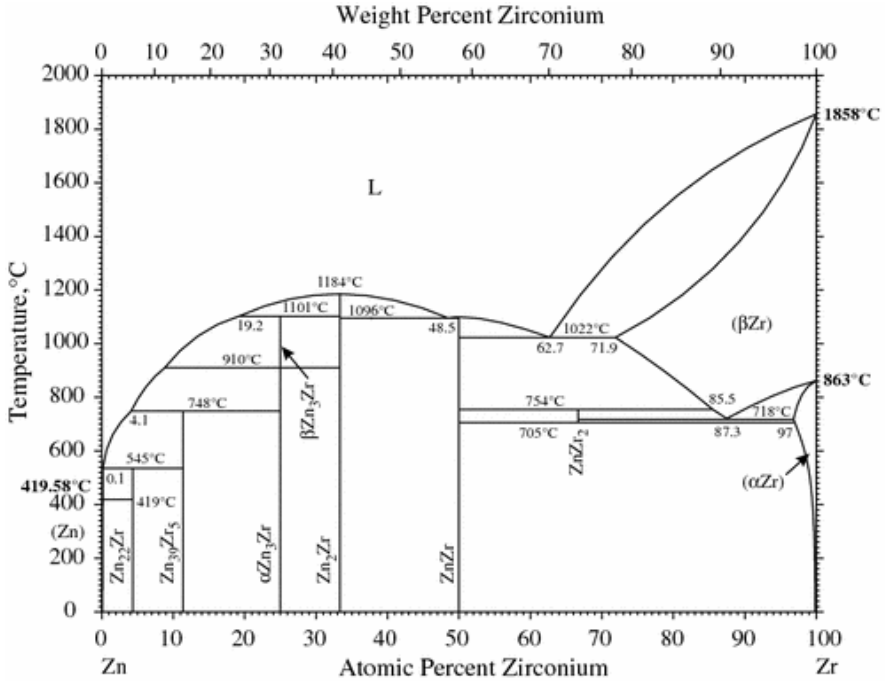

Figure 2.4. Zn-Zr binary phase diagram [127].

2.2.1.4. Rare Earth Elements (REEs)

The most commonly utilized rare earth elements (REEs) in magnesium alloys are cerium (Ce) and neodymium (Nd). These elements are added in small quantities, typically ranging from 1-5 wt%, and can significantly influence the microstructure and properties of the material [41,150,151]. Cerium functions as a grain refiner in magnesium alloys, aiding in microstructure refinement and enhancing the material's mechanical properties. It can also serve as a modifier, reducing the size and quantity of intermetallic phases formed during casting. Lanthanum is primarily employed to enhance the high-temperature properties of magnesium alloys, contributing to increased stability at elevated temperatures and mitigating the susceptibility to hot tearing during casting. Neodymium is commonly combined with other REEs like cerium and lanthanum to further enhance the mechanical properties of magnesium alloys. Additionally, it can improve corrosion resistance and lower the risk of environmental stress corrosion cracking in the material. Overall, the incorporation of REEs in magnesium alloys can enhance their strength, ductility, and corrosion resistance, making them suitable for various applications in industries such as aerospace, automotive, and consumer electronics. However, despite their benefits, the

utilization of rare earth elements, such as in ZE10 (Mg-1Zn-0.2Ce-MM), WE43 (Mg-4Y-3Nd-0.5Zr), and WE54 (Mg-5Y-3.5Nd-0.5Zr) alloys, remains limited due to their high cost [127].

2.2.2. Application Areas of Magnesium Alloys

Magnesium alloys stand as the third most employed structural metal subsequent to steel and aluminum alloys. Featuring a density approximately one-quarter that of steel and two-thirds that of aluminum, magnesium, being the lightest structural metal, presents considerable advantages, particularly in applications emphasizing weight reduction. The unique properties of magnesium and its alloys, such as low density, high specific strength, good machinability, and excellent castability, render them highly versatile across various industries. Some common applications encompass.

1. Automotive Industry: Magnesium alloys find extensive utilization within the automotive industry owing to their low density, impressive strength-to-weight ratio, and commendable corrosion resistance. These alloys are employed in diverse automotive components, including steering wheels, engine blocks, transmission cases, and seat frames.
2. Aerospace Industry: Magnesium alloys are used in the aerospace industry due to their low density, high specific strength, and good thermal conductivity. They are used in various aerospace components, such as aircraft parts, rocket casings, and missile components.
3. Medical Industry: Magnesium alloys are biocompatible and have good mechanical properties, which make them suitable for medical applications. They are used in various medical devices, such as implants, screws, and plates.
4. Electronics Industry: Magnesium alloys are used in the electronics industry due to their good electromagnetic shielding properties. They are used in various electronic devices, such as laptops, mobile phones, and cameras.
5. Sports Equipment Industry: Magnesium alloys are used in the sports equipment industry due to their low density and high strength-to-weight ratio. They are used in various sports equipment, such as golf clubs, tennis rackets, and bicycles.

6. Defense Industry: Magnesium alloys are used in the defense industry due to their lightweight and high strength-to-weight ratio. They are used in various defense applications, such as armored vehicles, aircraft components, and weapon systems.

Overall, magnesium and its alloys have numerous applications across various industries due to their unique properties and advantages. Some examples of these are shown in Figure 2.5 In most of these applications, magnesium alloys are used after casting.

Figure 2.5. Most of these applications, magnesium alloys are used [152,153].

The incorporation of magnesium alloys in the automotive industry can be traced back to the 1920s. An early instance involved the utilization of magnesium for engine parts

in Indy 500 race cars in the United States. In 1937, Germany produced approximately 4 million units of magnesium parts using presses. Additionally, the first magnesium crankcase was manufactured by the general engine company in 1931. By around 1970, magnesium components found applications in air-cooled gearboxes and engines within the automotive sector.

However, the rise in engine power and operating temperatures prompted a shift from air-cooled engines to water-cooled engines, leading to a reduction in the usage of magnesium components. Despite this shift, since the 1990s, certain applications such as magnesium seat frames, passenger doors, and steering frames have been produced by notable brands like Mercedes and BMW. Furthermore, magnesium alloys have proven to be well-suited for use in various portable electronic devices [153].

2.2.3. Casting Methods of Magnesium Alloys

Magnesium alloys offer higher castability than castings made of aluminum and copper because they have special solidification characteristics like particularly good fluidity and minimal susceptibility to hydrogen porosity. 98% of the parts made from magnesium alloys that are employed structurally are created by casting, which is the procedure that predominates in the production of magnesium alloy products [154,155]. For casting magnesium alloys, there are three distinct types of techniques. These include gravity casting, low-pressure casting, and high-pressure casting. Other casting techniques include ablation casting, lost foam casting, compression casting, and semi-solid casting [156]. Each of these casting methods has its own advantages and disadvantages, and the choice of method depends on factors such as the complexity of the part, the quantity of parts to be produced, and the required surface finish and dimensional accuracy.

2.2.3.1. High Pressure Casting

High pressure die casting (HPDC) is a casting method that is commonly used for the production of high-volume, high-quality, and complex-shaped parts made of non-ferrous metals, including magnesium alloys. HPDC involves injecting molten metal under high pressure into a metal mold, or die, that has been designed to produce the desired part geometry [157].

The process begins with the preparation of the die, which is typically made of steel and consists of two halves that are hinged together. The die is then coated with a release agent to prevent the molten metal from sticking to it. The molten magnesium alloy is melted in a furnace and then transferred to a shot chamber, where a plunger is used to inject the metal into the die cavity under high pressure. The molten metal solidifies rapidly as it is cooled by the walls of the die, and the two halves of the die are opened to release the solidified part [158].

HPDC offers several advantages over other casting methods, including:

1. High production rates: HPDC can produce hundreds of parts per hour, making it ideal for high-volume production.
2. Excellent dimensional accuracy and surface finish: The high pressure used in the process ensures that the part is formed precisely and has a smooth surface finish.
3. Low porosity: The rapid cooling of the molten metal in the die cavity results in a low porosity part with high density.
4. Good mechanical properties: The rapid solidification of the molten metal in the die cavity results in a fine-grained microstructure, which improves the mechanical properties of the part.

However, HPDC also has some limitations, including high tooling costs, limited part size, and the need for careful process control to prevent defects such as porosity, shrinkage, and cold shuts [151,158,159].

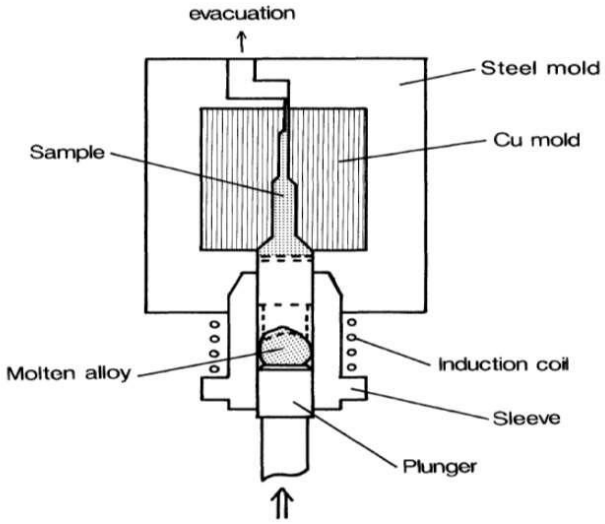

Figure 2.6. Depicts equipment used for high-pressure casting.

2.2.3.2. Low Pressure Casting

Low-pressure casting (LPDC) consists of a crucible under pressure with a feeder channel placed under the casting mold, as shown schematically in Figure 2.7. The pressure in the chamber where the crucible is located pushes the molten magnesium upwards through the channel that acts as the feeder, allowing it to be filled into the mold. Pressure continues until solidification is complete, and the runner channel acts as a feeder to remove shrinkage during solidification. If the appropriate design is made, when the pressure is reduced after solidification, the metal in the channel still remains liquid and returns to the crucible.

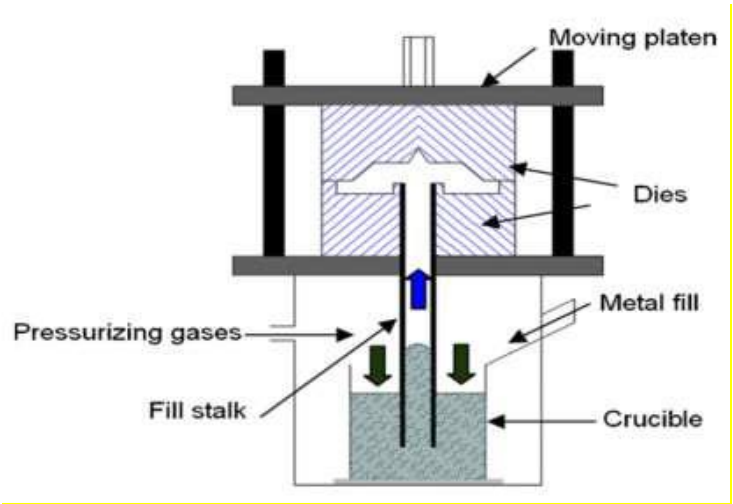

Figure 0.7. Low pressure casting method [160].

The low-pressure die casting method is well established in the aluminium die casting industry, and commercial equipment is readily available and easy to access, but this is not yet the case for magnesium alloys. With this method, low porosity and semi-automatic production of magnesium alloys are possible, and very high casting quality and high productivity can be achieved. Hollow castings that cannot be obtained with high pressure can be produced by the low-pressure casting method. In addition, the low-pressure casting system costs less than high-pressure casting. Despite all these advantages, it is not widely accepted in the commercial field because it is not suitable for the production of magnesium parts thinner than 3 mm and the casting cycle takes 2-4 times longer than high pressure. For this reason, the number of academic studies examining the process parameters and mechanical properties of the produced parts is very small [160,161]. Fu et al. produced the AM50 magnesium alloy using the low-pressure casting method with very low shrinkage and pore defects and determined the optimum process parameters. 15–22 sec. filling time, 8–12 sec. pressure dwell time, 390-410 °C mold and 705-710 °C casting temperatures, and 0.07 MPa casting pressure [160].

LPDC offers several advantages over other casting methods, including:

1. Good surface finish: LPDC produces parts with good surface finish and low porosity, which is ideal for parts that require a high degree of accuracy and a smooth surface finish.
2. Reduced scrap rate: The use of low pressure helps to reduce the incidence of defects, resulting in a lower scrap rate.
3. Improved mechanical properties: The slow and controlled solidification process produces a fine-grained microstructure, which results in improved mechanical properties.
4. Reduced tooling cost: LPDC has lower tooling costs compared to high-pressure die casting methods.

However, LPDC also has some limitations, including slower cycle times, the need for skilled operators, and limited part size [160].

2.2.3.3. Gravity Casting

Gravity casting, also known as permanent mold casting or gravity die casting, is a casting method used to produce medium to high-volume, dimensionally stable, and high-quality parts made of non-ferrous metals, including magnesium alloys. The gravity casting process involves pouring molten metal into a reusable metallic mold, or die, which is typically made of steel or iron. The die consists of two or more sections that are hinged together and contain a cavity that is the exact shape of the part to be cast. The molten metal is poured into the die, and gravity fills the mold cavity. Once the metal solidifies, the die is opened, and the part is removed [155].

The gravity casting process offers several advantages over other casting methods, including:

1. Good surface finish: Gravity casting produces parts with good surface finish and low porosity, which is ideal for parts that require a high degree of accuracy and a smooth surface finish.
2. Dimensional stability: The use of permanent molds and controlled cooling rates result in parts that are dimensionally stable and have consistent wall thickness.
3. Low cost: The reusable nature of the die means that the cost of tooling is lower compared to other casting methods.
4. Wide range of alloys: Gravity casting can be used to cast a wide range of non-ferrous metals, including magnesium alloys.

However, gravity casting also has some limitations, including:

1. Limited complexity: The design of the part must be such that it can be easily cast and removed from the mold.
2. Limited size: Gravity casting is typically used for parts that weigh less than 50 kg.
3. Limited production rate: The production rate of gravity casting is slower compared to other casting methods such as high-pressure die casting.

4. Limited material utilization: The gating and riser system used in gravity casting can result in significant material waste.
5.

Overall, gravity casting is a reliable and cost-effective casting method for producing medium to high-volume, high-quality parts made of non-ferrous metals, including magnesium alloys.

2.2.4. Deformation Mechanism of Magnesium Alloys

The deformation mechanism of magnesium alloys involves the movement of dislocations within the crystal lattice of the material. Dislocations are defects or irregularities within the crystal structure of the metal, and their movement is what allows the material to deform under an applied load. In magnesium alloys, the most common deformation mechanism is slip, which involves the movement of dislocations along specific crystal planes. Slip occurs when an applied stress causes the dislocations to move along these planes, resulting in plastic deformation of the material. The slip planes in magnesium alloys are closely packed planes with a hexagonal arrangement of atoms, which makes them more prone to deformation along these planes. Various sliding systems are shown in Figure 2.18. In magnesium, the lowest critical shear stress (0001) was found at the base plane and in the $< 11\bar{2}0 >$ direction. According to the von Mises criterion, five independent shear systems are required for uniform plastic deformation[4,162]. Magnesium has only two independent sliding systems and a twin mechanism at room temperature. This limits the deformation of magnesium at room temperature. Additional sliding systems must be activated to improve the formability of the magnesium. By increasing the temperature, the prismatic and pyramidal sliding systems shown in Figure 2.8 can be activated in magnesium.

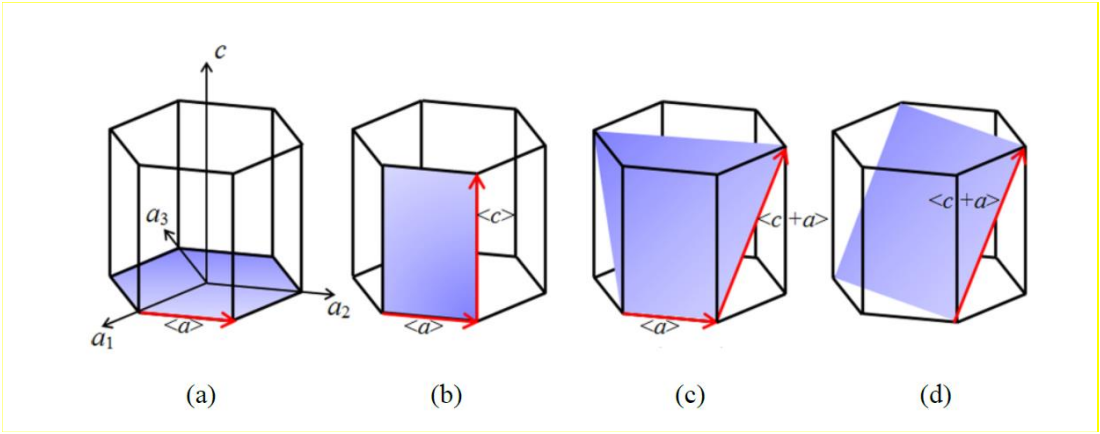

Figure 0.8. Slip systems in magnesium. a) (0001) basal shift, (b) $(10\bar{1}0)$ prismatic shift, (c) first order $(10\bar{1}1)$ pyramidal shift, and (d) second order $(11\bar{2}2)$ pyramidal shift [163].

Another deformation mechanism in magnesium alloys is twinning, which involves the formation of new crystal planes in the material. As seen in Figure 2.9, the critical shear stress required for twinning is lower than that of non-spatial (prismatic and pyramidal) planes, and twinning becomes active when shear systems are constrained. This explains why twinning occurs in hexagonal materials at low temperatures and high deformation rates [163].

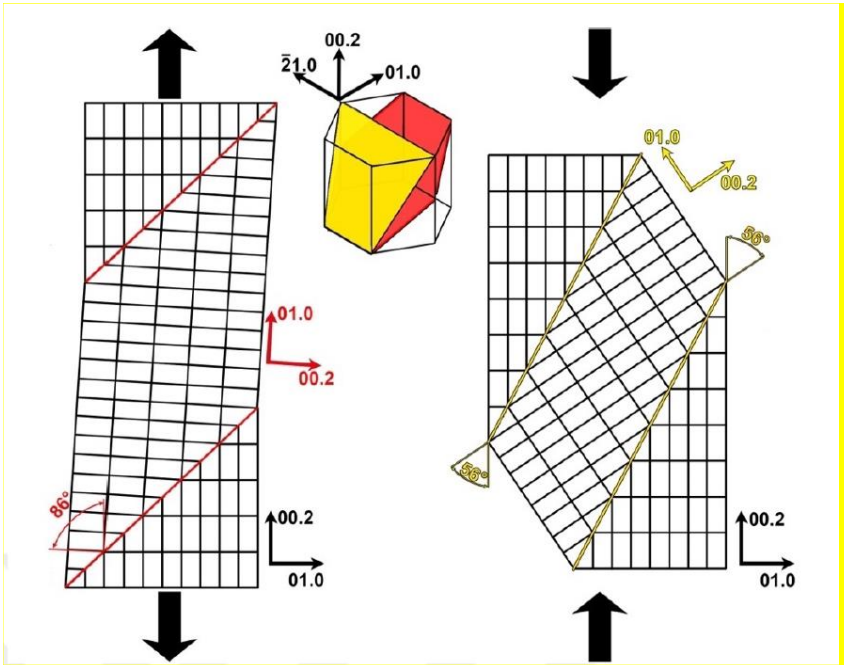

Figure 2.9. Schematic representation of twinning systems in magnesium. a) tension twinning and b) compression twinning[164].

Twinning occurs when the material is subjected to a deformation that is not aligned with the slip planes, causing a change in the crystal orientation of the material. Twinning results in a different type of deformation than slip, which leads to different mechanical properties of the material. The deformation behavior of magnesium alloys can also be influenced by factors such as temperature, strain rate, and microstructure. At higher temperatures, magnesium alloys tend to exhibit greater ductility and lower strength, while at lower temperatures, the opposite is true. Similarly, the strain rate can affect the deformation behavior of the material, with higher strain rates leading to more brittle behavior. The microstructure of magnesium alloys, including the size, distribution, and orientation of the grains, can also have a significant impact on the deformation behavior of the material. Fine-grained magnesium alloys tend to have higher strength and ductility compared to coarse-grained alloys. In addition, the presence of second-phase particles, such as intermetallic compounds, can also affect the deformation behavior of magnesium alloys. The specific features that distinguish twinning from crystallographic shift are as follows.

1. Twinning represents a deformation mechanism that occurs in a singular direction. It generates either tensile or compressive strain along the c-axis but not simultaneously in both directions.
2. Twinning has limited capacity to provide strain. The amount of plastic deformation caused by twinning is very small.
3. Twinning acts as a barrier to dislocation shift and has a grain-reducing effect when it occurs at a high rate.
4. Twinning allows crystals to be rearranged, depending on the type of twin system.

Overall, the deformation mechanism of magnesium alloys is a complex process that involves the movement of dislocations within the crystal lattice of the material, and is influenced by factors such as temperature, strain rate, and microstructure. Understanding these factors is important for designing and engineering magnesium alloy components with the desired mechanical properties.

2.2.5. Extrusion of Magnesium Alloys

Extrusion is a manufacturing process that involves forcing a material through a shaped die to create a continuous profile. Magnesium alloys are often extruded to create various parts and components for different industries, such as automotive, aerospace, and electronics. The extrusion of magnesium alloys requires a carefully controlled process due to the material's low ductility and high reactivity with oxygen. The extrusion process involves heating the magnesium alloy billet to a specific temperature, typically between 350°C and 450°C, to make it soft enough to be shaped. The billet is then pushed through the die using a hydraulic press, with the speed and pressure controlled to achieve the desired shape and surface finish. The basic direct extrusion system is shown schematically in Figure 2.10. Extrusion is one of the most important thermomechanical processes for magnesium alloys, because besides the technical and economic advantages of extrusion, it provides production in a wide product profile [165].

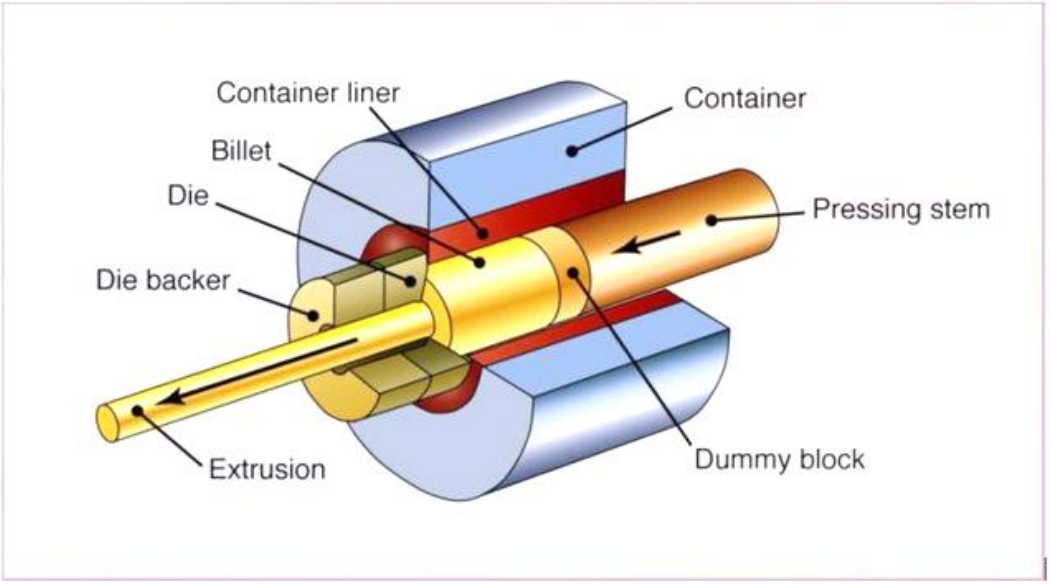

Figure 0.10. Schematic representation of the extrusion process.

There are several benefits to extruding magnesium alloys, including their high strength-to-weight ratio, , good corrosion resistance and excellent machinability . Additionally, extruded magnesium alloys can be easily formed into complex shapes

with tight tolerances, renders them suitable for diverse applications across various fields.

However, there are also some challenges associated with extruding magnesium alloys, including their high susceptibility to cracking and their tendency to form a surface oxide layer during processing. To overcome these challenges, extrusion processes are often performed under controlled atmospheres, such as in a vacuum or with the use of protective gases, to minimize oxidation and prevent cracking.

Extrusion is a complex process for magnesium alloys as it involves the relationship between process variables and the high-temperature properties of the material. Theoretical process variables include extrusion speed, extrusion temperature, and extrusion rate. Texture, microstructure, and mechanical properties are shaped according to these variables[166].

2.2.5.1. Extrusion Speed

The extrusion speed is a critical parameter in the extrusion process, which determines the production rate, efficiency, and quality of the extruded product. The extrusion speed depends on various factors, including the material properties, billet temperature, die design, and extrusion press capacity. In general, the extrusion speed is determined by the cross-sectional area of the extrusion and the output rate required. The speed can range from a few millimeters per second for complex shapes with tight tolerances to several meters per second for simpler profiles with less stringent requirements. Figure 2.11 shows the variation of the extrudability of different alloys as a function of temperature and the effect of increasing extrusion speed on the surface of the alloy. In Figure 2.11 (a), it is seen that the extrusion limit of the aluminum alloy shown as AA6063 is wider than the magnesium alloys and that the M1, ZM21, and AZ31 alloys are at competitive levels with aluminum alloys. AZ61 and ZK60 alloys, which have higher strengths than these alloys, can be shaped at lower deformation rates. ZK60 alloy is more ductile and malleable, as well as more durable, than AZ61 alloy, thanks to the small-grained structure provided by the zirconium (Zr) element in its content [167]. In Figure 2.11 (b), it is clearly seen that the hot cracking on the surface gradually increases with the increase in the extrusion speed of the AZ31 alloy.

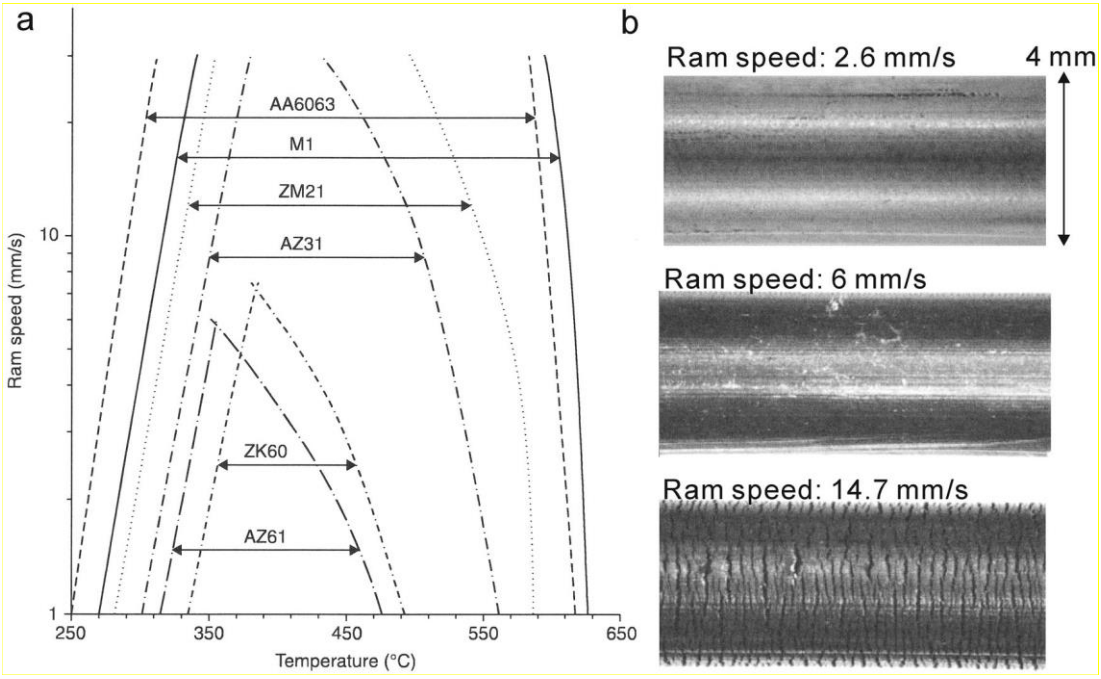

Figure 0.11 (a) The extrusion limit diagrams for several commercial magnesium alloys and the aluminum alloy AA6063 are displayed. Additionally, part(b) demonstrate the surface appearance of as-extruded magnesium alloy AZ31 under different processing conditions. The rod extrusion took place at a temperature of 375°C, with varying ram speeds of 2.6, 6, and 14.7 mm/s, using rods with a 4-mm diameter [167].

2.2.5.2. Extrusion Temperature

The extrusion temperature is a critical parameter in the extrusion process of magnesium alloys. The temperature affects the material properties, flow behavior, and extrusion quality. The extrusion temperature of magnesium alloys typically ranges from 350°C to 450°C, depending on the specific alloy composition and extrusion process requirements. At lower temperatures, the material is less ductile, making it more difficult to form complex shapes. At higher temperatures, the material becomes more ductile, allowing for easier deformation and improved surface finish. However, excessively high temperatures can lead to issues such as melting, burning, or oxidation, which can result in product defects.

Illustrated in Figure 2.12, utilizing such data, one can discern a general trend where the yield strength (YS) of an extruded alloy typically diminishes with increasing extrusion temperature. For instance, Mg-3Zn-0.2Ca-0.5Y exhibited a tensile yield

strength of 309 MPa when extruded at 150°C. However, this value notably decreased to 160 MPa when the extrusion process was carried out at 300°C [168]. This outcome is typical of the majority of magnesium alloys and shows that lower extrusion temperatures are more likely to result in higher YS. The UTS of an extruded Mg alloy reduces or changes only slightly with an increase in extrusion temperature, as illustrated in Figure 2.12 (b). In the traditional conundrum for metallurgists, an increase in extrusion temperature increases the elongation of alloys that have been extruded. As an illustration, when the extrusion temperature was raised from 300°C to 400°C, there was a substantial enhancement in elongation observed for the Mg–0.2Zn–0.3Ca–0.14Mn alloy, increasing from 20.6% to 32%. Notably, the Mg–1Zn–0.5Ca alloy exhibited an even more notable increase in elongation, going from 8% to 44%, as depicted in Figure 2.12(c) [167].

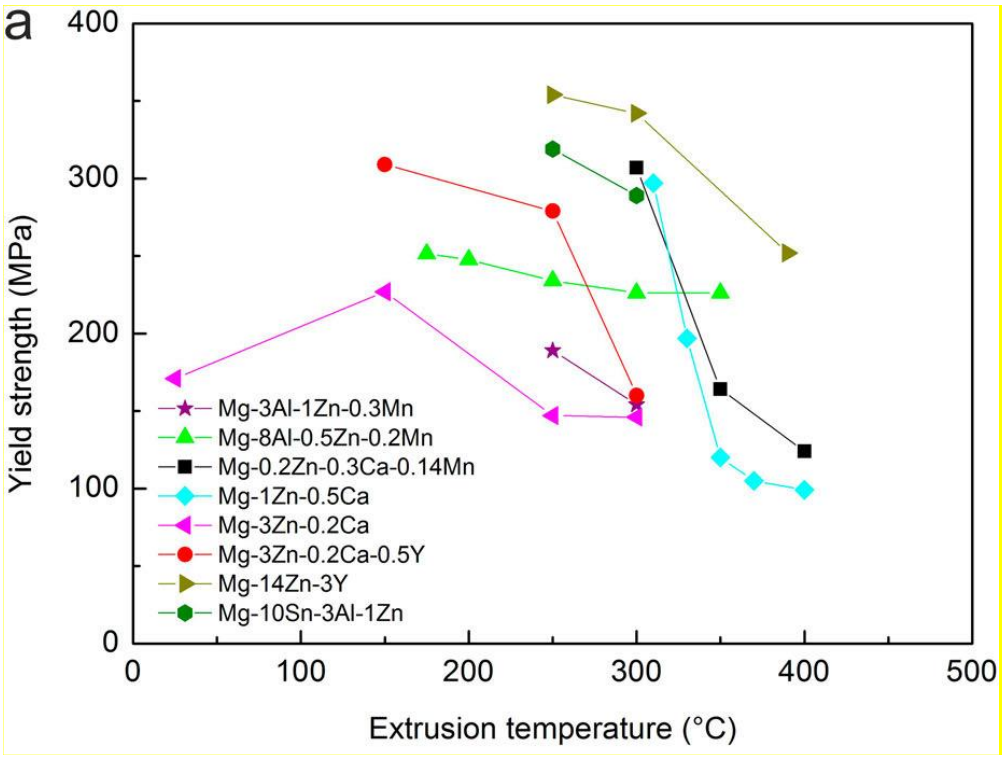

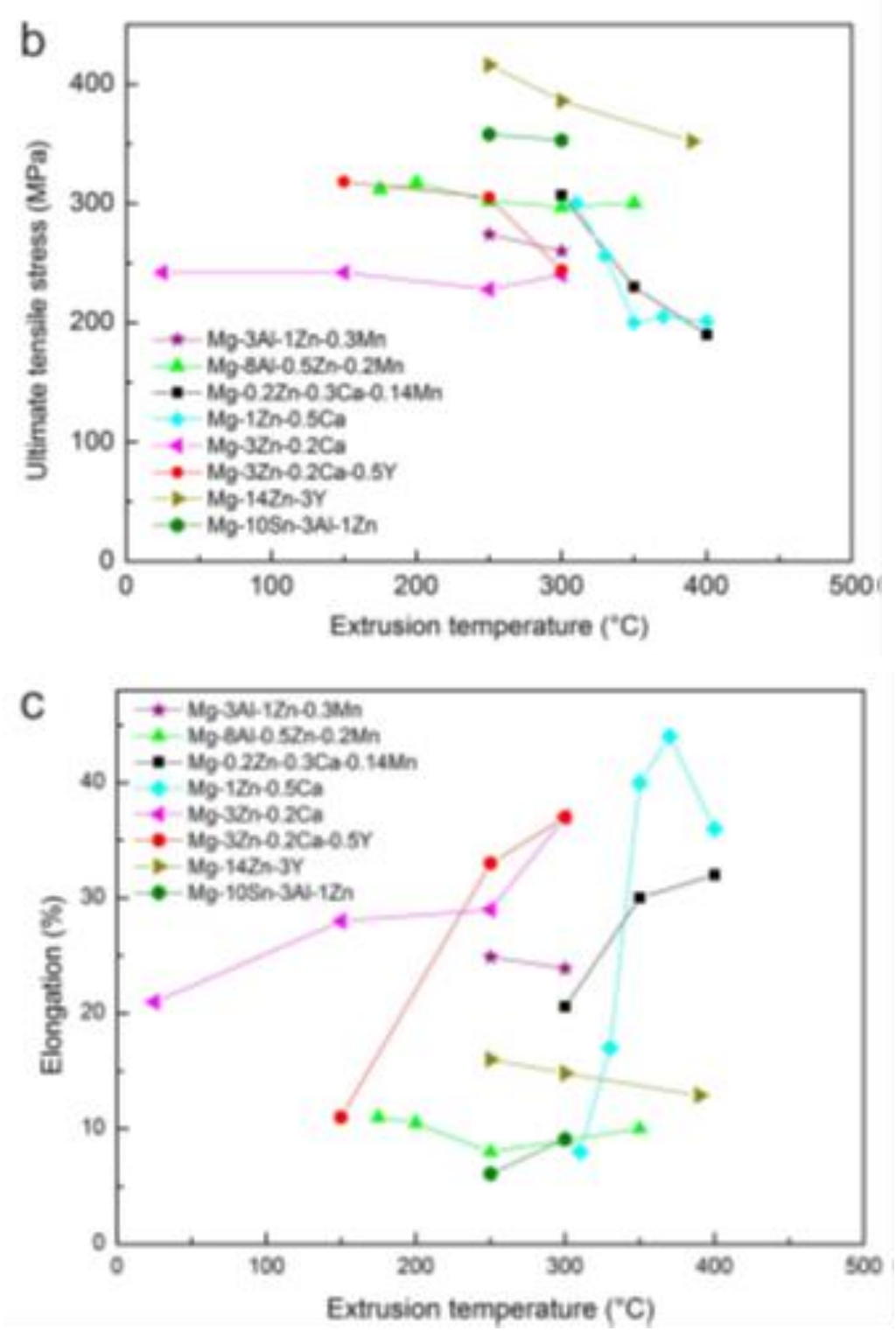

Figure 2.12. The diagram demonstrates alterations in (a) tensile yield strength, (b) ultimate tensile strength, and (c) elongation concerning different extrusion temperatures for magnesium extrusion alloys that underwent processing with identical extrusion speed and extrusion ratio [167].

Similarly, in a study by Zhang et al., the recrystallized grain size increased as the extrusion temperature rised from 310 °C to 400 °C [130]. These changes in the microstructure also seriously affected the mechanical properties, while the yield and tensile strengths decreased with increasing extrusion temperature, the amount of elongation increased.

2.2.5.3. Extrusion Rate

The extrusion ratio refers to the ratio between the cross-sectional area of the billet and the cross-sectional area of the extruded product. The extrusion rate indicates the amount of mechanical work done during extrusion. While low extrusion rate means low plastic strain, high extrusion rate causes high strain formation.

Different findings have been obtained in studies on the effect of extrusion rate on the grain size of the final product. Chen et al. observed a decrease in grain size from 25 μm to 4 μm as the extrusion rate increased from 7 to 100 at a constant extrusion rate of 250 °C for the AZ31 alloy [169]. Ishihara et al., again in AZ31 alloy at 450 °C at constant extrusion speed, extrusion ratio from 10 to 100.

The grain size increased from 30 μm to 170 μm [170]. Uematsu et al. observed only a small change in grain size from 5.9 μm to 4.3 μm as the extrusion rate increased from 39 to 133 in the AZ80 alloy at a constant extrusion rate at 330 °C [171]. The main reason for these different findings is due to the fact that the first extrusion temperatures are different, and the extrusion rate increases, resulting in an increase in the material exit temperature.

PART 3

MAGNESIUM METAL MATRIX COMPOSITES

Magnesium metal matrix composites (MMC) are a type of advanced material made by combining magnesium with other materials to enhance its mechanical properties. These composites typically consist of magnesium as the matrix material and a reinforcing material, such as ceramic or metallic particles, fibers, or whiskers. MMC are attractive for a range of applications because of their exceptional balance between strength and weight, coupled with a lightweight nature, and superbly efficient heat transfer capabilities. These properties make them ideal for use in the aerospace, automotive, and electronic industries, among others. The properties of MMC can be further enhanced by perfecting the fabrication process and selecting appropriate reinforcement materials. However, some challenges exist in producing MMC, such as difficulties in achieving uniform distribution of the reinforcement materials and maintaining the integrity of the matrix material during the fabrication process.

Below is a comprehensive analysis of the literature with information on studies on Mg-MMK produced using various reinforcements.

3.1. CERAMIC PARTICLES

Ceramic particles such as silicon carbide, alumina, and titanium dioxide are commonly used as reinforcements in Mg-MMK. They offer high strength, stiffness, and wear resistance, but can be challenging to distribute evenly within the magnesium matrix. There are several types of ceramic particles that can be used as reinforcements in Mg-MMK, including:

3.1.1. Silicon Carbide (SiC) Particles

SiC particles offer high strength, stiffness, and excellent wear resistance. They are also relatively affordable compared to other types of ceramic particles.

Gupta et al. [172] has studied characterize the properties of the Mg/SiC composites, several tests are conducted. The mechanical properties, including tensile strength, hardness, and impact resistance, are evaluated using standardized testing methods. The results demonstrate the influence of SiC content and distribution on the mechanical behaviour of the composites. The composites with optimized microstructures exhibit enhanced strength and toughness compared to the pure Mg alloy. The research also suggests future directions for optimizing the composite manufacturing process and further enhancing the performance of Mg/SiC composites. Prakash et al. [173] in this study provides insights into the mechanical and wear behaviour of Mg-SiC-Gr hybrid composites, showcasing their potential as advanced engineering materials. The findings contribute to the development of composites with enhanced properties, expanding the possibilities for their utilization in various industries. Hubler et al.[174] this paper concludes by summarizing the cyclic deformation behaviour of Mg-SiC nanocomposites on both the macroscale and nanoscale. The findings highlight the enhanced fatigue resistance of the nanocomposites due to the presence of SiC nanoparticles, which act as effective reinforcements and inhibit crack propagation. The nanoscale observations provide valuable insights into the underlying deformation mechanisms and dislocation interactions, elucidating the mechanisms responsible for the improved fatigue performance. According to research by Matin et al. [175] summarizing the microstructure and mechanical properties of Mg/SiC and AZ80/SiC nanocomposites fabricated through the stir casting method. The findings demonstrate the potential of these nanocomposites to exhibit that SiC nanoparticles significantly reduce the grain size of magnesium matrices and the presence of nanoparticles increases the hardness, tensile strength and ductility values compared to the pure matrices. In addition, Choi H et al. [176] reported that Mg-1%SiC nanocomposites were produced using an ultrasonic cavitation-based casting method. The addition of SiC particles enhances the strength, stiffness, and hardness of the composites compared to the pure Mg matrix. The improved mechanical properties are attributed

to the effective load transfer and strengthening mechanisms provided by the dispersed nanoparticles. Additionally, Penther, D et al. [177] examine the influence of silicon carbide (SiC) nanoparticles on the production method, internal structure, and hardness of magnesium (Mg)-SiC nanocomposites formed through mechanical milling and hot extrusion. The findings demonstrate the potential for improving the mechanical properties, such as hardness, through the addition of SiC nanoparticles. The research contributes to the understanding of Mg-SiC nanocomposites and offers insights for optimizing the fabrication process to achieve desirable microstructures and mechanical properties in these nanocomposites. Ponhan, in their research [178], the researchers explored how the microstructural characteristics and properties of Mg-SiC nanocomposites were affected by varying the content of SiC nanoparticles and the duration of the milling process. These nanocomposites were created via powder metallurgy techniques that encompassed high-energy ball milling. The findings emphasize the importance of optimizing SiC content and milling parameters to achieve desirable microstructures and enhanced mechanical properties. The research contributes to the understanding and development of Mg-SiC nanocomposites for various applications .Zhang, L.[179] conducted a study focusing on the dry sliding wear performance of magnesium-based nanocomposites utilizing a ball-on-disk wear test apparatus. The findings suggest that augmenting the SiC content correlates with an improvement in the wear resistance of these nanocomposites, offering potential benefits in wear-prone applications. The research advances the understanding of wear mechanisms in Mg-SiC nanocomposites and provides insights for optimizing their composition for improved wear performance.

3.1.2. Aluminum Oxide (Al_2O_3) Particles

Al2O3 particles offer high strength, stiffness, and good thermal stability and chemical resistance. Ghasali, E., et al [180] reported the corrosion behaviour of two types of Mg-metal matrix nanocomposites reinforced separately with Al2O3 and Si3N4 particles in their study. According to corrosion tests, the presence of ceramic reinforcements can influence the surface properties and bioactivity of the composites, affecting their ability to support tissue growth and mineralization. In addition, they claimed that, compared to the Mg-Si_3N_4 composite, the Mg-Al_2O_3 composite showed

a lower corrosion current density. Singh A et al.[181] report that in their study, Al2O3 particles varying between 3–12% were added to the pure Mg matrix. It has been noted that comparing the wear behaviour of the Mg and Mg/Al_2O_3 composites, it is possible to assess the effect of the reinforcement on the composite's wear resistance. The addition of Al2O3 particles can potentially improve the hardness and wear resistance.

3.1.3. Titanium Carbide (TiC) Particles

TiC is a ceramic material known for its high hardness and wear resistance, making it an ideal candidate for reinforcing the softer Mg matrix. Aydın, F .el al. [182] investigated the mechanical, wear, and corrosion performances of TiC-reinforced AZ91 matrix composites produced by powder metallurgy methods, including hot pressing. Significant improvements in hardness and wear resistance were observed with the addition of TiC. On the other hand, they reported that the corrosion rate increased with the addition of TiC particles due to the presence of galvanic reactions. Anasori et al. [183] has investigated the mechanical properties of TiC and Ti2AlC-reinforced Mg (AZ31, AZ61, and AZ91) composites. The addition of TiC and Ti_2AlC particles to the Mg alloy matrix can significantly improve the mechanical properties of the composites. These reinforcements act as strengthening agents, enhancing the composite's strength, hardness, and stiffness. TiC and Ti_2AlC have high hardness and thermal stability, providing resistance against deformation and wear. Dash et al. [184] investigated the bending and abrasion properties of Mg/TiC composites in their study. The results of the three-point bending test showed that the maximum bending strength and bending stress were obtained in the AZ91D/20% TiC composite, and the inclusion of TiC particles can enhance the wear resistance of the composites by providing hardness and wear-resistant properties. Falcon et al. [185] evaluated the corrosion behavior of TiC particle reinforced Mg-Al alloy in 3.5% NaCl solution in their study. As a result of the tests, the corrosion of Mg-Al/TiC composites can be influenced by several factors, including the composite's microstructure, particle distribution, and the interaction between the matrix, reinforcement, and the corrosive medium, and they reported that the composite exhibited a lower corrosion rate than the base alloy. In addition, Meenashisundaram et al. (2015) [186] synthesized 0.58%, 0.97, and 1.98% TiC nanoparticle-reinforced composites with Mg matrix using melt deposition and hot

extrusion methods. The tensile properties of the synthesized nanocomposites revealed a significant improvement in the tensile breaking stress of pure Mg and an increase in the compressive yield strength of pure Mg by 0.2% with the addition of nano TiC. Narayanasamy et al. (2015) [187] aimed to develop TiC-MoS2 hybrid composites using powder metallurgy techniques. The hardness value of the hybrid composite increased with the presence of TiC compared to the matrix material. They also reported that the presence of MoS2 particles showed a slight decrease in hardness. The report highlighted a notable enhancement in the abrasion resistance of the produced composites in contrast to the magnesium base material. This improvement was attributed to the synergistic impact resulting from the incorporation of both reinforcements. In the author work Narayanasamy et al. (2018) [188] the study delved into the wear characteristics of magnesium metal matrix composites fortified with varying weight percentages (0, 5, 10, 15, and 20 wt%) of TiC, manufactured through powder metallurgy. Their findings indicated that the resulting composites displayed a uniform microstructure and notable enhancements in both mechanical and tribological properties. Notably, composites featuring higher TiC content showcased heightened wear resistance, albeit accompanied by an increase in the coefficient of friction. Reyes et al. (2016) [189] in their study, Mg-AZ91/TiCp composite was produced using spontaneous infiltration technique at 950 °C with argon atmosphere, and its microstructure and mechanical properties were evaluated. As a result of XRD, Mg, TiC, Al, and Mg17Al12 phases were determined. It was stated that the hardness of the produced composites increased up to 316 HV. Selvakumar et al. (2015) [190]
The study examined the dry sliding wear performance of magnesium (Mg) matrix composites reinforced with titanium carbide (TiC) and molybdenum disulfide (MoS2), created using the powder metallurgy method. According to their findings, the abrasion resistance of the resulting composites exhibited a substantial improvement in comparison to the base magnesium matrix. This enhancement was attributed to the combined effects provided by both types of reinforcements [191].

3.1.4. Aluminum Nitride (AlN) Particles

AIN can be used as reinforcements in Mg-MMK to enhance the properties of the composite material. AlN is a ceramic material that offers high thermal conductivity,

high electrical insulation, and good thermal shock resistance. And this some literature to give some information about the characterising of AIN.

Chen et al. [192]. This study focuses on investigating the effect of different particle contents of AlN on the mechanical properties and fracture behaviour of the Mg-Al matrix. The researchers conducted a series of tests to evaluate the mechanical properties of the composites, including tensile testing, hardness measurement, and impact testing. They also examined the fracture behaviour and analyzed the microstructure of the composites using scanning electron microscopy (SEM) and energy-dispersive X-ray spectroscopy (EDS). The results indicated that 5% AlN reinforcement showed the highest densification and flexural strength, and with increasing reinforcement content, the fracture mode of the composites changed from plastic to brittle. Songwei et al. [125]. In this study, AZ31 alloy samples were prepared with different conditions: with and without the addition of AlN particles, and with and without the application of electromagnetic stirring during the casting process. The microstructure of the as-cast samples was then examined and analyzed. The combined effect of AlN particles and electromagnetic stirring was found to produce the most pronounced improvement in the microstructure. The presence of AlN particles, along with the agitation provided by electromagnetic stirring, resulted in a highly refined and more homogeneous microstructure in the as-cast AZ31 alloy.

Li et al. [126] produced an AlN-particle-reinforced Mg-Al matrix composite by casting. As a result, it was reported that the AlN particles acted as reinforcing agents, effectively strengthening the composite material. They enhanced the tensile strength, hardness, and impact resistance of the composite. The improved mechanical properties were attributed to the load transfer between the Mg-Al matrix and the AlN particles, as well as the restriction of dislocation movement by the AlN particles. In the author literature Nano-aluminium nitride (AlN) particle-reinforced magnesium (Mg) composites have been extensively studied to explore their microstructural and mechanical properties. As a result of microstructural characterization investigations, nano-AlN particle-reinforced Mg composites exhibit enhanced microstructural characteristics and improved mechanical properties, including increased strength, hardness, and potentially enhanced wear resistance, creep resistance, and fatigue

performance. Among the developed composites, Mg/0.8AlN has been reported to show superior strength (30% improvement) and Mg/0.2AlN has improved ductility (80% improvement)[78].

The selection of the ceramic particle reinforcement will depend on the specific application requirements and the desired properties of the composite material. Other factors to consider when selecting a ceramic particle reinforcement include its cost, availability, and compatibility with the magnesium matrix material. Additionally, it is important to ensure that the ceramic particles are evenly dispersed within the magnesium matrix to maximize the performance of the composite material.

3.2. CARBON FIBERS

Carbon fibres are commonly used as reinforcements in Mg-MMK due to their high strength, low weight, and excellent stiffness. However, they are expensive and can be difficult to produce consistently.

There are several types of carbon fibers that can be used as reinforcements in Mg-MMK, including:

3.2.1. Polyacrylonitrile (PAN) Based Carbon Fibers

PAN-based carbon fibers are the most used type of carbon fiber reinforcement in Mg-MMK. They offer high strength, stiffness, and fatigue resistance, and are relatively affordable compared to other types of carbon fibers [193]. Yusof et al. (2012) [194] summarizing the key findings and highlighting the importance of understanding the post-spinning and pyrolysis processes for PAN-based carbon fibres and activated carbon fibres. It emphasizes the need for optimization and control of process parameters to achieve desired Fiber properties and tailoring the characteristics of activated carbon fibres for specific applications. Lindsay et al.(2007) [195] studied combining IGC and XPS techniques, researchers can gain valuable insights into the surface properties, chemical composition, and reactivity of PAN-based carbon fibres after electrochemical treatment. These analyses can help elucidate the effects of the

treatment on the Fiber surface and provide a better understanding of the structure-property relationships in the context of carbon Fiber applications.

3.2.2. Pitch-Based Carbon Fibers

Pitch-based carbon fibers offer higher strength and stiffness than PAN-based fibers but are also more expensive[196]. Viala et al. [197] investigating the effect of magnesium on the microstructure, composition, and mechanical properties of carbon fibres can provide valuable insights for tailoring and optimizing carbon fiber characteristics for various applications, including high-performance composites, energy storage devices, and structural materials.

3.2.3. Rayon-Based Carbon Fibers

Rayon-based carbon fibers are less commonly used in Mg-MMK but offer good strength and stiffness properties. Xiao et al.[198] find that while hot stretching improves the microstructures and properties of both PAN-based and rayon-based carbon fibres, PAN-based fibres tend to exhibit more significant enhancements due to their higher degree of graphitization and orderliness.

3.2.4. Carbon Nanotubes (CNTs)

CNTs offer high strength and stiffness, as well as excellent electrical and thermal conductivity.

Shi et al. (2019)[199] developed magnesium (Mg) matrix composites reinforced with carbon nanotubes (CNTs) using a three-stage preparation method involving mixed ball milling, melt processing, and hot extrusion. To induce an interfacial reaction on the CNT surface, aluminum (Al) was introduced into the composite melt at a mass ratio of 0.3% before casting. The study concluded that the Mg-6Zn-0.3Al/CNT composites exhibited a notable increase in both yield strength (by 21.1%) and ultimate strength (by 9.3%) compared to Mg-6Zn/CNT composites.

Aung et al. (2010) [200] investigated the corrosion resistance of composites reinforced with pure magnesium and 0.3% and 1.3% by weight CNTs in a 3.5% NaCl solution by using a dip test and electrochemical measurements. They reported that the corrosion rate increased significantly with the presence of CNTs, due to the microgalvanic effect between the cathodic CNTs and the anodic Mg matrix.

Habibi et al. (2011) [201] produced Mg/Al-CNT hybrid nanocomposites using powder metallurgy and hot extrusion. In their final report, their microstructure indicated that the hybrid Al-CNT nanoparticles up to 1.00 wt% Al content were highly uniformly dispersed, and the compressive strength of all hybrid Mg/Al-CNT nanocomposites was significantly higher compared to pure Mg.

The selection of the carbon fiber reinforcement will depend on the specific application requirements and the desired properties of the composite material. Other factors to consider when selecting a carbon fiber reinforcement include its cost, availability, and compatibility with the magnesium matrix material. Additionally, it is important to ensure that the carbon fibers are evenly dispersed within the magnesium matrix to maximize the performance of the composite material.

3.3. WHISKERS

Whiskers, such as silicon carbide and alumina, offer high strength and stiffness, but are challenging to distribute evenly within the magnesium matrix.

In addition to the whiskers mentioned earlier, there are several other types of whiskers that can be used as reinforcements in Mg-MMK. These include:

3.3.1. Boron Carbide (B_4C) Whiskers

B_4C whiskers offer high strength and stiffness, as well as good wear and corrosion resistance.

Kumar et al. (2018) [202] investigated the electrochemical and mechanical behaviour of B_4C/Al–Mg–Si composites produced using the powder metallurgy method. They reported that with increasing B_4C content, the corrosion resistance decreased and the hardness of the composite increased. Krishnan et al. (2020) [203] investigated the wear behaviour of pure Mg and Mg- B_4C (5-15%) composites developed by powder metallurgy technique. According to the results, it was concluded that the Mg-15% B_4C sample had excellent wear behaviour, and the surface roughness of Mg decreased from 3.718 to 0.647 μm with the increase in B_4C addition. Majzoobi et al. (2020) [204] carried out the production of composites by powder compression technique using Mg matrix and 1.5%, 3%, 5%, and 10% reinforced B_4C nanoparticles. They stated that the highest strength was obtained in 1.5%, 3%, and 5% B_4C -reinforced composites, respectively. In addition, Jutanaiman et al. (2020) [205] carried out the production of magnesium composites by the mixing casting method using magnesium as matrix and 2, 4, 6, and 8 % micro B_4C as reinforcement. The best mechanical properties in magnesium composites were obtained by adding 8% B_4C. They reported that the mechanical properties of the magnesium composite increased due to the increase in the number of B_4C particles causing new interfaces that would inhibit dislocation motion and the dispersed B_4C particles acting as load-retaining elements. Rahmani et al. (2019) [206] conducted a study on the hardness and wear resistance of Mg-B4C nanocomposites, employing both dynamic and quasi-static compression methods for production. Their findings revealed that the Mg-10% B4C nanocomposite exhibited approximately a 50% increase in hardness and approximately a 70% improvement in wear resistance compared to pure Mg. Rahmani et al. (2021) [207] examined the corrosion characteristics of Mg-B4C composites. The findings indicated that these composites exhibited a reduced corrosion rate attributed to their decreased porosity and elevated relative density. For instance, as reported in the study, the measured corrosion rate for the sample reinforced with 5% volume of B4C particles was 54% lower than that observed for the pure sample.

Singh et al. (2017) [208] outlined their study where magnesium-based metal matrix composites reinforced with B4C particles were effectively created using an economical conventional mixing casting technique. Their wear experiments distinctly demonstrated that the wear resistance of the cast composites surpassed that of unreinforced magnesium. This improvement was attributed to dispersion hardening

induced by the presence of carbide particles. Yao et al. (2015) [209]: In their research, the study focused on B4C/Mg composites created through a metal-supported pressure-less infiltration technique, analyzing the wear behavior and mechanisms of this material. The findings indicated that the B4C/Mg composites exhibited superior wear resistance compared to pure Mg across different applied loads. Notably, while abrasion was identified as the primary wear mechanism for pure Mg, adhesion and delamination were observed in the case of B4C/Mg composites under low loads.

3.3.2. Silicon Nitride (si3n4) Whiskers

Si3N4 whiskers offer high strength and stiffness, as well as good thermal stability and corrosion resistance. Jong et al [210] from the University of Michigan have conducted comprehensive research on the synthesis and characterization of silicon nitride whiskers. Their work has contributed to the understanding of whisker growth mechanisms, optimization of synthesis parameters, and characterization of the physical and chemical properties of silicon nitride whiskers. Wang et al (2023) [211] studied the addition of magnesium oxide (MgO) in a multiphase additive during the synthesis of βSi_3N_4 whiskers has a significant effect on the formation process and morphology. MgO acts as a catalyst, promotes the growth of βSi_3N_4 whiskers, influences their morphology, enhances crystallinity, and stabilizes the desired β-phase. However, more research is needed to fully understand the underlying mechanisms and optimize the use of MgO in controlling the formation and properties of βSi_3N_4 whiskers.

3.3.3. Carbon Nanotubes (CNTs)

CNTs offer high strength and stiffness, as well as excellent electrical and thermal conductivity. Dimitrios Bikiaris's research focused on the microstructure and properties of PP/CNT nanocomposites, including dispersion, interfacial interaction, alignment, and their effects on mechanical, electrical, thermal, gas barrier, and rheological properties. These investigations aimed to establish structure-property relationships and optimize the performance of PP/CNT nanocomposites [212]. Han et al (2010) [213] Fina conducted a comprehensive review on the thermal conductivity

of CNTs and their polymer nanocomposites. They analyzed the intrinsic thermal conductivity of CNTs, factors influencing their thermal conductivity, and the mechanisms behind the thermal conductivity enhancement in polymer nanocomposites. Their work provides valuable insights for understanding and designing CNT-based materials with improved thermal conductivity.

The selection of the whisker reinforcement will depend on the specific application requirements and the desired properties of the composite material. Other factors to consider when selecting a whisker reinforcement include its cost, availability, and compatibility with the magnesium matrix material. Additionally, it is important to ensure that the whiskers are evenly dispersed within the magnesium matrix to maximize the performance of the composite material.

The selection of the reinforcement material depends on the specific application requirements and the desired properties of the composite material. Additionally, the fabrication process used to produce the Mg-MMK must be optimized to ensure even distribution of the reinforcement material within the magnesium matrix and to maintain the integrity of the matrix material during processing.

PART 4

WEAR AND CORROSION BEHAVIOR OF MAGNESIUM-BASED MATERIALS

In addition to their superior qualities compared to other materials, magnesium-based materials have limited wear and corrosion resistance, which limits their application in industry[214]. When analysing magnesium-based materials, it is very important to accurately express the wear and corrosion mechanisms. Information about wear mechanisms, types of corrosion, and corrosion mechanisms in magnesium-based materials is given in this section.

4.1. WEAR BEHAVIORS

Abrasion is one of the most important problems that limit the useful life of the materials used and cause material loss as a result of two materials touching each other. The weak hardness of Mg and its alloys prevents them from being used as gears, pistons, cylinders, or shaft bearings due to significant wear losses[214]. It is common to use particle-reinforced MMK to increase the wear resistance of magnesium-based materials. These materials show different wear processes at different loads and speeds, among other wear circumstances. The primary wear mechanisms in these materials include adhesion, delamination, wear, oxidation, melting, and thermal softening.

4.1.1. Adhesive Wear

In adhesive wear, especially at high loads, material transfer occurs and is seen as spreading and plastic deformation on the surface. This type of wear occurs less in composites than in non-reinforced alloys[215,216]. Figure 4.1 indicates the surface where adhesive wear occurs.

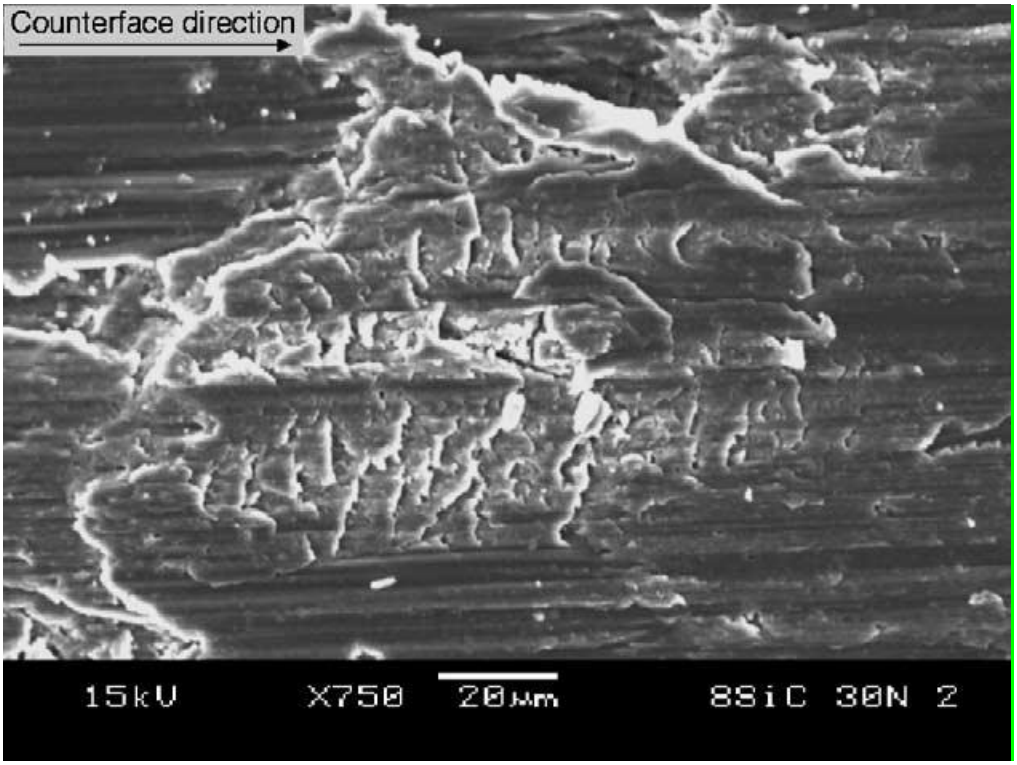

Figure 0.1. Adhesive wear surface appearance[215].

4.1.2. Abrasive Wear

In this form of wear, grooves and scratches usually appear parallel to the direction of sliding. Wear is caused by material tearing or breaking due to hard protrusions on the steel ball or hard particles on the contact surfaces [215,216]. Figure 4.2 schematically represents how abrasive wear occurs. An image of an abrasive-worn surface is shown in Figure 4.3.

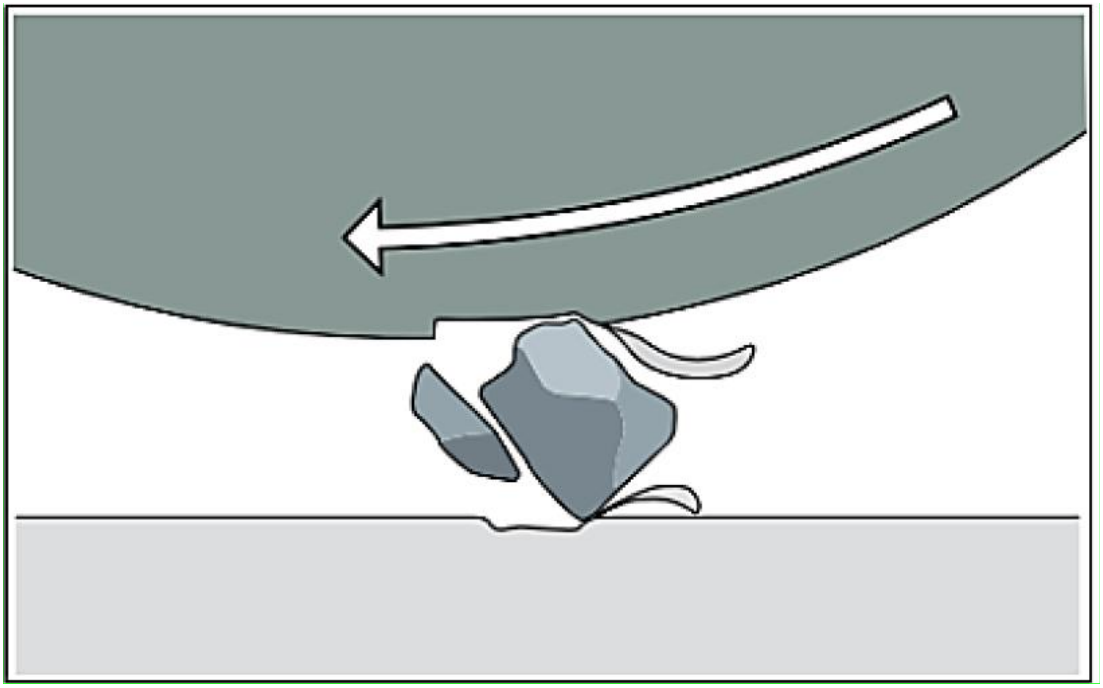

Figure 0.2. Abrasive wear formation [217].

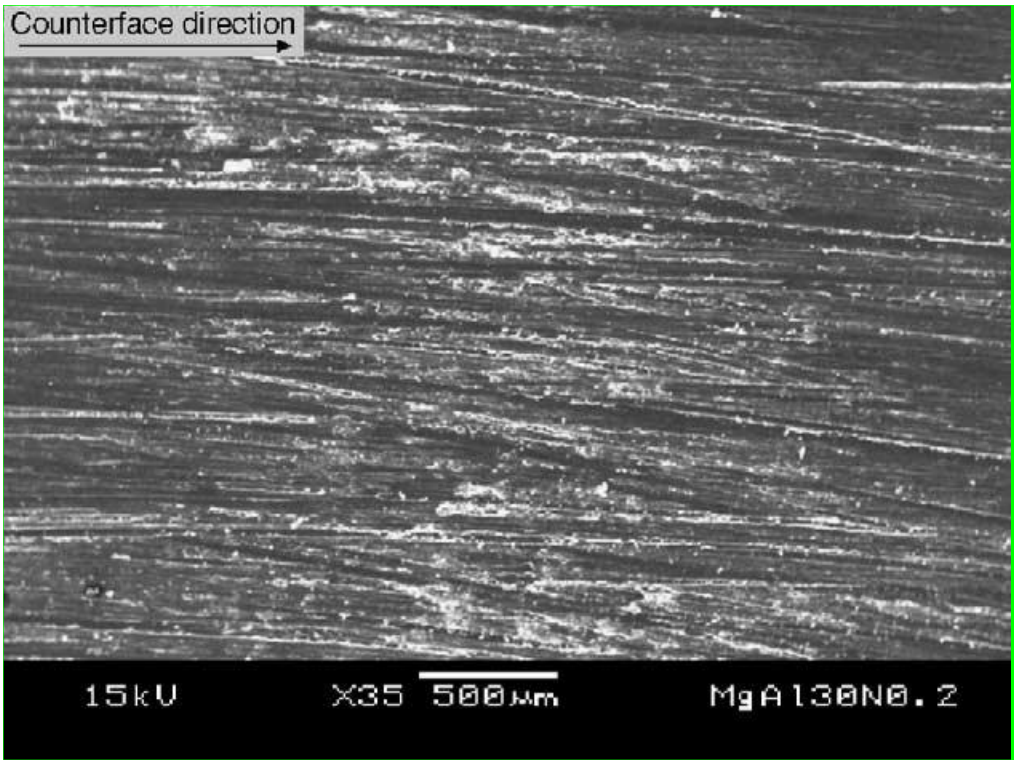

Figure 0.3. Abrasive eroded surface image [215].

4.1.3. Oxidative Wear

Oxidative wear occurs when the surface is oxidized as a result of the heat created by friction during sliding. Oxide wear deposits saturate the surface, providing a protective layer and reducing contact and wear rates as a result of repeated sliding. Said oxide films are formed when the surface temperature rises to a level suitable for oxidation to occur and reaches a certain thickness [216]. The oxidatively degraded surface image is shown in Figure 4.4.

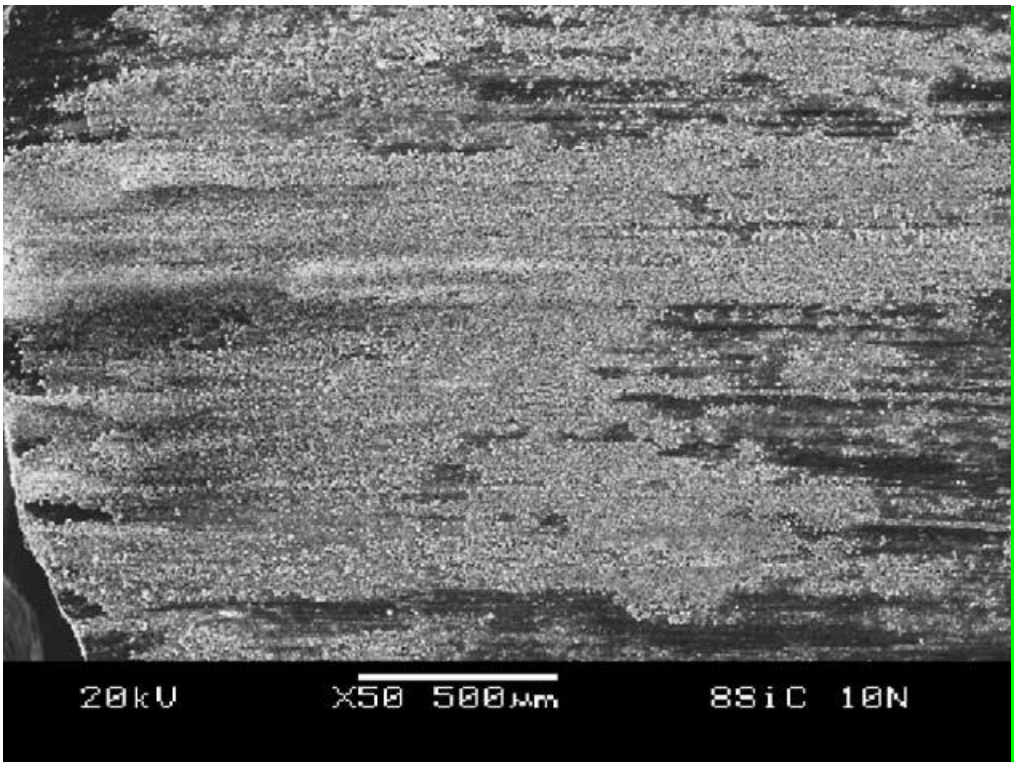

Figure 4.4. Oxidatively degraded surface appearance [215].

4.1.4. Delamination

Delamination usually occurs with the formation of vertical cracks in the direction of shear. This process is usually due to fatigue, and repeated sliding causes subsurface cracks to expand, eventually shearing the surface and forming long, thin wear plates [215,216]. Figure 4.5 shows a delaminated, eroded surface.

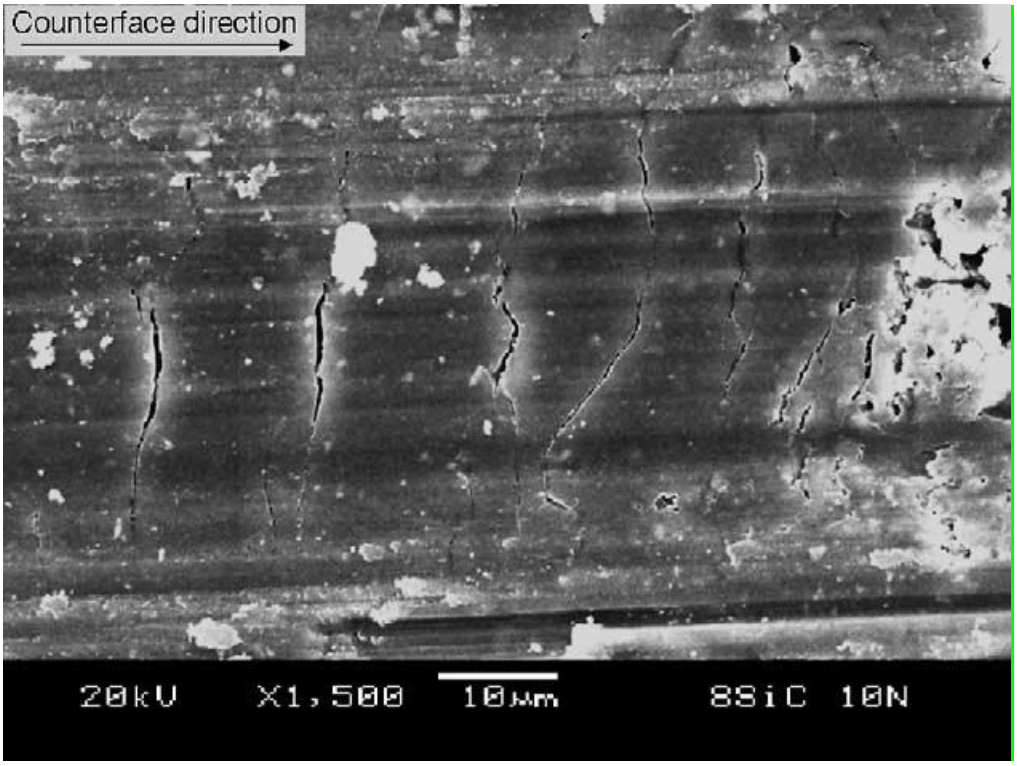

Figure 0.5 Delaminated eroded surface image [215].

4.1.5. Thermal Softening and Melting

The large plastic deformation causes this wear, and the material protrudes from the interface and resolidifies around the pin. When too much material is transferred to the disc, it leaves a lot of wear residue behind. The frictional heat at the friction interface causes this wear [216].

Figure 4.6 [216] depicts the creation of a wear map between normal loads against sliding speeds in order to provide a more concise summary of the wear processes of magnesium and its composites. Changes between mechanisms happen gradually, and the lines shown are only approximations. It is possible to see the broad patterns shown below.

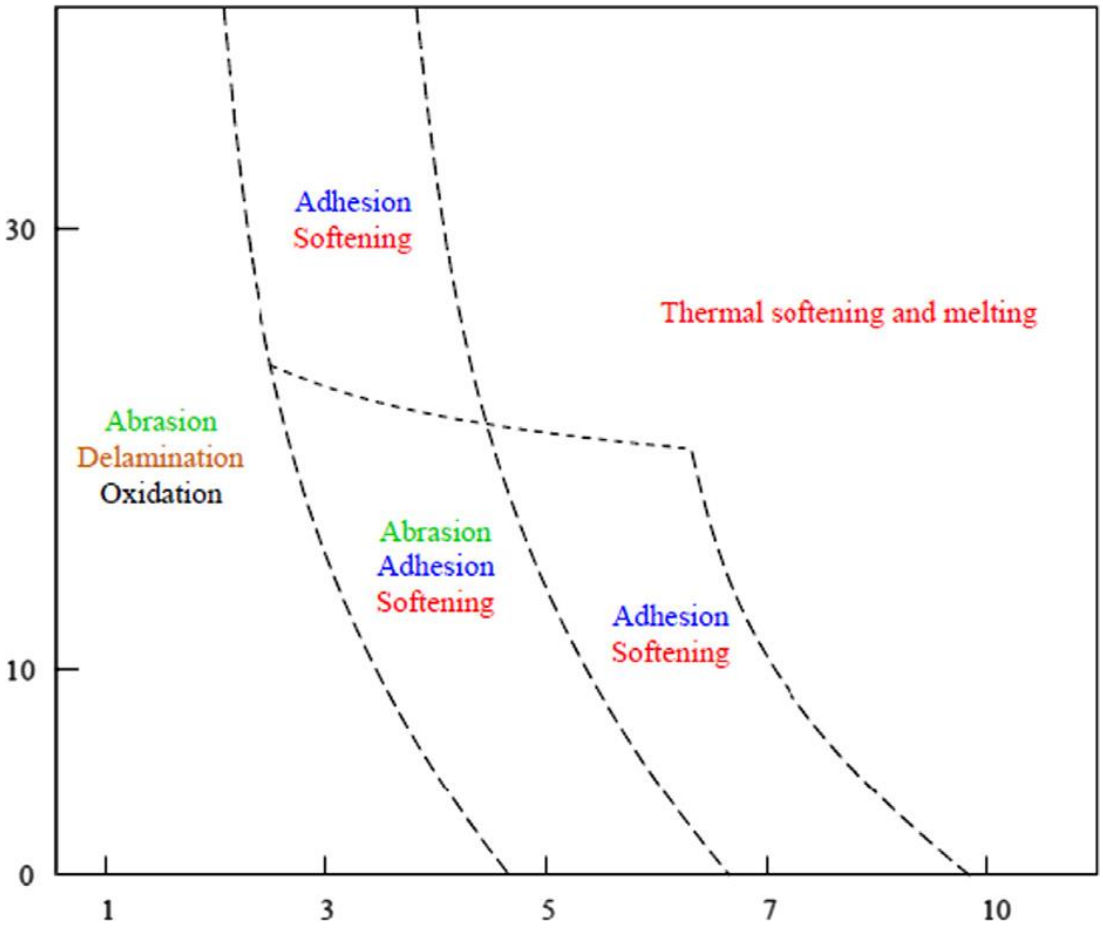

Figure 4.6. Simplified wear mechanism map depicting wear behavior of magnesium and its composites [216].

4.2. CORROSION BEHAVIORS AND TYPES OF CORROSION

Corrosion is often defined as a substance losing its metallic properties due to an electrochemical or chemical interaction with its surroundings. The utilization of magnesium-based materials in construction applications has been severely limited due to their low resistance to corrosion. Nonetheless, corrosion is inhibited by the oxide layer that forms on the magnesium surface. For two reasons, the corrosion rate of magnesium alloys is low. The first is secondary phases and contaminants causing galvanic corrosion. Second, compared to surfaces composed of aluminum and stainless steel, the hydroxide layer that forms on the magnesium surface is less stable [218].

Many unusual types of corrosion occur in magnesium and magnesium alloys.

4.2.1. Galvanic Corrosion

Magnesium has one of the lowest electronegative potentials leading to galvanic corrosion among engineering metals. Galvanic corrosion can be seen as macro and micro (Figure 4.7) [219].

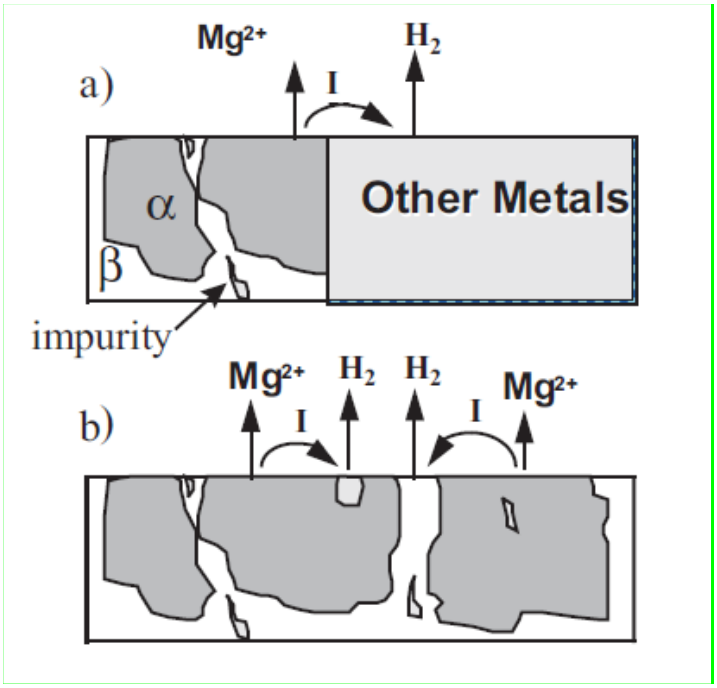

Figure 4.7 a) External galvanic corrosion. b) Galvanic corrosion inside [219].

The β-Mg17Al12 secondary phase, located at the AZ91 alloy's grain boundaries and containing 9% aluminum, exhibits cathodic activity in contrast to the matrix (Table 4.1). [220]. Table 4.1 displays the corrosion potential values of magnesium and magnesium secondary phases after two hours in a 5% NaCl solution with a pH of 10.5. The β-Mg17Al12 secondary phase exhibits corrosion resistance due to a thin passive layer that develops on its surface [220].

Table 4.1. Values of magnesium's corrosion potential and the main secondary phases of magnesium in a 5% NaCl solution [220].

Metal	Ecorr ,V_{SCE}
Mg	-1.66
Mg_2Si	-1.66
Al_6Mn	-1.53
Al_4Mn	-1.44
Al_8Mn_5	-1.26
$Mg_{17}Al_{12}$	-1.21
Al_8Mn_5(Fe)	-1.19
Beta-Mn	-1.18
Al_4MM	-1.16
Al_6Mn(Fe)	-1.11
Al_6(MnFe)	-1.01
Al_3Fe(Mn)	-0.96
Al_3Fe	-0.75

There are two impacts of the secondary phase of β-Mg17Al12 on magnesium corrosion. These effects are the barrier and the galvanic cathode. When the volume fraction of the β phase in the matrix is too low, the β-Mg17Al12 phase acts as a micro galvanic cathode and speeds up the corrosion of the matrix. When the volume of the β phase is large, it functions as a barrier to stop the alloy from corroding. [221]. The galvanic corrosion between the major phases of magnesium and Mg-Al alloys is schematically shown in Figure 4.8 [222].

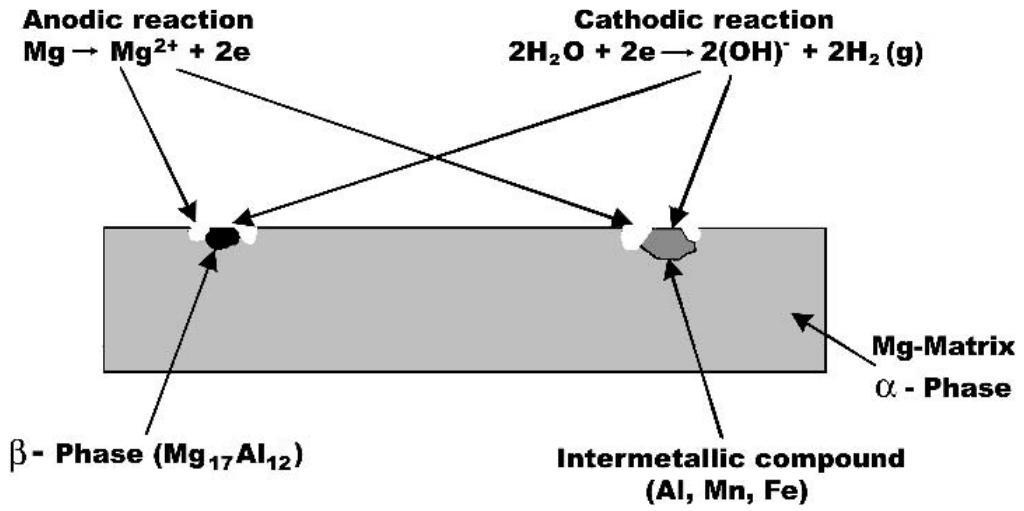

Figure 4.8. Diagram showing the progression of galvanic corrosion in Mg-Al alloys between the main phases [223].

4.2.2. Intergranular Corrosion

This kind of corrosion is not common in materials made of magnesium. Corrosion cannot pass through the grain because the grain boundary phases are cathodic to the grain. Most often, corrosion occurs in grains and at grain borders. [219].

4.2.3. Pitting Corrosion

Localized corrosion attack on metal surfaces is known as "pitting corrosion." Pitting occurs when the Mg17Al12 network in the magnesium-aluminum alloy system is attacked. Magnesium is considered an inactive metal. Pitting corrosion occurs when magnesium encounters chlorine ions in a non-oxidizing environment and has free corrosion potential. Corrosion cavities were discovered in defect areas near some second-phase particles such as Mg17Al12 and AlMn. As an example, Figure 4.8 shows cavities formed around Al-Mn particles in magnesium AM60 alloy immersed in a 3.5% NaCl solution [217].

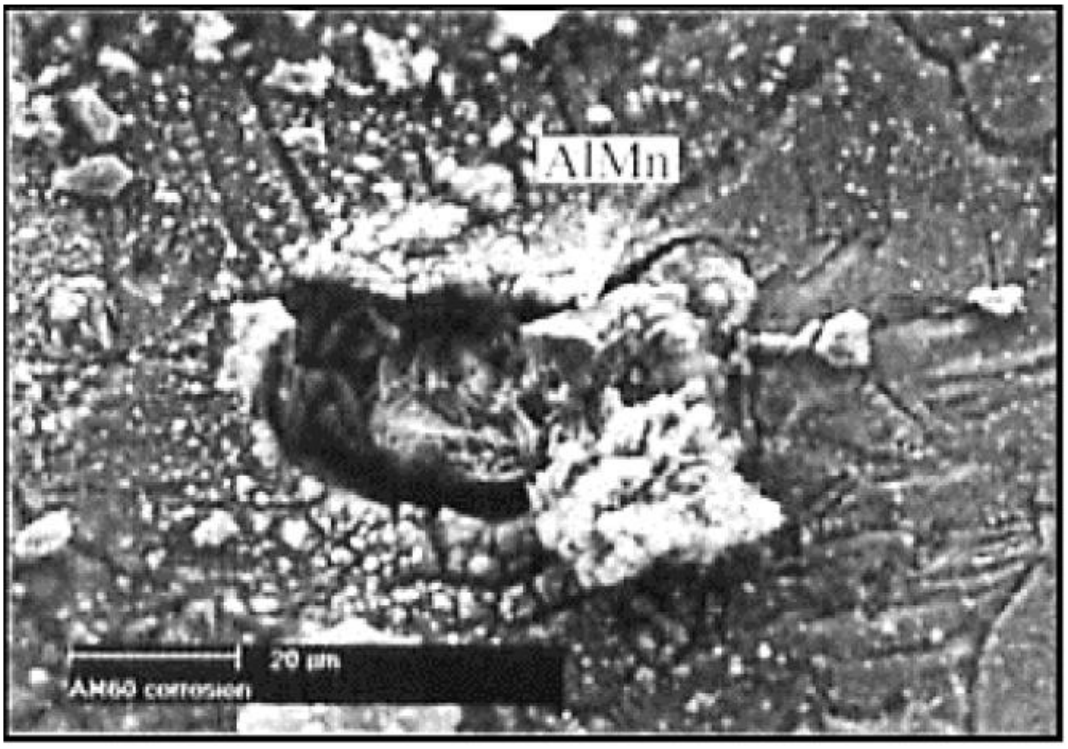

Figure 4.9. Pitting corrosion image of magnesium AM60 alloy after submersion in an aqueous solution of 3.5% NaCl [217].

4.2.4. Stress Corrosion Crack

For stress corrosion to occur, the metallic material must be supported in the direction of tension or compression as well as a crack initiation and a supporting electrolyte. Under most environmental conditions, commercially pure magnesium is not susceptible to stress corrosion cracking (GST) when applied to a load greater than its yield strength. In magnesium alloys, the presence of aluminum and zinc as alloy components increases the susceptibility to GCC. Aluminum and zinc-free magnesium alloys are the most resistant to GCS [217].

4.2.5. High Temperature Corrosion

As the temperature increases, the MgO film formed on the surface provides protection at temperatures below 450°C. As the oxidation temperature increases, the MgO coating is porous and non-protective. In general, the corrosion rate increases as the temperature increases. It increases the oxidation rate of Al and Zn [219].

4.3. FACTORS AFFECTING CORROSION

Alloying elements, impurity elements, phase components and microstructure affect the corrosion of Mg-based materials.

4.3.1. Al and Zn Effect

A continuous and layered structure of Al, Mg and Mg17Al12 is formed along grain boundaries. The resulting ß phase acts as a corrosion barrier. In addition, as the amount of Al increases, the composition of the hydroxide film on the surface also changes. It is possible to form a protective layer rich in Al. Corrosion resistance is higher in Al-rich areas close to ß precipitates. Zn increases the tolerance limits of other elements by changing the surface film characteristic [219].

4.3.2. Impurity Elements

Impurity elements adversely affect the corrosion resistance of magnesium alloys, and examples of these elements are iron, nickel, and copper. The precipitation of iron as Al-Fe compounds causes galvanic corrosion in magnesium as it is more cathodic compared to the magnesium matrix. Nickel, which is more harmful than iron in pure magnesium and magnesium alloys due to its limited solubility in solids, is found in a different phase in magnesium alloys. It is well known that the tolerance limit value for nickel varies with the casting process and is not affected by manganese or other alloying elements. In Mg-Al-Zn alloys, copper has a negative effect on the corrosion resistance of magnesium. Galvanic corrosion occurs as more copper is added to the Mg-Al-Cu-Zn phase, where the corrosion potential becomes more noble [219].

4.4.3. Effect of Phases

The ß phase (Mg17Al12) has a significant effect on the AZ91 alloy. Regarding the matrix, this phase is cathodic. The ß phase behaves passively over a wide pH range. At this stage, a lower pH level is expected to result in thicker film production [224]. The Mg17Al12 phase acts as a corrosion barrier and is inert in chloride solutions compared to the Mg matrix [225]. The formation of a thin passive coating on the surface of the ß phase explains its high strength.

4.4.4. Microstructure

In terms of corrosion, grain size and phase distribution factors are important. Thin and evenly dispersed cathodic phases have lower corrosion resistance. Corrosion resistance is also adversely affected by micropores. As a result, there is more corrosion per unit area [219]. The corrosion resistance of AZ series magnesium alloys increases with increasing aluminum content. According to theory, the distribution and amount of phase influence how well magnesium alloys resist corrosion to aluminum. However, since the AZ31 alloy consists of the matrix phase, the ß-phase theory cannot be applied to it. As a result, the corrosion behavior of the alloy is affected by the grain size, crystal defects and surface condition [226].

PART 5

EXPERIMENTAL STUDIES

In this research, varying proportions of AIN and SiC alloys were combined with ZK60 magnesium alloy. The alloys were prepared through a low-pressure casting technique by incorporating the elements. Following the casting process, the homogenized samples were extruded at a temperature of 300°C, utilizing an extrusion ratio of 16:1. The study encompassed an investigation into the microstructure, hardness, compressive strength, wear resistance, and corrosion properties.

5.1. PRODUCTION OF ALLOYS.

The study generated ZK60 alloys, encompassing both the ZK60 alloy compositions and ZK60 composites strengthened with 15% SiC and 15% SiC + 0.2/0.5% nano AlN. These compositions are outlined in Table 5.1. The reinforcing elements, namely silicon carbide (SiC) and aluminium nitride (AlN), were of 99% purity. The size of SiC particles ranged from 60 to 70 μm, while AlN particles measured 790 nm. Visual representations of SiC and AlN can be observed in Figure 5.1 using scanning electron microscope (SEM) images.

Table 0.1. Displays the gram quantities of the constituents within the examined ZK60 alloy and ZK60 matrix composites, normalized for 1000 grams.

Alloy and composites	SiC (gr)	AlN (gr)	Mg (gr)	Zn (gr)	Zr (gr)	Mg (gr)
ZK60	0	0	0	60	5	935
ZK60I	150	0	114	60	5	735
ZK60II	150	2	114	60	5	733
ZK60III	150	5	114	60	5	730

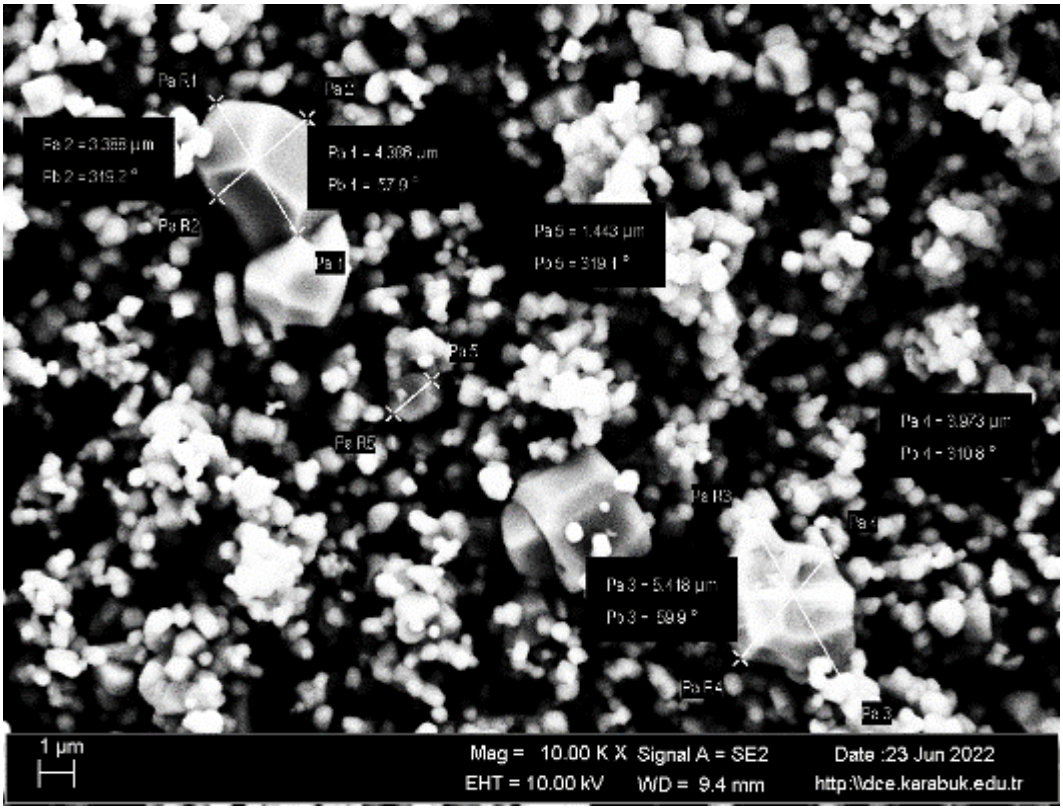

(a)

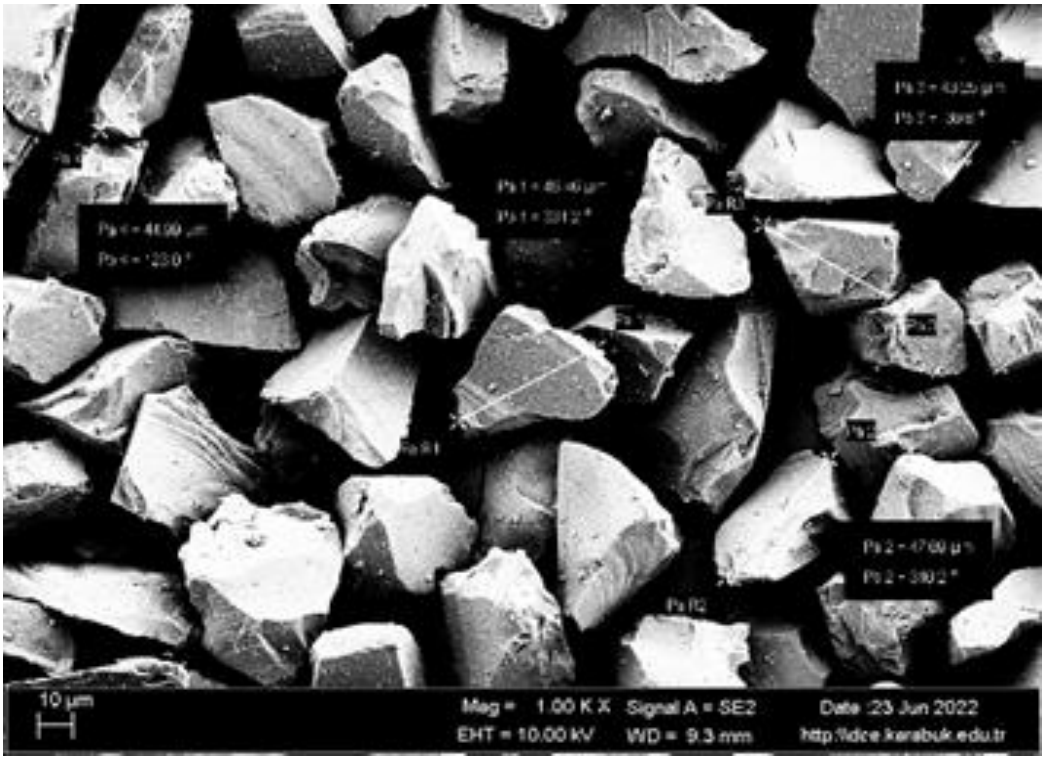

(b)

Figure 5.1. Presents images of (a) aluminum nitride (AlN) and (b) scanning electron microscope (SEM) visualization of SiC powder.

5.1.1. Preparation of Powder Mixtures

In order to achieve uniform dispersion of particles and prevent the formation of clumps that may occur during the process of mixing powders, liquid-based mixing and powder metallurgy techniques are used. At this stage, a mixture of 9% magnesium and 15% micro silicon carbide particles is blended for one hour in a V-type mixer. After being immersed in ethanol, the powder combinations in the ultrasonic vibration equipment are subsequently mixed together (Figure 5.2). After subjecting the combination to ultrasonic energy, it is then agitated in ethanol for a further three hours using a temperature-controlled magnetic stirrer. The addition of magnesium and silicon carbide particles to the aluminium nitride is done gradually in order to prevent clumping.

V-type mixer

Ultrasonic vibration device

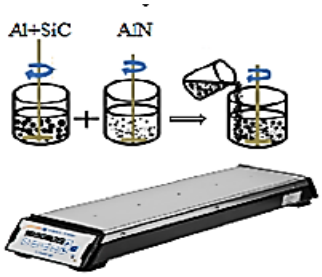

Magnetic stirrer

Figure 5.2. Preparation of the powder mixtures.

5.1.2. Compression and consolidation of powder mixtures

The AlN nanoparticles and SiC microparticles are pulverized at a temperature of 350°C at this stage. Figure 5.3 illustrates the use of a hydraulic press with a capacity

of thirty tons to exert force on the material, causing it to be inserted into a mold with a diameter of 32 mm and a length of 30 mm. Once the capsules have been enveloped in aluminum foil, as seen in figure 5.4, the sintering process is conducted for a duration of three hours at a temperature of 500°C. This is done inside a safeguarding environment consisting of SiO2 and graphite particles.

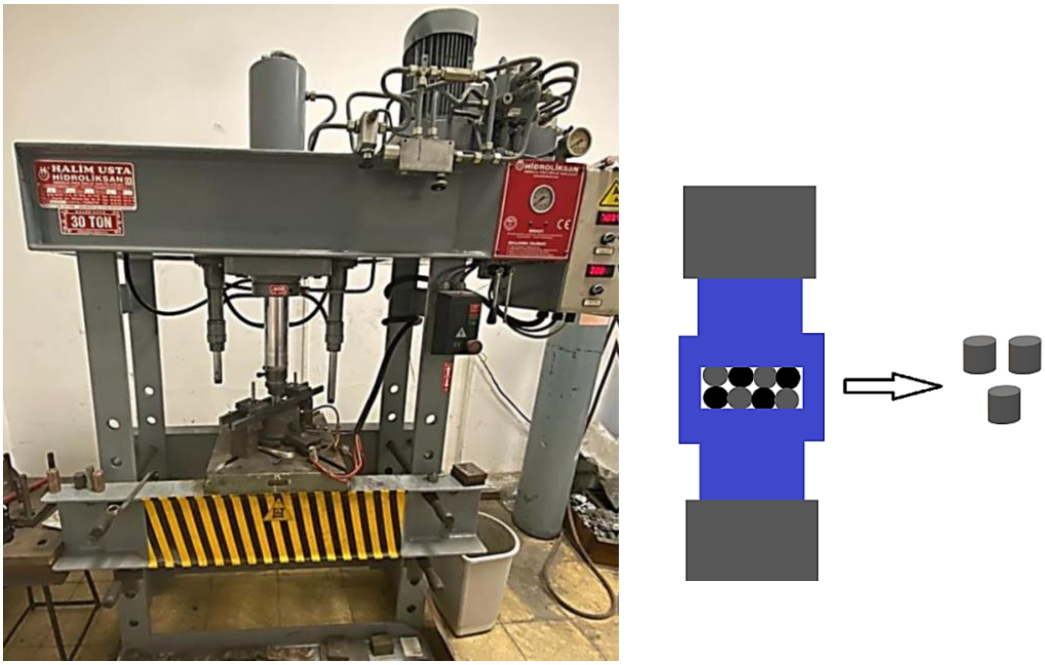

Figure 5.3. Schematic representation of the hydraulic press and pressing process used in the pressing and extrusion stage.

Figure 5.4. Protherm brand heat treatment furnace.

5.1.3. Induction Mixing and Casting Process

Using an induction melting furnace with gas shielding, alloys are melted. In order to keep the environment to prevent atmospheric contact during the melting process, a constant supply of CO2+0.8 SF6 gas combination is delivered to the ladle. With the aid of a mechanical mixer made of graphite, the melt in the crucible is mixed. First, in the casting procedure, pure Mg is added to the graphite crucible, and melting is anticipated. After thorough blending, a mixture of 6% zinc and 0.5% zirconium is added to the completely molten magnesium. A mechanical mixer spinning at 200 rpm for 30 minutes creates a vortex after the mixture reached a semi-solid state (about 450 °C). Capsules containing 9% Mg/SiC15, 9% Mg/SiC15 / AlN0.2, and 9% Mg/ SiC15 / AlN0.5 are introduced into the mixture after the furnace temperature reaches 750 C. An further two hours are spent stirring. After melting and mixing are finished, casting is created into cylinder-shaped casting molds (Figure 5.5).

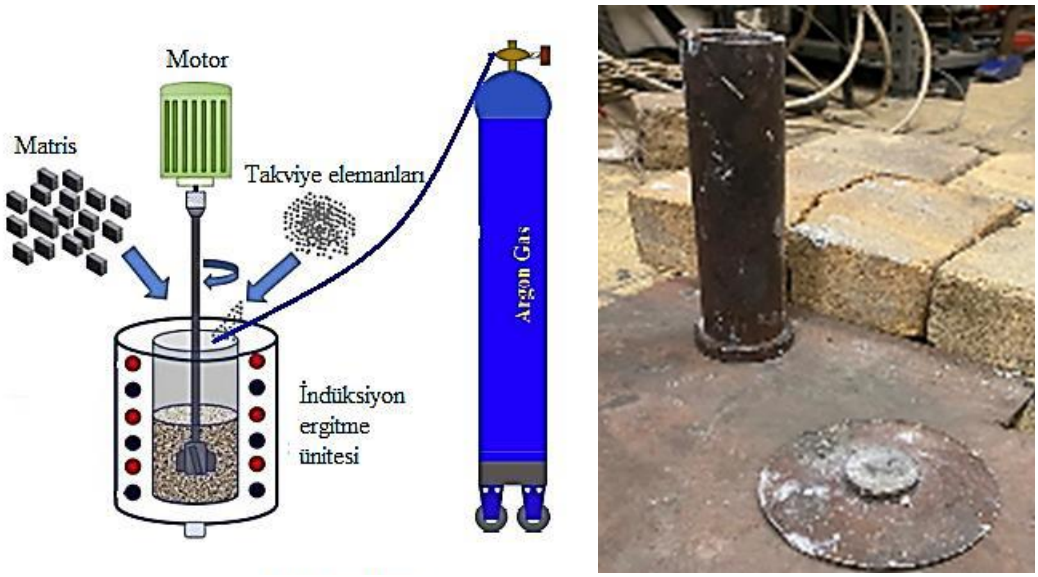

Figure 5.5. Cylindrical casting mold.

5.1.4. Homogenization

To prevent segregations from developing in the structure after casting and to homogenize the alloy composition, homogenization heat treatment is done to all

samples. Following their wrapping in aluminium foil, the cast ingots are immersed in a mixture of SiO2 and graphite sand and subjected to homogenization at a temperature of 420 °C for a duration of 24 hours, as seen in figure (5.6). The samples that were taken out of the furnace were immediately cooled by immersion in water in order to retain the homogenized structure.

Figure 0.6. Protherm brand heat treatment furnace.

5.1.5. Extrusion

An alloy extrusion process is carried out using a hydraulic press that has a capacity of 30 tons. The extrusion process utilizes a billet with a diameter of 32 mm and an extrusion exit with a diameter of 10 mm. The alloy undergoes extrusion at a temperature of 400 °C, with a velocity of 0.3 mm/s. The production of cylindrical extrusion samples with a diameter of 10 mm is achieved by spinning the punch connected to the press and applying pressure to a cylindrical billet with a diameter and length of 30 mm each. The billet is placed in the mold shown in figure (5.7), which has been heated to the required extrusion temperature. The formula below was used to compute the extrusion rate

$$(\text{EO}).EO = \frac{A_O}{A_S} \qquad (5.1)$$

The variable A_0 represents the cross-sectional area of the billet, whereas As represents the cross-sectional area of the sample produced after extrusion. For all extrusion operations in this investigation, a 9:1 extrusion ratio was used, based on the billet diameter of 30 mm and the extrusion outlet diameter of 10 mm, as specified in Equation 5.1.

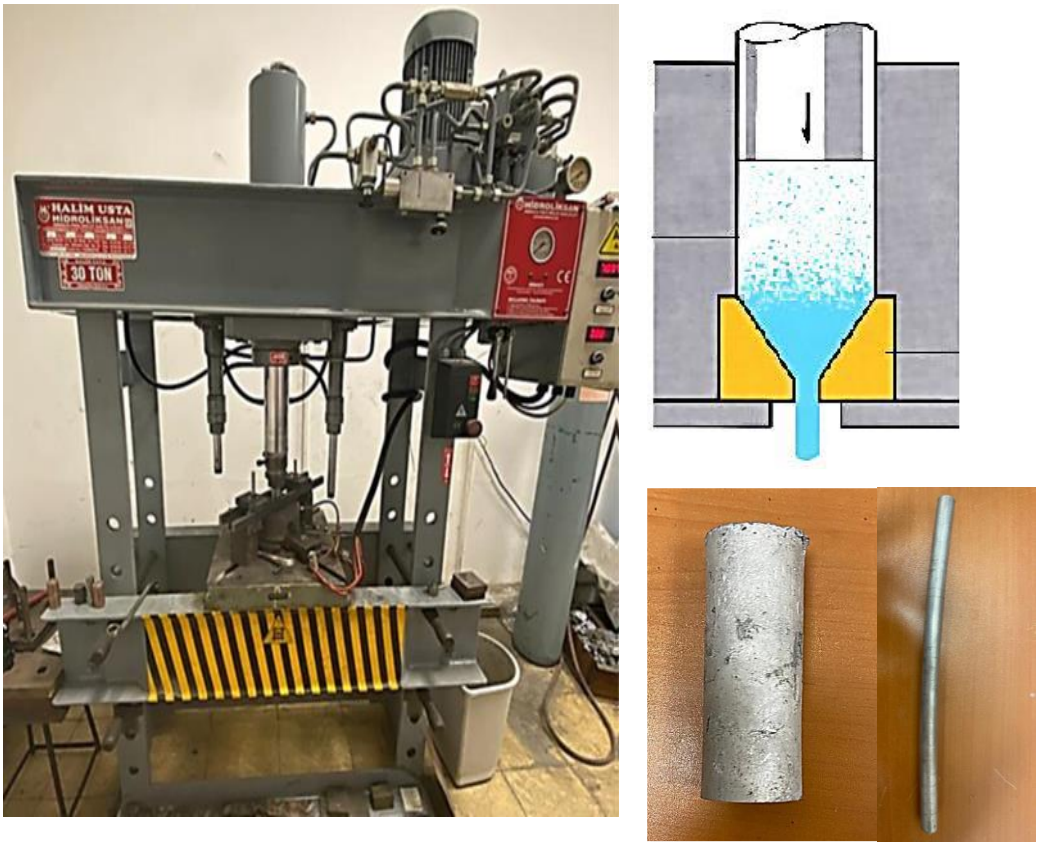

Figure 5.7. The hydraulic press and Images of produced samples.

5.2. CHARACTERIZATION OF ALLOYS

The microstructure of the produced composite materials was examined following casting, homogenization, and extrusion. The samples were merely examined for hardness, compression, wear, corrosion, and thermal conductivity testing after extrusion.

5.2.1. Density Measurement

After fabrication, the experimental The densities of the samples were measured using Archimedes' principle. For this, firstly, the weights of the parts were calculated with the precision measuring device shown in Figure 5.8.

Figure 5.8. PRECISE XB 220A precision balance used in the experiments.

5.2.2. Microstructure Characterization

The microstructure pictures of the manufactured samples were generated using an optical microscope and SEM (Scanning Electron Microscopy), while the component phases were identified using the XRD (X-Ray Diffraction) technique.

5.2.2.1. Metallographic Studies

The samples undergo initial sanding using SiC paper with a grid size of either 600, 800, 1000, 1200, or 2500 for metallographic examinations. The surface cleaning is then completed by polishing with 1 µm alumina paste. The sample is then etched to disclose its internal structural features after being dipped in a picric acid solution (The mixture consists of 6 grams of picric acid, 5 milliliters of acetic acid, 10 milliliters of distilled water, and 100 milliliters of ethyl alcohol). Using an optical microscope, metallographic analyses of the produced samples are performed. Microstructure images of each produced alloy after casting, the process of homogenization and extrusion was seen using a Nikon optical microscope and a Carl Zeiss Ultra Plus Gemini scanning electron microscopy (SEM) with energy dispersive spectroscopy (EDS) capabilities, as shown in figure 5.9. All samples were cut in appropriate sizes before imaging and cold molded in a cylindrical form with a mixture of epoxy resin and hardener. Subsequently, the surfaces of the Microtext brand were prepared for etching by using the conventional metallographic technique using a sanding and polishing apparatus. An etching solution consisting of 6 grams of picric acid, 5 milliliters of acetic acid, 10 milliliters of distilled water, and 100 milliliters of ethyl alcohol was used.

Grain size analysis was performed by examining 6 different microstructure images of each alloy by linear intersection method in accordance with ASTM E112 standard [180]. The volume ratio of the secondary phases in the structure after casting and homogenization was determined with the help of Image-J program.

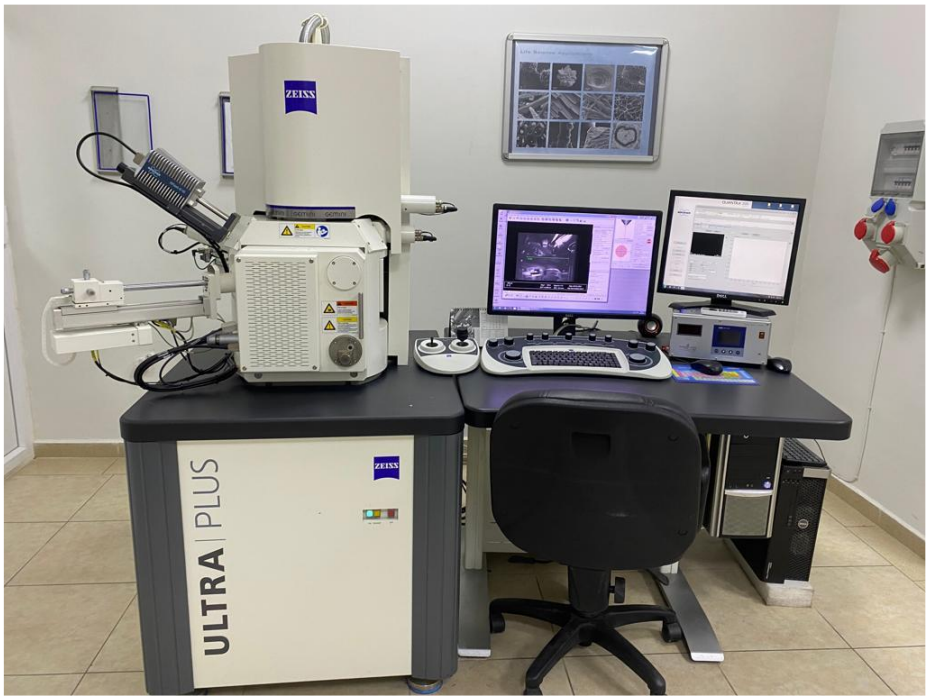

Figure 0.9. Carl Zeiss Ultra Plus Gemini Fesem SEM analyzer.

5.2.2.2. XRD Analysis

The XRD profiles of all samples were acquired using a Rigaku Ultima IV apparatus. The scanning angles ranged from 10° to 90°, with a scanning speed of 3°/min (Figure 5.10). The identification of the constituent phases in the post-casting structure was achieved by correlating the peaks seen in the XRD profiles with those present in the standard cards.

Figure 0.10. Rigaku brand XRD device.

5.2.3. Hardness Test

The specimens' Brinell hardness ratings are determined using a Brinell hardness testing instrument. A 2.5 mm diameter ball with a load of 187.5 N is used in the Brinell hardness test. Three distinct indentations are created for each sample, and their hardness levels are averaged by measuring the corresponding diameters, as seen in Figure 5.11.

Figure 0.11. The Brinell hardness device.

5.2.4. Compressor Test

The compression values of the samples are obtained using the Zwick Roel 600 kN compression device, as shown in figure 5.12. The samples used for the compression test have dimensions of roughly 10 mm in diameter and 12 mm in length. The compression speed employed is 0.5 mm/min. Three instances are generated for each parameter, and the compressor values are determined by calculating the mean.

Figure 0.12. The compression device Zwick Roel 600 kN device.

5.2.5. Characterization of Corrosion Properties

An analysis of the corrosive characteristics of casting and Extrusion samples were fabricated by constant immersion in salt solution and electrochemical potentiodynamic polarization tests. For both corrosion tests, the surfaces of the samples The surface was polished using sandpaper with a grain level of 1200 and there were no residues, voids, etc. on the surfaces. Factors that may affect the corrosion rate, such as.

5.2.5.1. Immersion Test

Immersion test specimens were extracted from casting and extrusion specimens with an outer diameter of 8 millimeters and a length of 15 millimeters in a cylindrical fashion. The surfaces of these specimens were then sanded and washed with pure water using an ultrasonic device. Due to the immersion test, the surface dimensions of the samples were computed to be $2\pi r^2 + 2\pi rh$. This was done in order to get the results of the computations. After calculating the surface areas of the samples and measuring their initial weight with a balance with 0.0001 g sensitivity before dipping, they were

left suspended with the help of a net in 3.5% NaCl solution placed in equal amounts in glass jars Figure 5.13. The specimens that were placed in the solution were recovered at certain time intervals of 3, 6, 9, 12, 24, 48, and 72 hours. Following removal, the surfaces of the items were purified and their weights were measured and documented. To eliminate the corrosion products that formed on the surface, the samples were immersed in a chromic acid solution with distilled water at a concentration of 180 g/L for 10 minutes, repeated hourly. then, the samples underwent ultrasonic cleaning using alcohol and were then submerged in a 3.5% NaCl solution. Weight losses were computed for each hour, and the overall average corrosion rates were established. Each sample underwent three immersion corrosion tests, and the average of the data was calculated. Following the 72-hour immersion test, SEM was used to capture pictures of the damaged surfaces of each sample, allowing for a detailed examination of the corrosion processes.

Figure 5.13. Illustrates the subsequent step, in which the specimens were submerged within an ultrasonic vibration apparatus.

5.2.5.2. Potentiodynamic Polarization Test

The corrosion resistance of the newly produced composites is evaluated in a 3.5% NaCl solution at room temperature, utilizing both the Tafel technique and an electromechanical test approach. For this purpose, a Gamry type PC4/300 mA potentiostat/galvanostat coupled with computer controlled DC105 corrosion analysis is employed to generate the potentiodynamic curves, as shown in Figure 5.14.

Before initiating the corrosion assessment, the samples are crafted in dimensions of 10x10 mm, enclosed by copper wire, and placed within Bakelite material. The wire's end is deliberately separated from the Bakelite to guarantee conductivity. After the exposed area of the sample has been polished to a smoothness of 2000 grit, a strong adhesive tape with a circular opening of 0.25 cm^2 is affixed to its surface. This method guarantees uniform exposure to the corrosion testing for all samples.

Within the 1 mV/s scan zone, the potentiodynamic polarization curves are shown, which range from -0.25 V (vs Eoc) to +0.25 V (vs Eoc). As in a standard three-electrode cell configuration, the sample surface operates as the working electrode in this experimental setup, with a graphite rod acting as the counter electrode and a calomel electrode as the reference electrode.

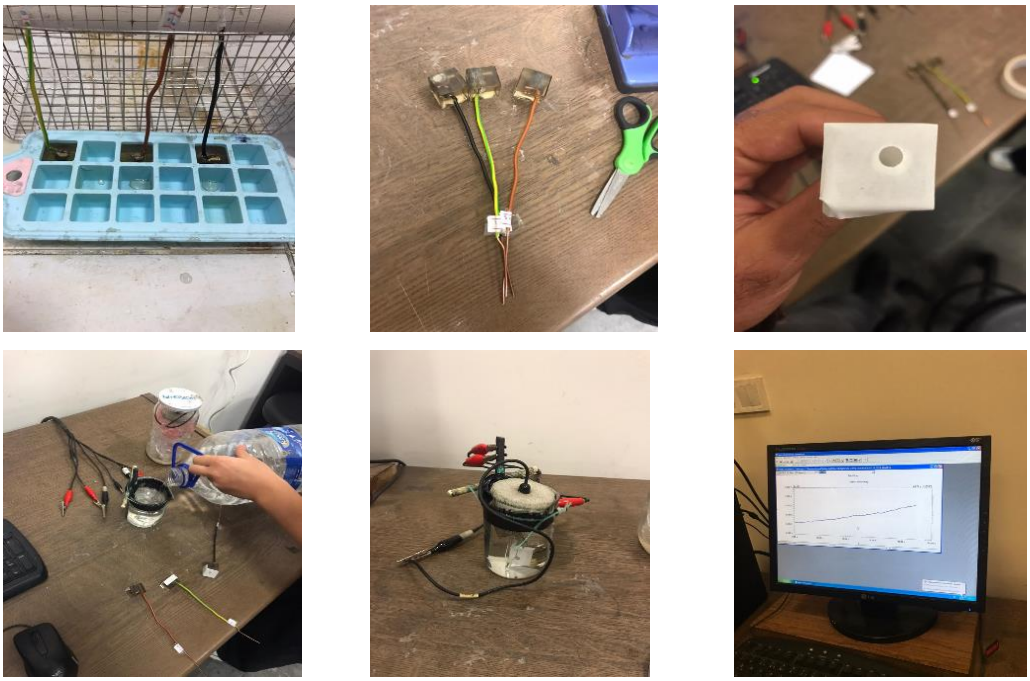

Figure 0.14. The preparation of samples to Potentiodynamic Polarization Test

5.2.6. Wear Test

Wear tests were conducted on both casting and extrusion specimens employing a reciprocating wear testing apparatus, as depicted schematically in Figure 5.15. The tests were carried out under three different modes: constant load, constant speed, and constant distance. Prior to the wear tests, the samples were trimmed to match the bed provided as a sample inside the gadget. Afterward, the surfaces were meticulously polished using sandpaper with a grain size of 1200 and thoroughly cleaned with alcohol.

The wear evaluations were conducted with a 20N load, a sliding speed of 0.1 m/s, and a total sliding distance of 1000 m. The frictional force throughout the wear process was quantified by means of a load cell affixed to the tribometer arm, with

instantaneous data being logged on the computer. The substance inserted was a high-hardness steel ball made of AISI 52100 grade.

Following the wear tests, the wear depths were quantified Using a Mitutoyo SJ-410 instrument for assessing surface roughness, employing a 2 μm standard probe in line with the ISO 1997 standard. The wear volume losses for each sample were calculated using the formula provided below.

$$V_w(mm^3) = \frac{2ab}{3}c \tag{5.2}$$

where V_w is the wear volume loss, c is the track length, a is the scar width, and b is the scar depth. The wear rates were calculated from the ratio of the volume losses calculated from here to the total distance. The worn surfaces underwent a thorough examination using Scanning Electron Microscopy (SEM), and the wear processes were identified. Each sample underwent three wear tests, and the average of the findings was calculated.

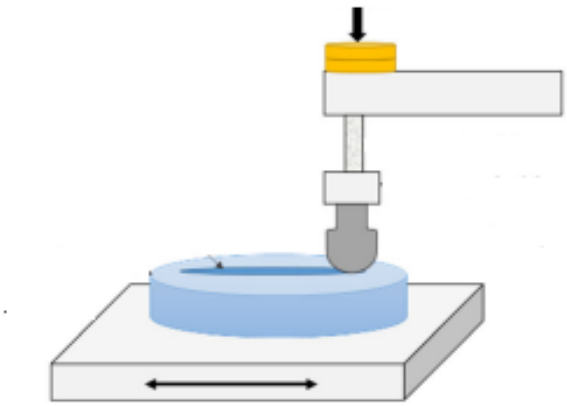

Figure 5.15. Schematic representation of the reciprocating wear tester.

PART 6

EXPERIMENTAL RESULTS AND DISCUSSION

This study presents the outcomes of various tests, encompassing density measurement, microstructure analysis, hardness assessment, compression testing, wear evaluation, and corrosion analysis, conducted on the compositions of the ZK60 alloy and ZK60 composites strengthened ZK60I,ZK60II, and ZK60III .

6.1. DENSITY MEASUREMENT RESULTS OF COMPOSITES

The samples, which are prepared at a ratio of 1:1 into pore water of known density are immersed in the water in turn. By making use of the difference between the weight of the samples in the air and the weight of the pure water, density determination is carried out without the need for volume measurement. Weighing during density measurement 0.0001 scale with gr sensitivity is used. Measurements are made 3 times for each sample and the results are averaged.

Principle equation is used while calculating density of the material using Archimedes scale method.

$$(\rho = \rho_w W_a (W_a - W_w) \tag{6.1}$$

Here ρ denotes the actual density of the material, ρ_w is the density of pure water as ($1 g/cm^3$), $W_a$is the weight of the material at air and W_w represent the weight of the material at water.

Hence the measured densities of the studied composites are presented in Table 6.1.

Table 0.1. The density results of composites.

Composites	**Density(gr/cm^3)**
ZK60	1.817
ZK60I	1.824
ZK60II	1.827
ZK60III	1.831

6.2. XRD RESULTS

The XRD analysis results for ZK60 are displayed in Figure 6.1. The ZK60 alloy exhibits the presence of the $MgZn_2$ and Zn_2Zr intermetallics alongside the predominant -Mg matrix. However, when examining the XRD outcomes of ZK60I (Figure 6.2), this composite showcases a primary matrix composed of -Mg, accompanied by intermetallic particles such as $MgZn_2$, Zn_2Zr, Mg_2Si, and SiC particles. The XRD data for the ZK60 composite reinforced with 15% SiC and 0.2% AlN is presented in Figure 6.3. This particular composite (ZK60II) reveals phases of $MgZn_2$, Mg_2Si, and Zn_2Zr intermetallics, as well as SiC and AIN nanoparticles. With the ZK60III composite, the XRD results exhibit additional peaks at 35°, 59°, and 70° angles as the AIN content is increased from 0.2% to 0.5% weight. This composite's XRD patterns (Figure 6.4) show the presence of the main -Mg matrix, along with $MgZn_2$, Mg_2Si, and Zn_2Zr intermetallics, SiC particles, and AIN nanoparticles. To simplify referencing, the composite ZK60I reinforcement is denoted as ZK60I , while the additional 0.2% and 0.5% AlN reinforced composites are denoted as ZK60II and ZK60III, respectively.

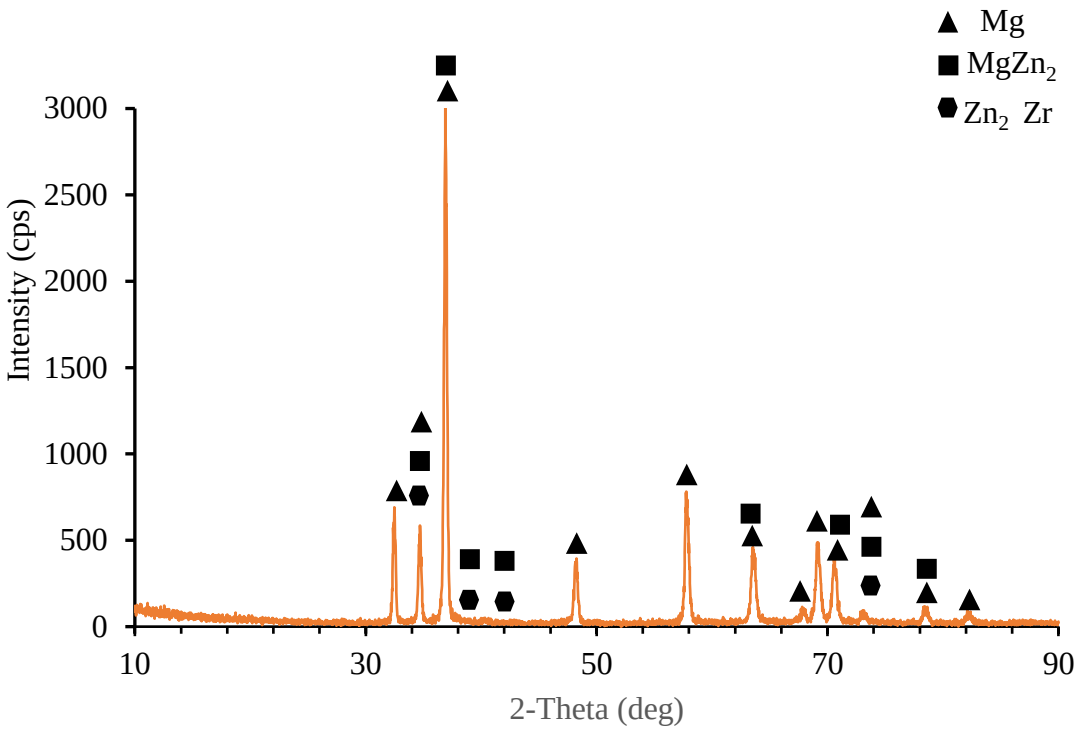

Figure 6.1. showcases the XRD (X-ray diffraction) patterns of the ZK60 alloy.

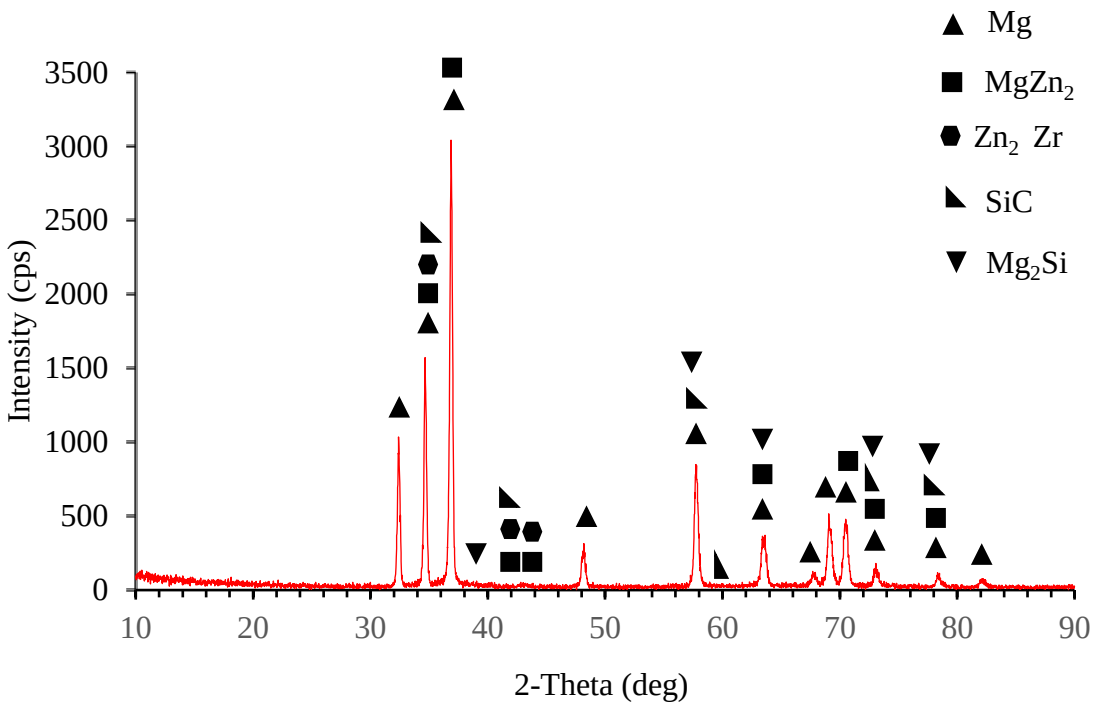

Figure 0.2. showcases the XRD (X-ray diffraction) patterns of the ZK60I.

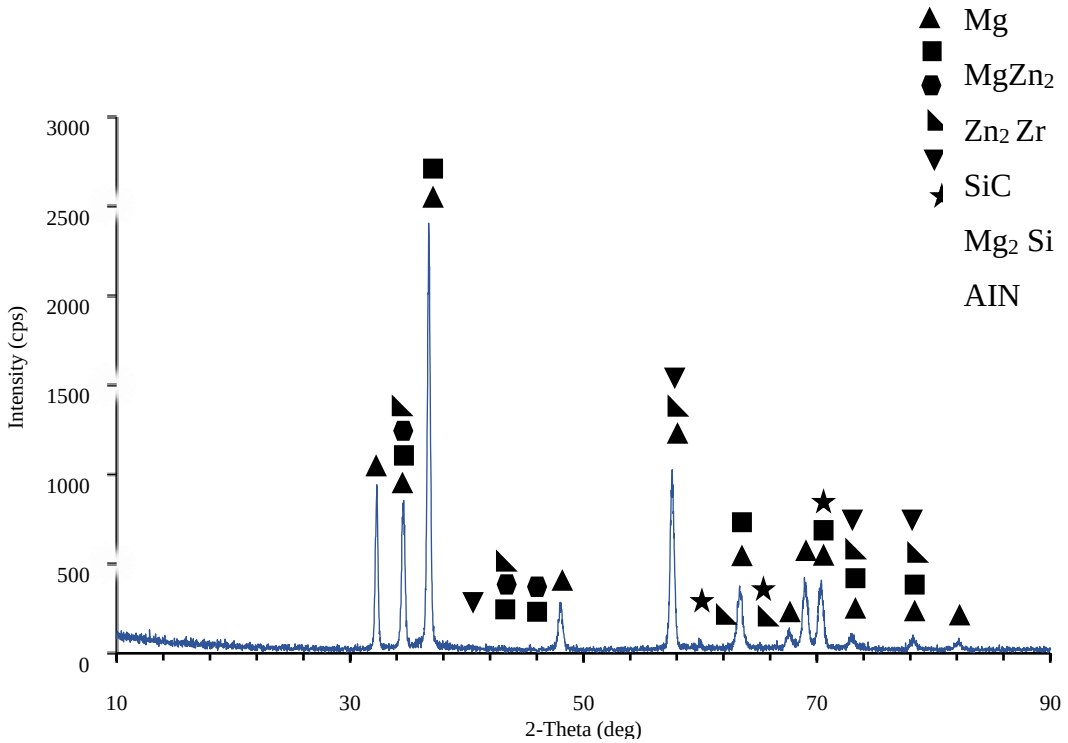

Figure 6.3. showcases the XRD (X-ray diffraction) patterns of the ZK60II.

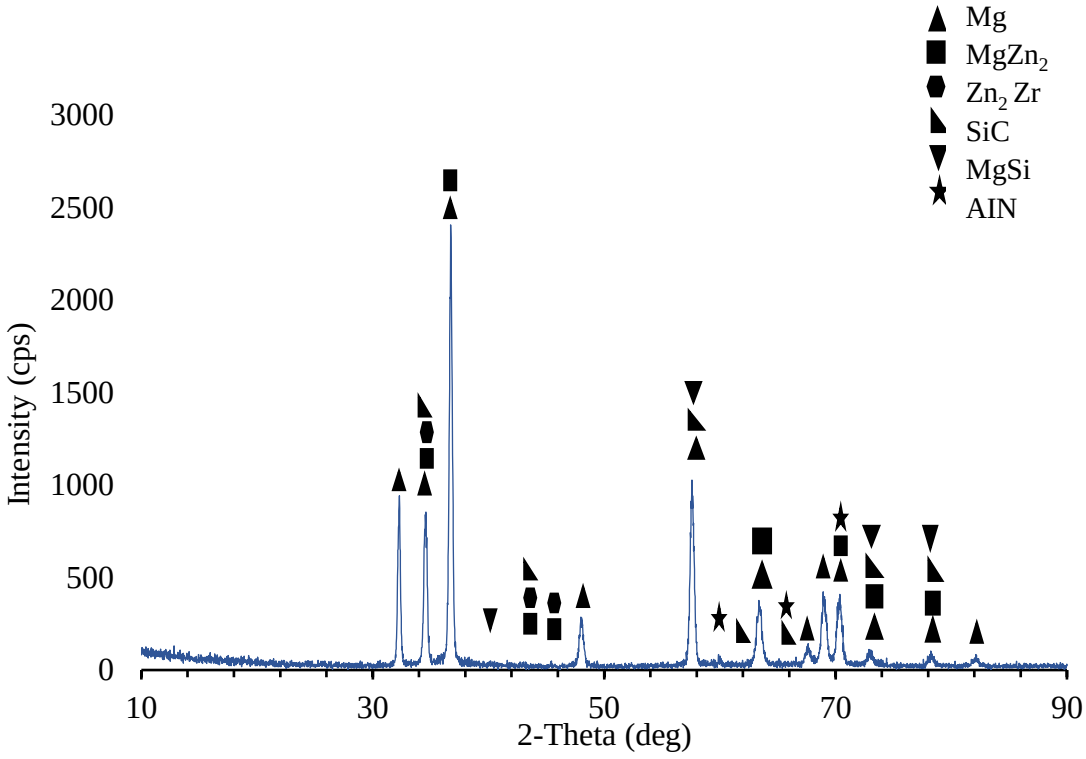

Figure 6.4. showcases the XRD (X-ray diffraction) patterns of the ZK60III.

6.3. MICROSTRUCTURE RESULTS

6.3.1 Optical Microstructure Images

Figures 6.5a, 6.5b, and 6.5c provide a comparative view of the microstructures of the cast, homogenized, and extruded ZK60 alloys. Correspondingly, Figures 6.5d, 6.5e, and 6.5f showcase ZK60I . ZK60II is illustrated in Figures 6.5g, 6.5h, and 6.5i, while ZK60III is depicted in Figures 6.5j, 6.5k, and 6.5l. Utilizing an image processing software application in accordance with ASTM standard (ASTM E112), in order to find the grain size, the average of five measurements was computed. Consequently, the mean grain sizes of the as-cast samples were calculated to be 65 µm for ZK60, 60 µm for ZK60I, 62 µm for ZK60II, and 48 µm for ZK60III. For the extruded samples, the average grain sizes were observed to be 32 µm for ZK60, 28 µm for ZK60I, 25 µm for ZK60II, and 23 µm for ZK60III.

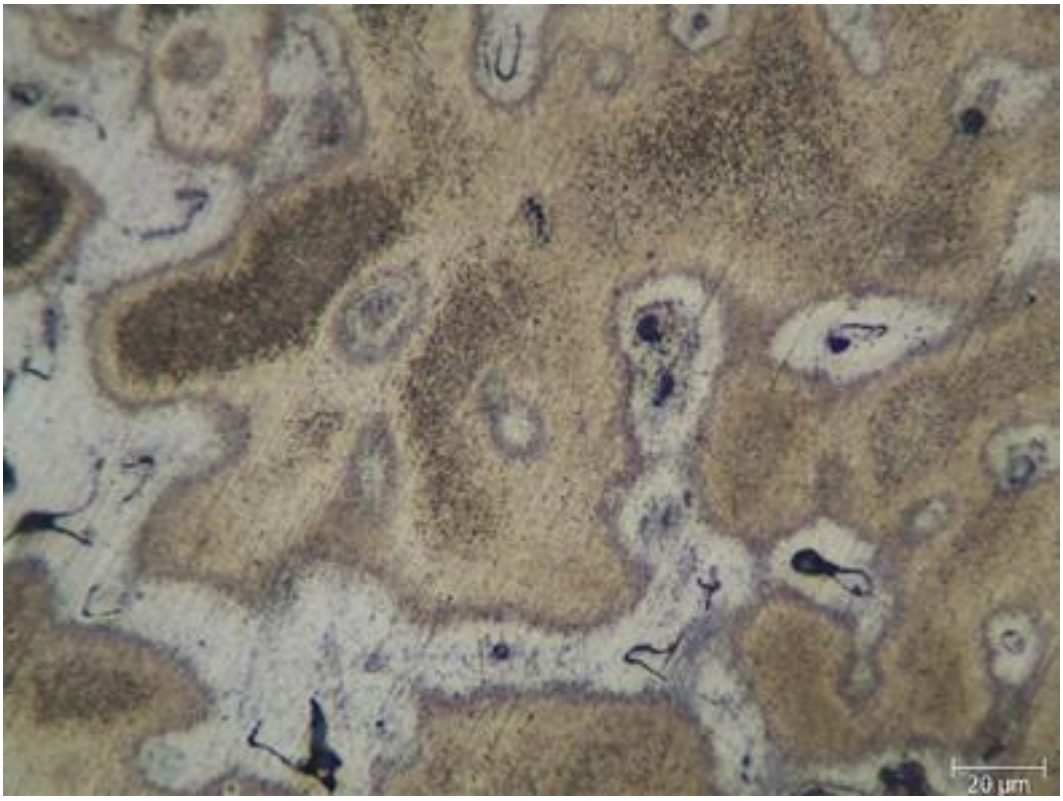

(a) ZK60 at 500 X after casting.

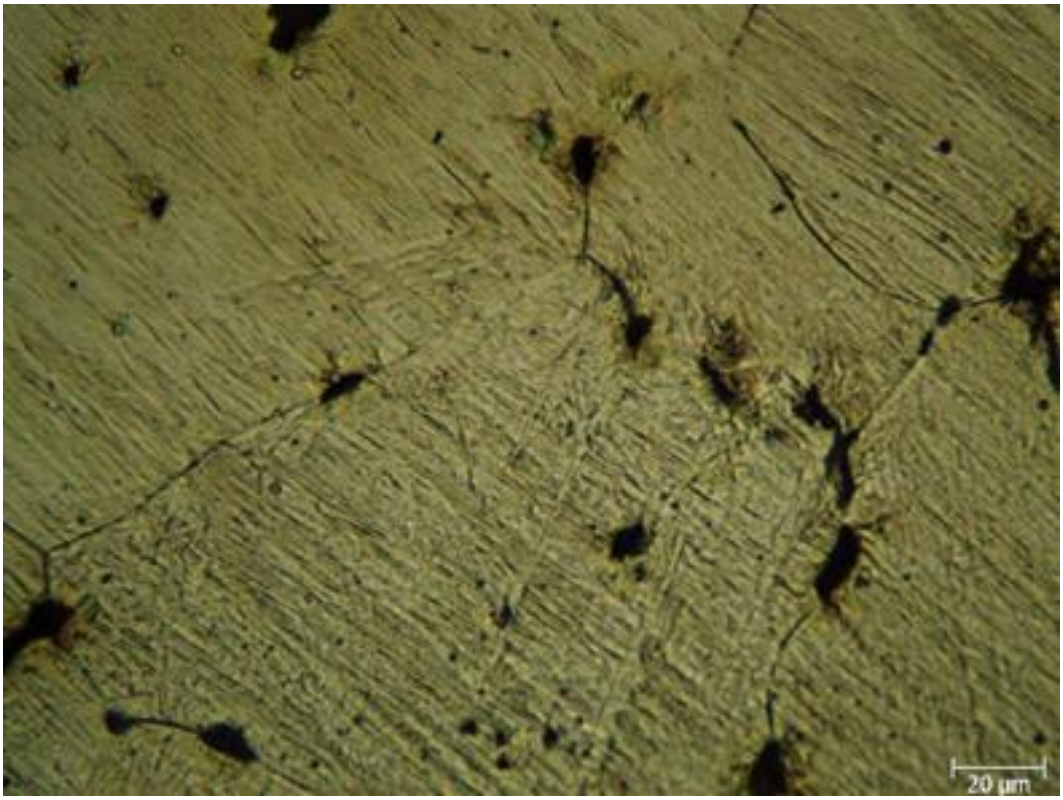

(b) ZK60 at 500 X After homogenization.

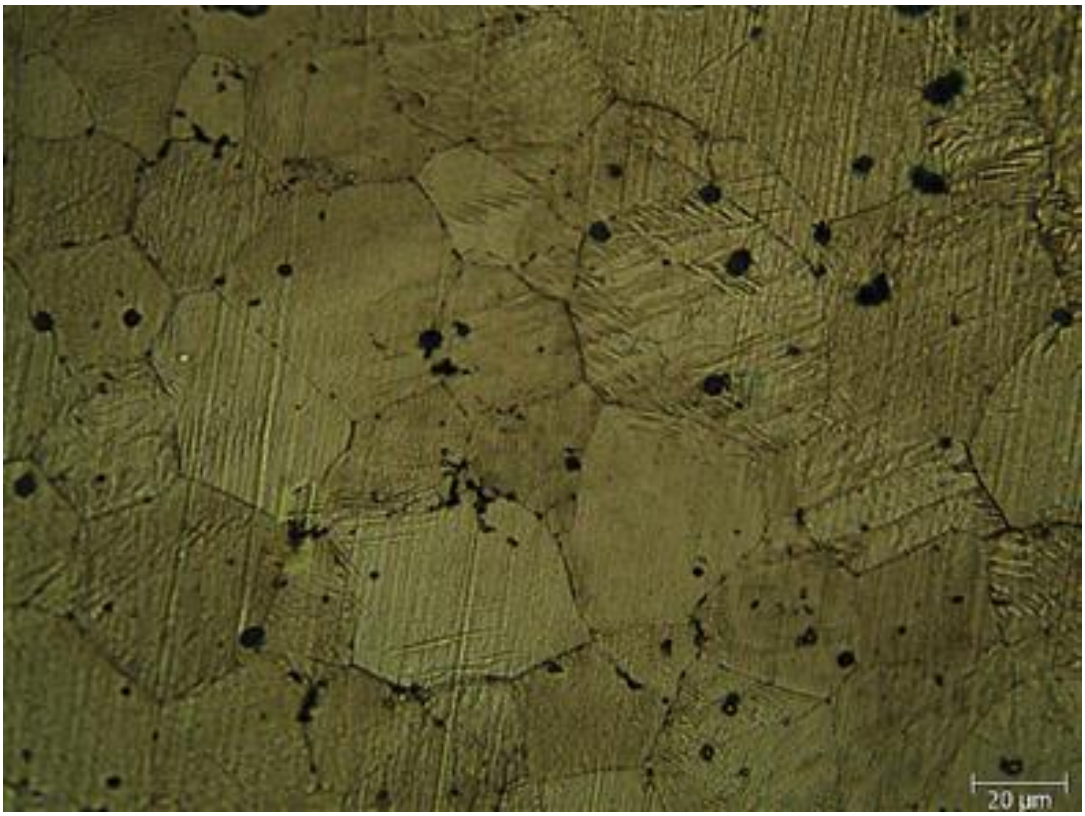

(c) ZK60 at 500 X after extrusion

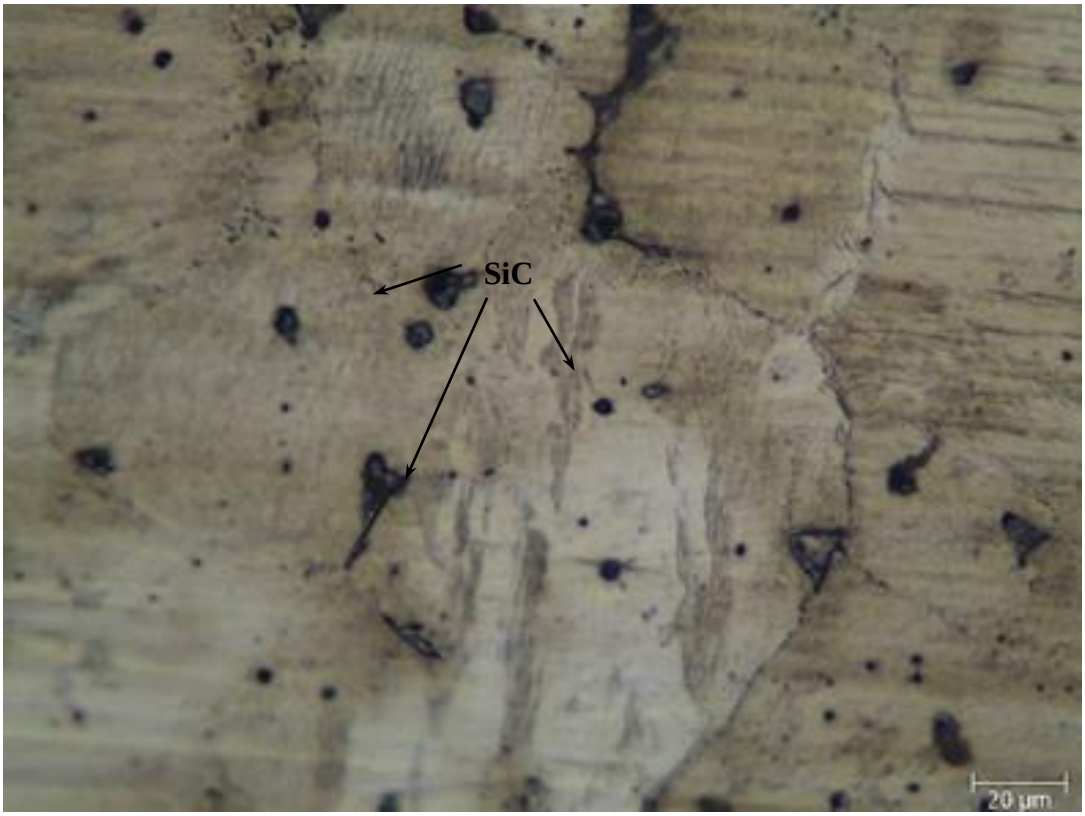

(d) ZK60I at 500 X after casting.

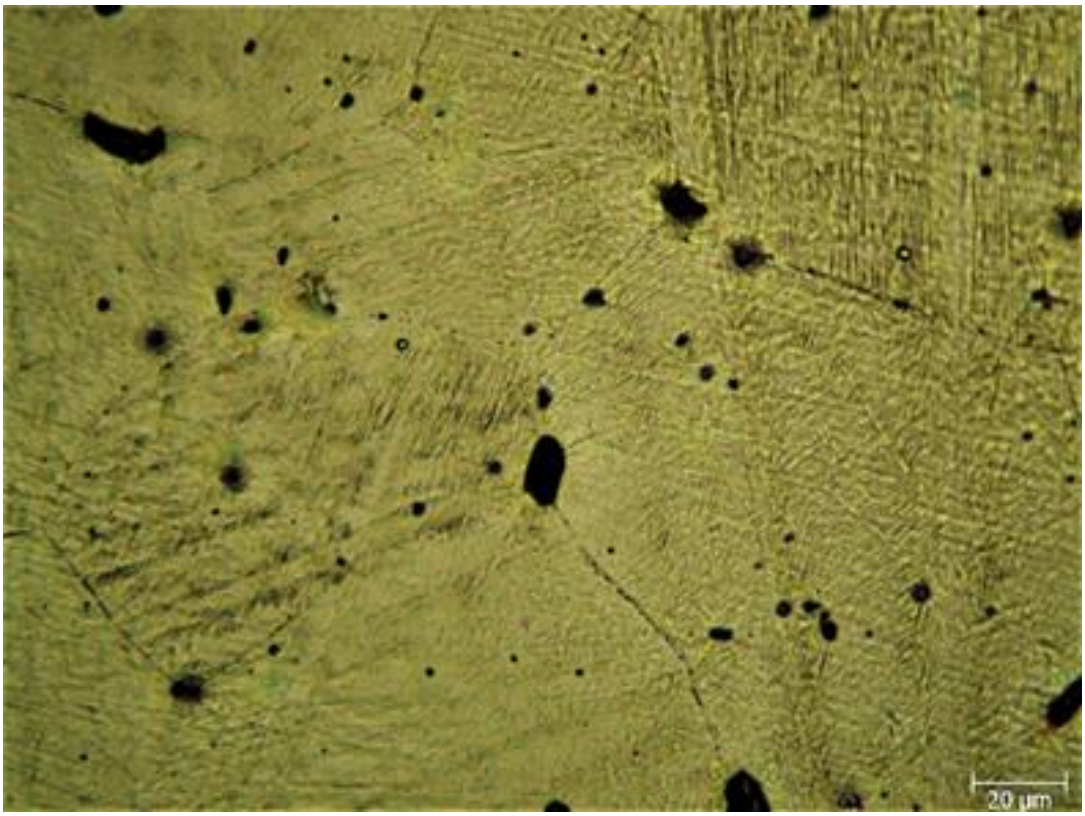

(e) ZK60I at 500 X after homogenization.

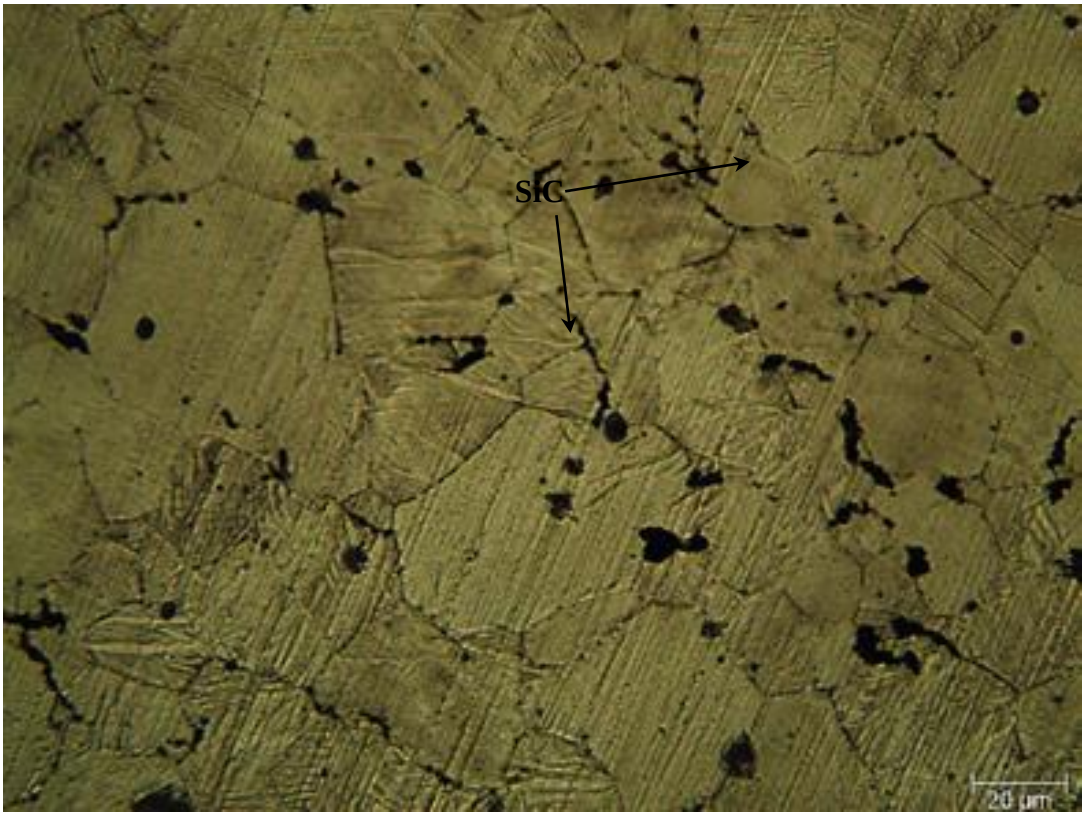

(f) ZK60I at 500 X after extrusion

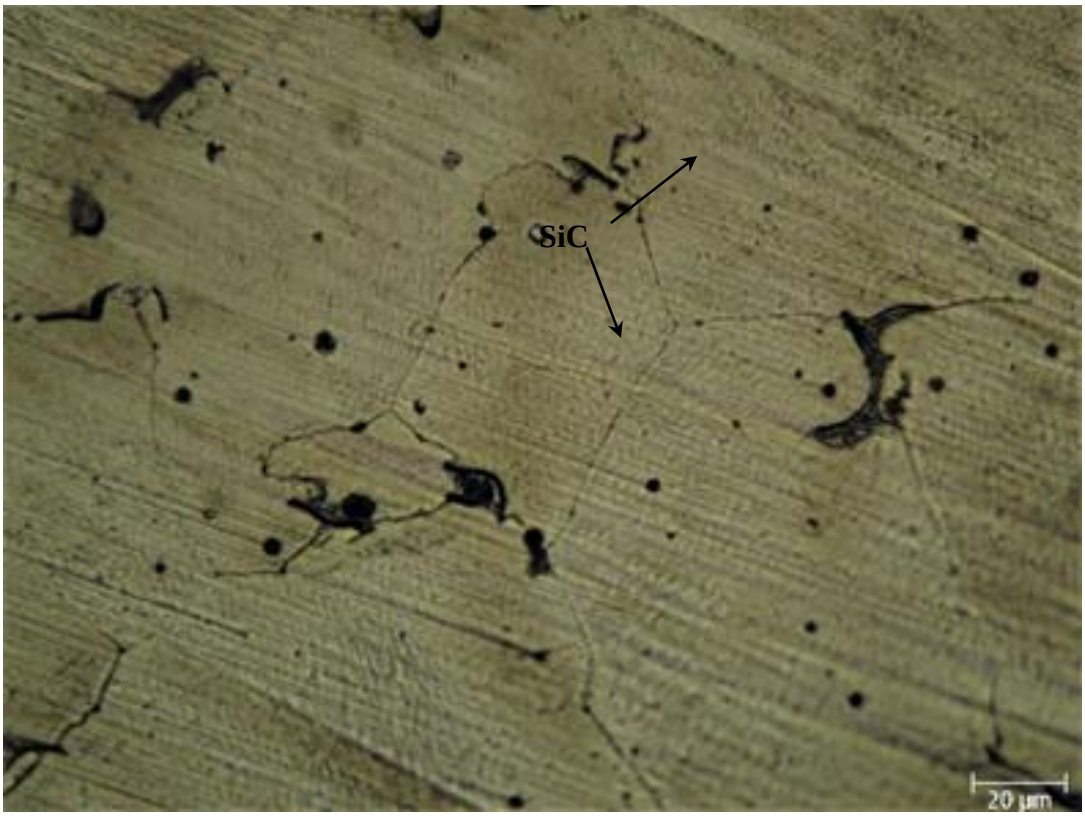

(g) ZK60II at 500 X after casting.

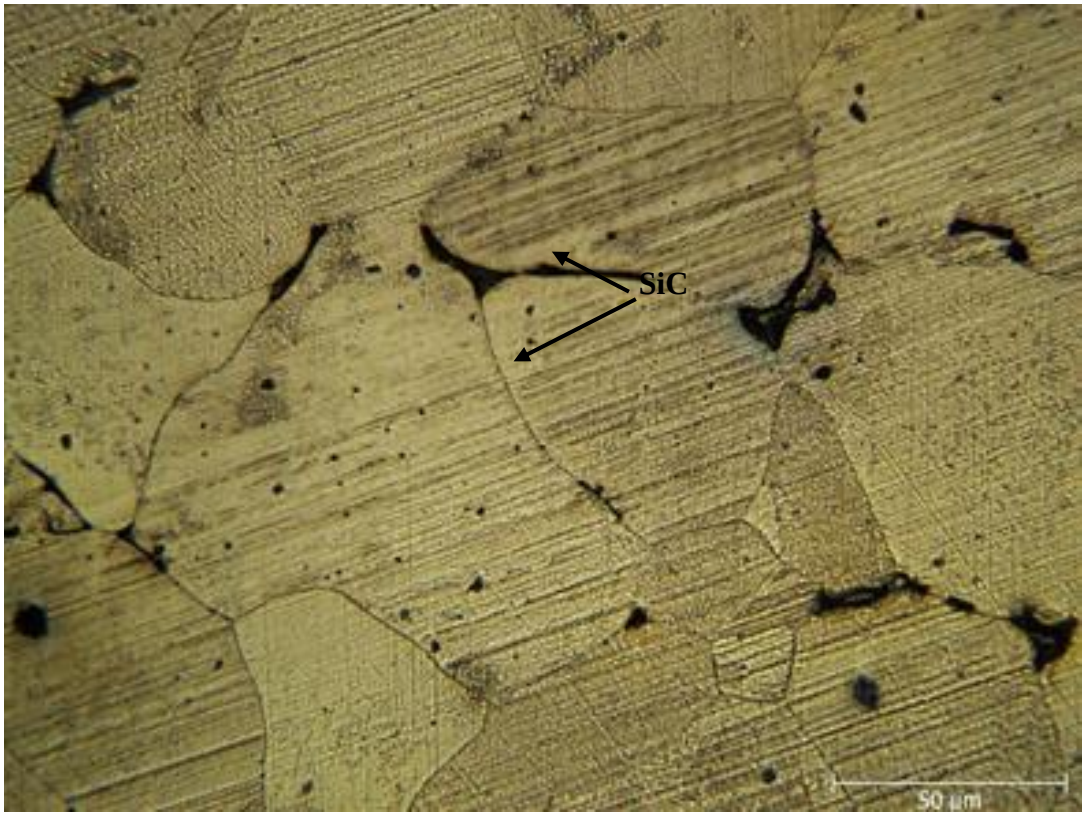

(h) ZK60II at 500 X after homogenization.

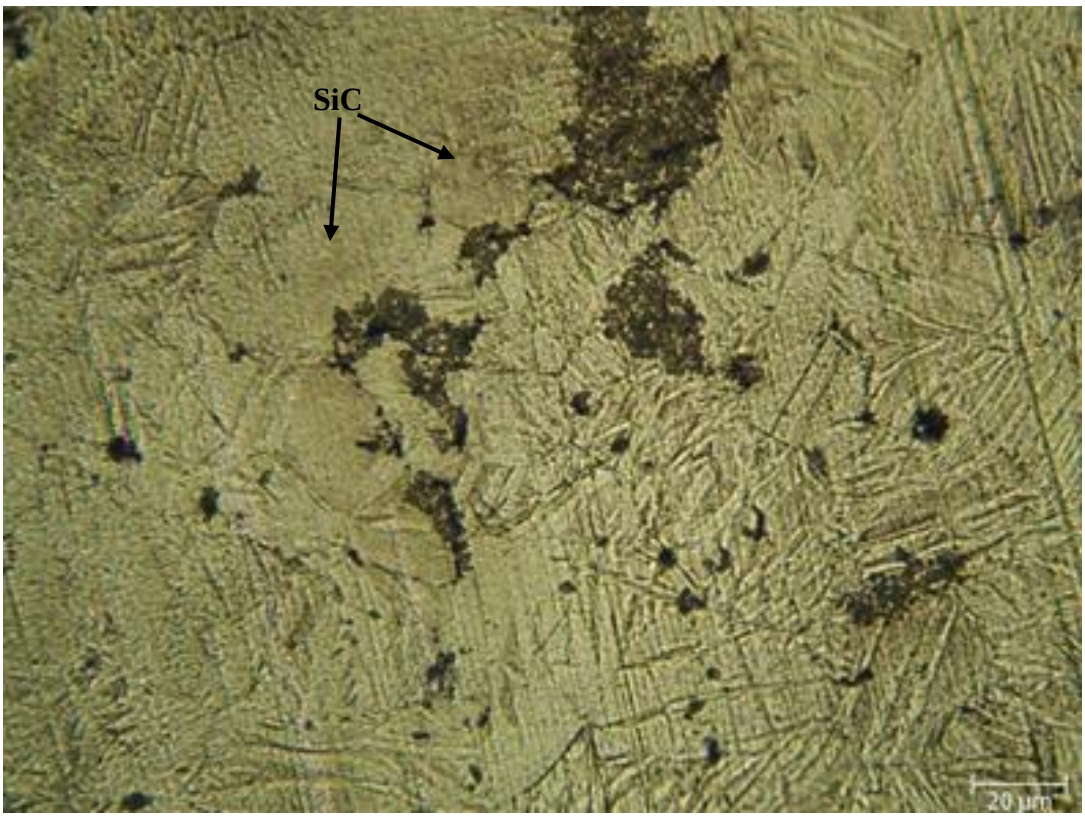

(i) ZK60II at 500 X after extrusion.

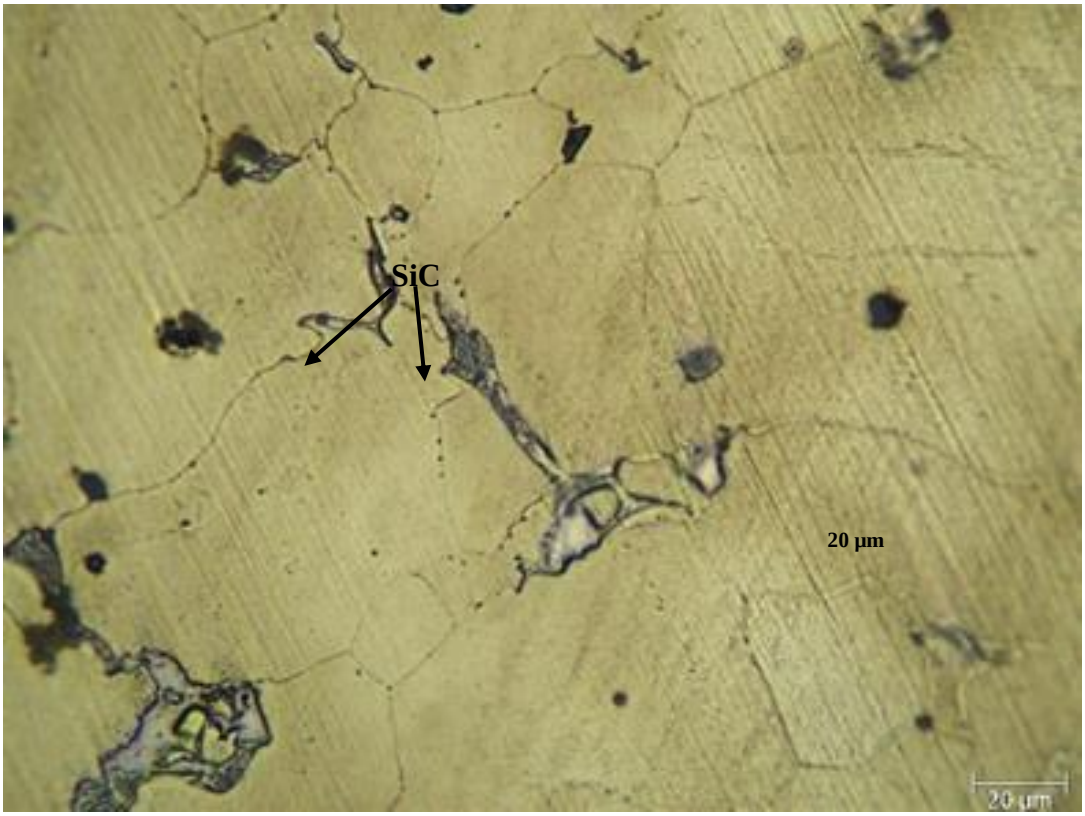

(j) ZK60III at 500 X after casting.

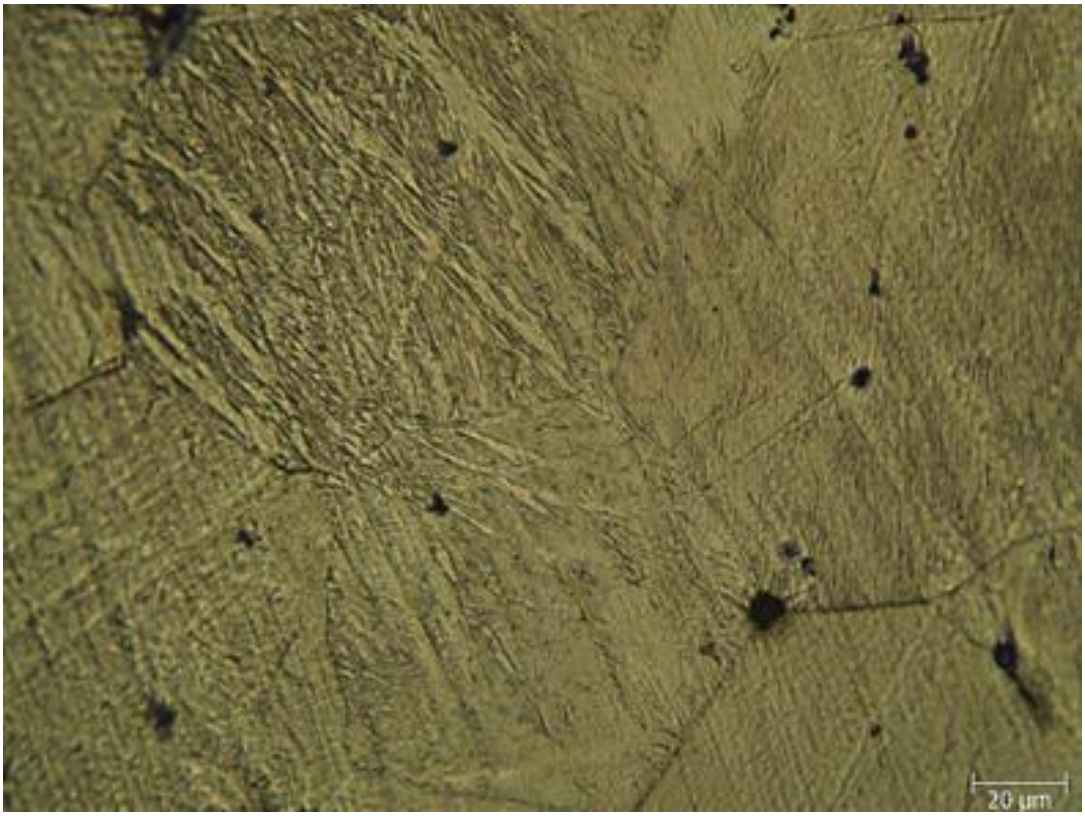

(k) ZK60III at 500 X after homogenization.

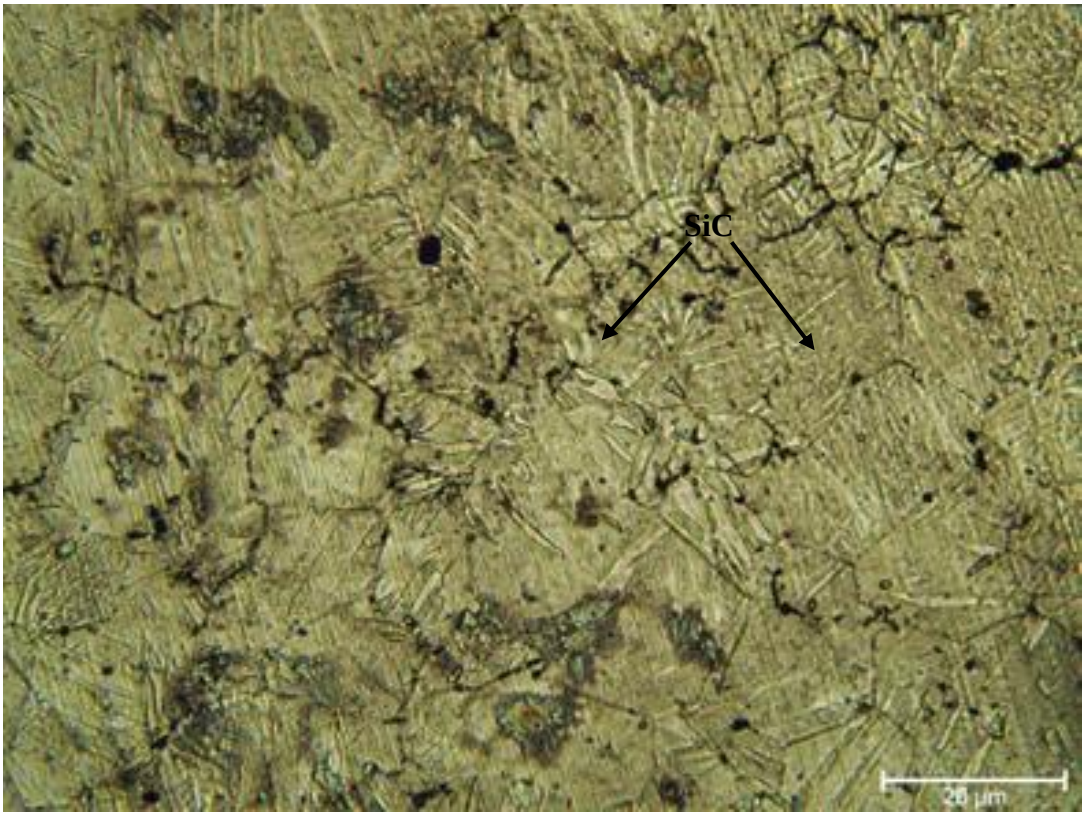

(l) ZK60III at 500 X after extrusion.

Figure 6.5. Light microscopy pictures of the following samples: ZK60 (a, b, and c), ZK60I (d, e, and f), ZK60II (g, h, and i), and ZK60III (j, k, and l).

The black, clearly visible microstructures particles are thought to be SiC. It has been noted that following extrusion, the ZK60 alloy's α-Mg grain size decreases with the addition of SiC and AlN. The post-extrusion microstructure images show that dynamic recrystallization (DRX), which occurred during hot extrusion, significantly reduced the grain size in all alloys.

6.3.2. SEM Microstructure Images and EDX Analysis

The ZK60I reinforced ZK60 composite is shown in Figure 6.6a in SEM pictures and Figure 6.6b in an EDX map analysis at a 2kX magnification. The elemental spectra of the sites marked with the digits 1–6 in Fig. 6.6a is shown in Table 3.

Figure 6.6a's section 1 has the components 4.48% carbon, 87.15% magnesium, and 8.45% zinc, which indicates the existence of the main matrix. This information is shown in Table 6.2. The structure of the SiC particles in the composite is shown by

the presence of 13.22% carbon and 36.19% silicon in the area illustrated by 2 and in Figure 6.6a. In addition, there is a trace quantity of Zr that may be found at the grain boundaries of the SiC particle. Additionally, the SiC particle is represented by area 3, and the SiC particle is represented by region 4, which shows a spectrum consisting of 11.9% carbon, 29.59% silicon, and 55.6% magnesium elements. Within area 5, there is an intermetallic compound composed of magnesium and zinc, and within region 6, there are a few trace quantities of fine-grained SiC particles. During the powder mixing process, certain SiC particles are naturally finer than others. This is because the steel balls that are contained inside the V-type mixer contribute to the particle size.

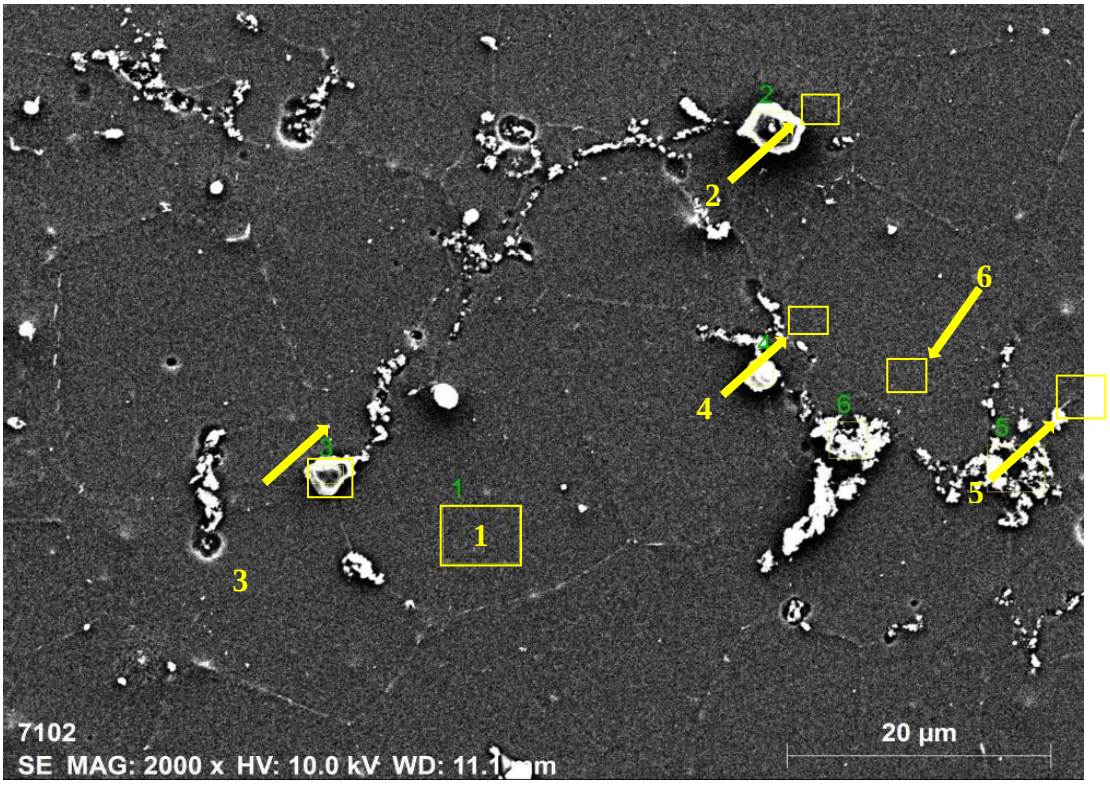

(a)

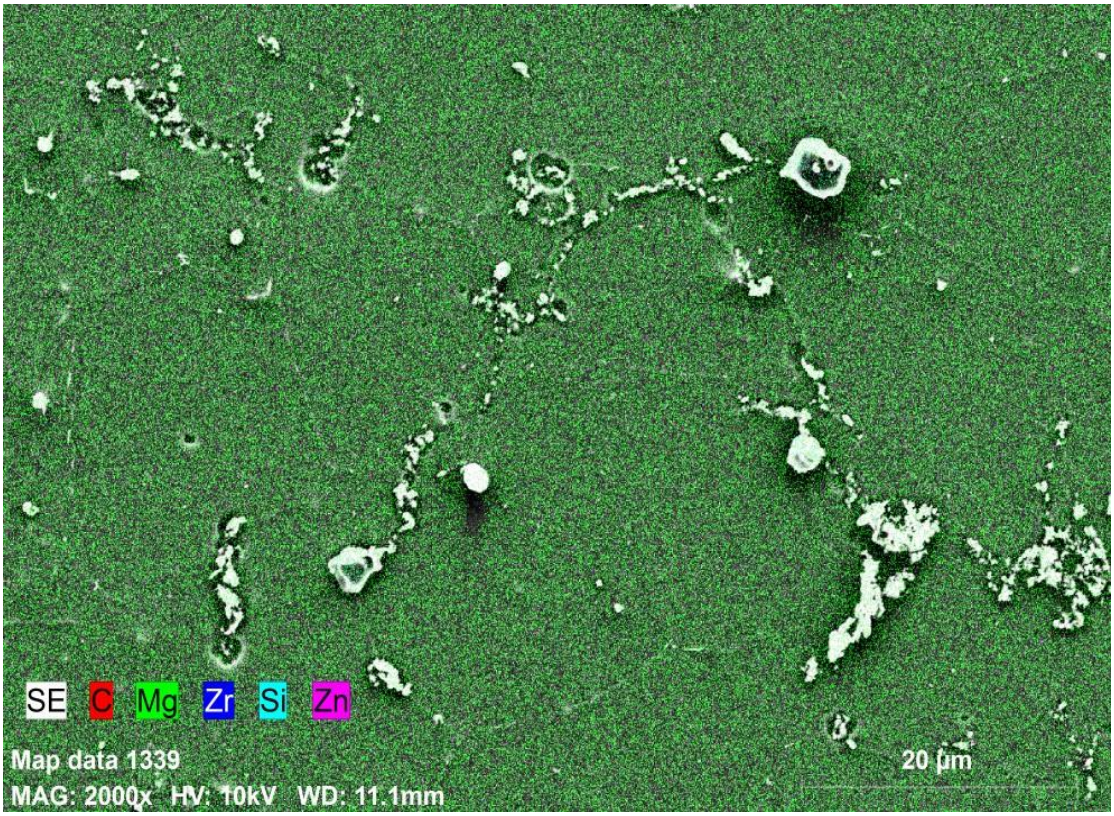

(b)

Figure 0.6. SEM microstructures of the extruded ZK60I sample; (a) the EDX analysis image at 2kX (indicating the 6 sites to be studied using EDX spectrum analysis); and (b) the elemental mapping of the EDX picture in Figure 6.6a.

Table 0.2. The spectrum analysis findings for the locations shown in Figure 6.6a for ZK60I are as follows:.

Aspects of	C	Mg	Si	Zn	Zr
1	4.46	87.15	0.00	8.40	0.00
2	13.22	47.16	36.19	2.18	1.25
3	7.23	57.79	32.97	1.75	0.27
4	11.90	55.60	29.59	2.89	0.02
5	8.58	83.64	0.09	7.43	0.25
6	12.27	80.20	0.43	7.10	0.00
Mean value	9.61	68.59	16.55	4.96	0.30
Sigma	3.42	17.03	18.06	3.00	0.48
Sigma mean	1.40	6.95	7.37	1.22	0.20

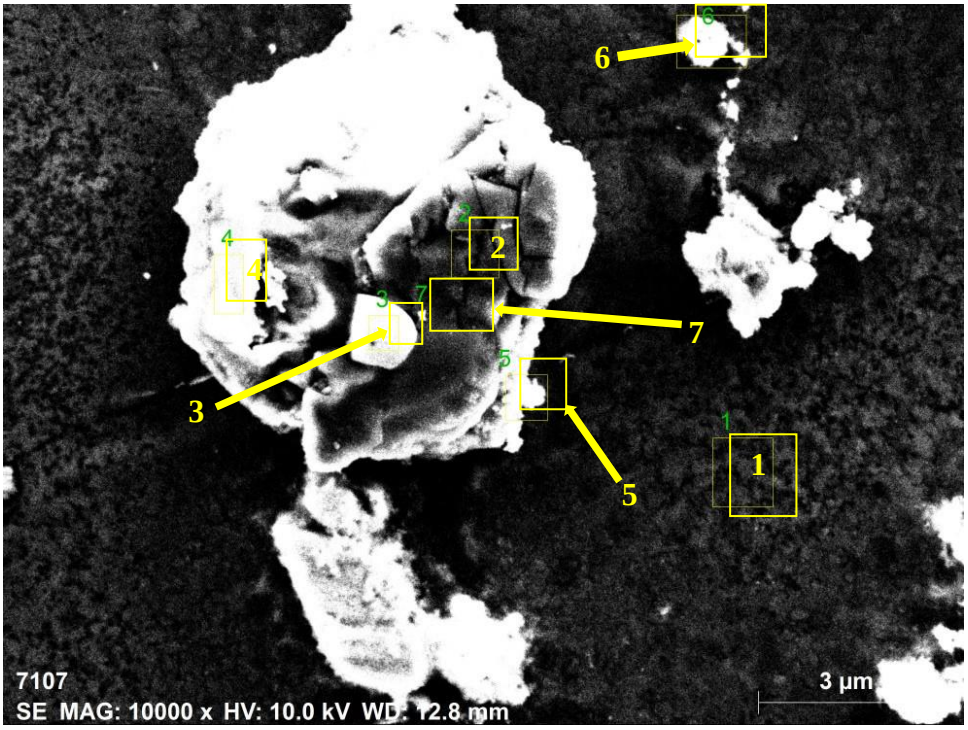

(a)

(b)

Figure 0.7. Shows ZK60 with ZK60I reinforcement SEM pictures. Part (a) shows sections indicated for EDX spectrum analysis in the 10,000X SEM picture, whereas part (b) shows the elemental mapping of Figure 6.7a's EDX image.

The findings of the energy-dispersive X-ray (EDX) spectrum analysis conducted on sections 1 through 7 of the ZK60 composite sample, which consists of 15% SiC and 0.5% AIN, are shown in Table 6.3. The slices may be recognized in the scanning electron microscope (SEM) picture shown in Figure 6.7a.

Table 0.3. Presents the results of the spectral analysis conducted on the different areas indicated in Figure 6.7a for the composite ZK60III.

Aspects of	C	N	Mg	Al	Si	Zn
1	6.53	1.81	82.86	1.06	0.19	7.55
2	3.13	31.35	1.52	62.65	0.08	1.27
3	11.63	20.18	0.94	60.78	6.21	0.27
4	28.82	3.19	7.18	5.66	53.86	1.28
5	2.92	0.00	83.89	11.70	0.00	1.49
6	15.14	2.68	71.06	2.65	1.44	7.04
7	2.75	36.72	0.79	58.82	0.13	0.79
Average	10.13	13.70	35.46	29.05	8.84	2.81
Sigma:	9.53	15.52	41.24	29.86	19.98	3.09
Sigma av:	3.60	5.86	15.59	11.29	7.55	1.17

According to the results of the elemental response spectrum analysis, which are shown in Table 6.3, there is a trace amount of magnesium zinc intermetallic present in area 1, which is the primary matrix material. The areas 2, 3, and 7 provide evidence that the SiC particle in area 4 is related to AlN nanoparticle reinforcements. This is proved by the existence of these reinforcements. The fifth section is a representation of the border that separates the main matrix, SiC particles, and AlN nanoparticles. Region 6 contains the basic matrix as well as a small number of SiC and AlN particles that have been finely separated.

6.4. MECHANICAL TEST RESULTS

6.4.1. Hardness Test Results

The outcomes of the Brinell hardness examination conducted on ZK60 specimens, involving casting, extrusion, and enhancement with SiC and AlN, are depicted in Figure 6.8. In contrast, the Brinell hardness test findings for as-cast ZK60 were 60.23, for ZK60 reinforced with ZK60I they were 73.33, for ZK60II the value was 78.29, and for ZK60III reinforcement, it measured 81.61 HB. After extrusion, the initial ZK60

displayed a hardness of 85.65 HB, which was increased to 96.86 HB by incorporating 15% SiC, to 101.23 HB with 0.2% AlN reinforcement, and to 103.94 HB with 0.5% AlN reinforcement. The mechanical qualities and hardness values of the specimens were also enhanced by the fine-grained structure resulting from substantial deformation during the extrusion process. Moreover, the augmentation in hardness was directly proportional to the added reinforcing content. The hardness elevation is attributed to the introduction of harder particles into the matrix, effective segregation of AIN particles at grain boundaries [227], Additionally, the homogeneous dispersion of reinforcing particles attributed to the deformation process caused by extrusion [139].

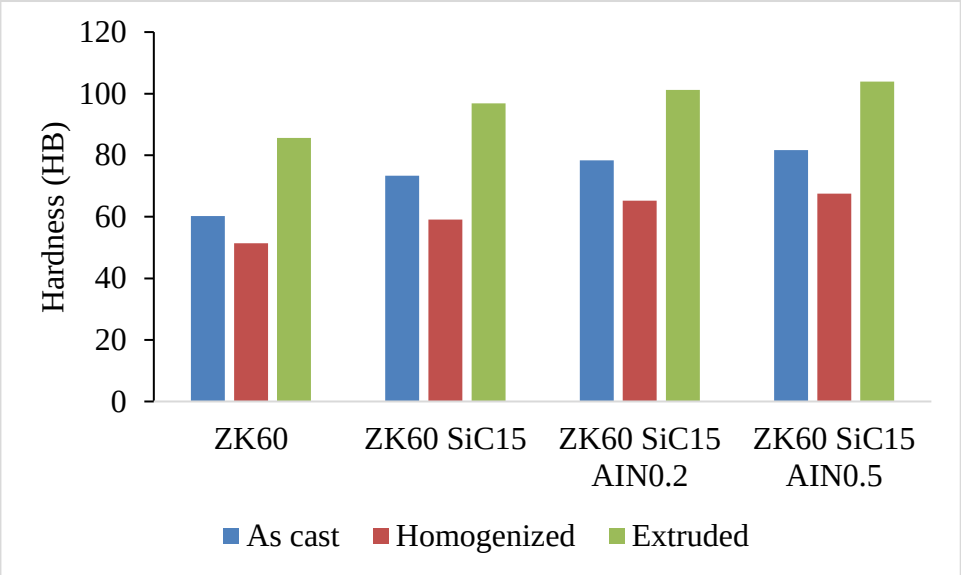

Figure 6.8. Contrasting the hardness test outcomes among the as-cast, homogenized, and extruded samples.

6.4.2. Compressor Test

Compression experiments for the materials ZK60, ZK60I, ZK60II, and ZK60III were carried out to examine the impact of reinforcements on the mechanical behaviours of the sample. Figure 6.9 displays the results of the stress-strain test. Figure 6.9 illustrates the compression test outcomes for both the unenhanced ZK60 and the reinforced composites, presenting the highest fracture stresses. The unreinforced ZK60's compression test result was 340 MPa; with SiC15 reinforcement, it increased

to 355 MPa; and ZK60I reinforcement, it increased to 370 MPa. Finally, it increased to 410 MPa for ZK60III.

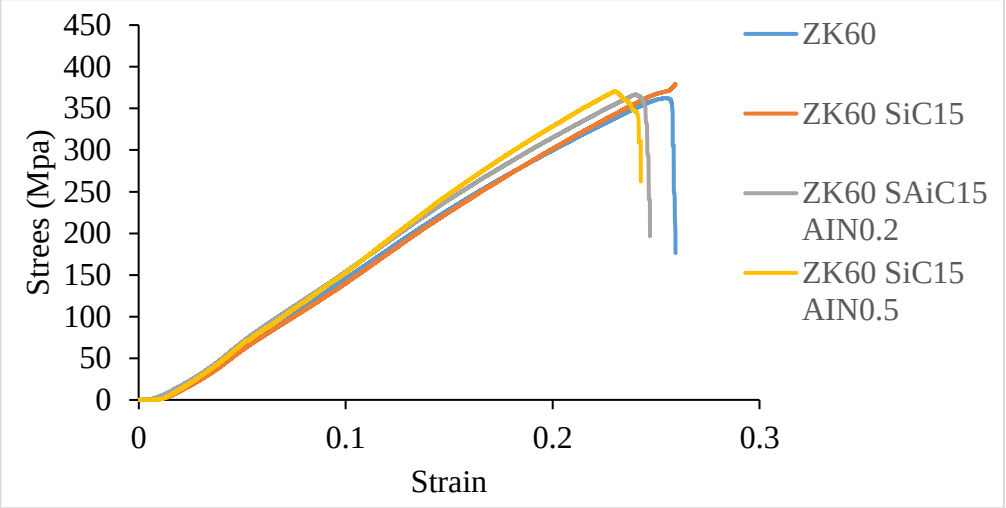

Figure 6.9. The results from the compression test conducted on the unenhanced ZK60, ZK60I, ZK60II, and ZK60III.

There has been an increase in the compression strength with the addition of reinforcements to ZK60, as shown by the compression results in Figure 6.10. When compared to ZK60 that hasn't been reinforced, the ZK60III reinforcement increases compressive strength by 20.5%. Because the reinforcement particles are more equally distributed throughout the primary matrix and have a more durable structure, the addition of the particles increases the strength. Additionally, the strength may be increased by increasing the dislocation density of the particles introduced to the microstructure. Furthermore, nanoscale reinforcements have a high dislocation density and stop dislocations from moving during deformation under stress [228].

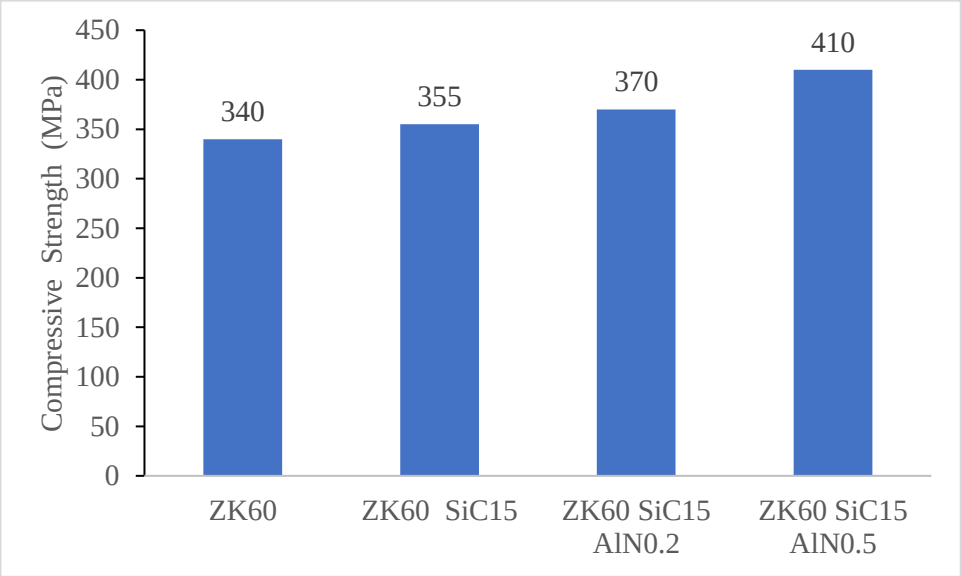

Figure 6.10. The comparisons of the maximum compressive strengths.

6.5. CORROSION TEST RESULTS

Corrosion tests of the produced composites were carried out in 3.5% NaCl solution in two diverse ways, potentiodynamic polarization and immersion corrosion test.

6.5.1. Immersion Test Results

The loss of weight during immersion of the hybrid composites made from ZK60, ZK60I, ZK60II, and ZK60III is shown in Figure 6.11 with regard to exposure periods. As shown in Figure 6.11, the immersion weight loss of the materials under investigation rase for up to 12 hours before stabilizing at the conclusion of the 72-hour exposure period. The post-extrusion samples' weight loss test findings for the ZK60, ZK60I, ZK60II, and ZK60III, respectively, are 7914.28, 7023.16, 5632.68, and 5332.03 mg/dm^2. Figure 6.12 displays the samples' daily corrosion rates (mg/dm^2 day). As can be seen, the corrosion rate first rose before falling as the exposure period went on. After two days, the graph's line started to stabilize. The corrosion rate of the composites following a three-day period is depicted in Figure 6.13. When considering corrosion rates, the initial corrosion rate of the unreinforced ZK60 at 2638.1 mg/dm² day The rate of decrease was observed to be 2341.1 mg/dm² day when 15% SiC was incorporated, and it further decreased to 1877.56 mg/dm² day when 0.2% AlN was

added. Lastly, the rate reached 1777.4 mg/dm² day when 0.5% AlN was introduced. Furthermore, Figure 15 illustrates the projected annual corrosion rates. These rates are determined by utilizing the densities of the samples ZK60, ZK60I, ZK60II, and ZK60III, and are as follows: 2090.73, 1848.19, 1479.84, and 1397.79 (mg/year), respectively.

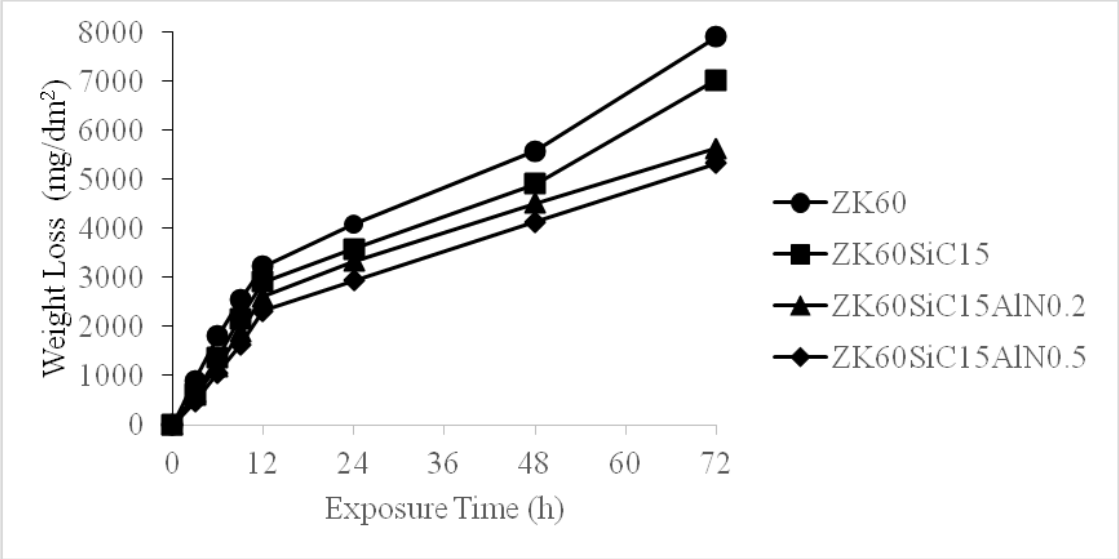

Figure 6.11. Displays the weight reductions (in mg/dm²) of the specimens during the initial 72-hour period.

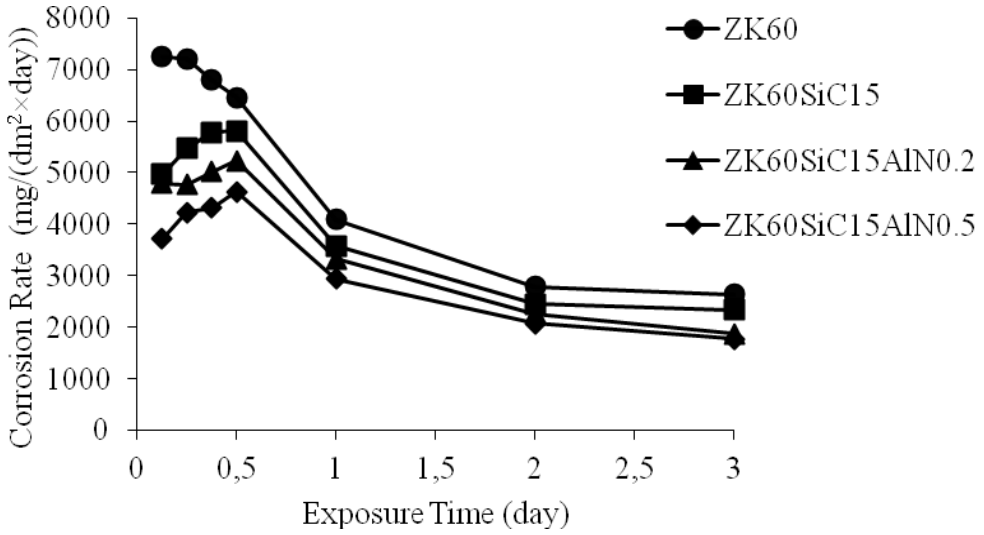

Figure 6.12. Depicts the rates of corrosion (measured in mg/dm²day) for the samples over the course of each day.

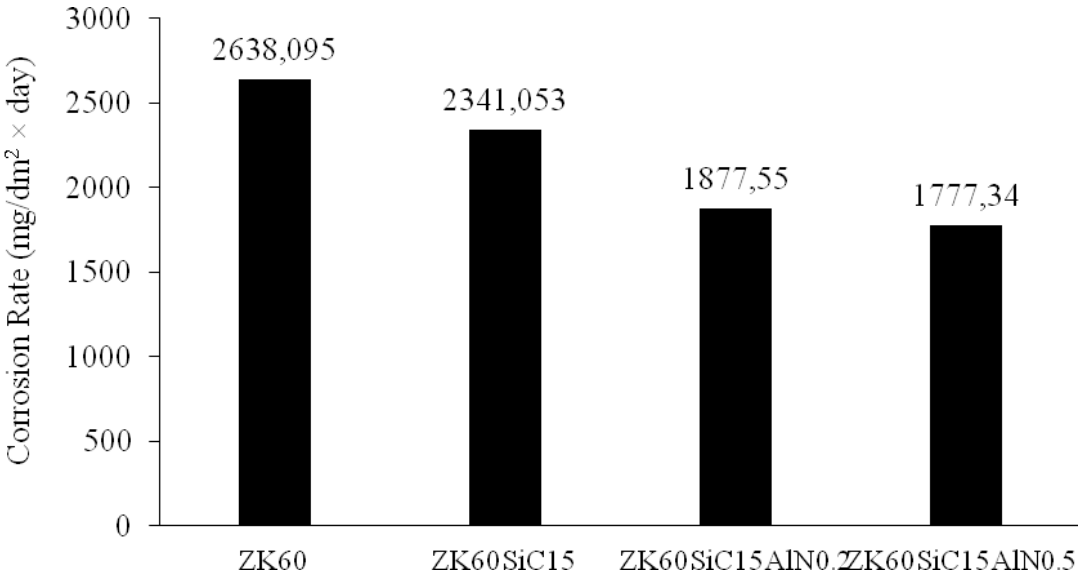

Figure 6.13. Illustrates the corrosion rates of the samples after a three-day duration.

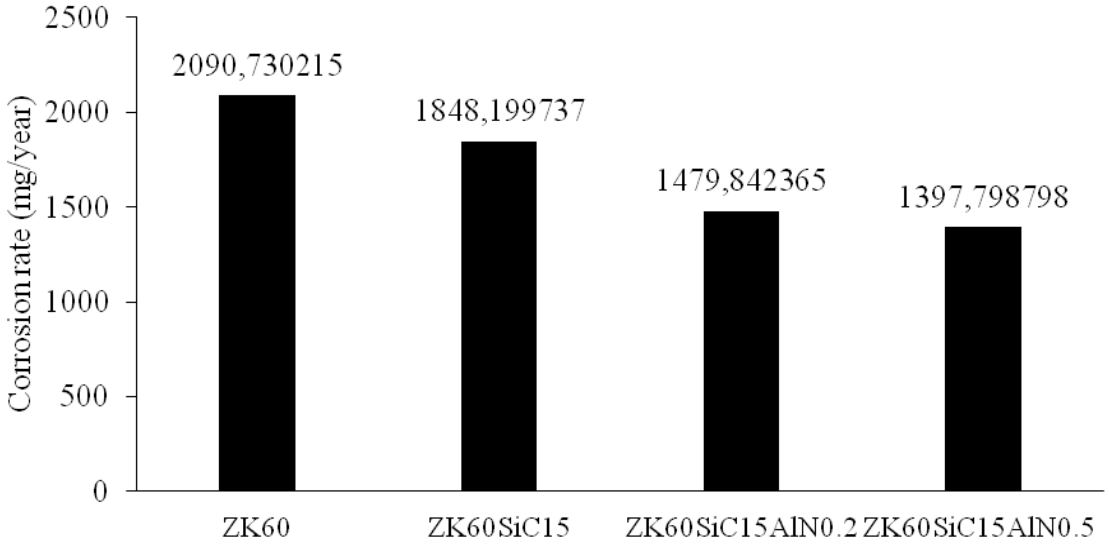

Figure 6.14. Demonstrates the corrosion rates (measured in mg/year) over successive years, estimated using the density values of the respective samples.

Analyzing the graphical representations in the figures, it is evident that the weight loss rises when the samples are submerged for longer periods of time. In Figure 6.13, corrosion started out slowly and then picked up speed between 6 and 12 hours after immersion. In other words, The rate of corrosion is delayed as the oxide layer that has formed on the surfaces of the samples stabilizes. The pictures demonstrate how adding reinforcements to the ZK60 alloy increases its corrosion resistance. The sample with the highest level of corrosion resistance contained ZK60III. After 72 hours, the weight

loss of ZK60I decreased from 7914.28 mg/dm^2 to 7023.16 mg/dm^2, as shown in Figure 6.11. The weight loss in hybrid composites decreased from 5632.68 mg/dm^2 in the 0.2% AlN-reinforced sample to 5332.03 mg/dm2 when the nanoparticle concentration was increased to 0.5%. After a duration of three days, the corrosion rate of the sample supplemented with 15% SiC and 0.5% AlN exhibited a reduction of 1.48 in comparison to the unreinforced ZK60 alloy.

Figures 6.15 and 6.16 display the SEM images of the surfaces of the corroded samples. Figure 6.15b shows the general elemental spectrum response graph of the corroded ZK60, and Figure 6.15a shows the SEM pictures of the corroded ZK60 at 5kX.

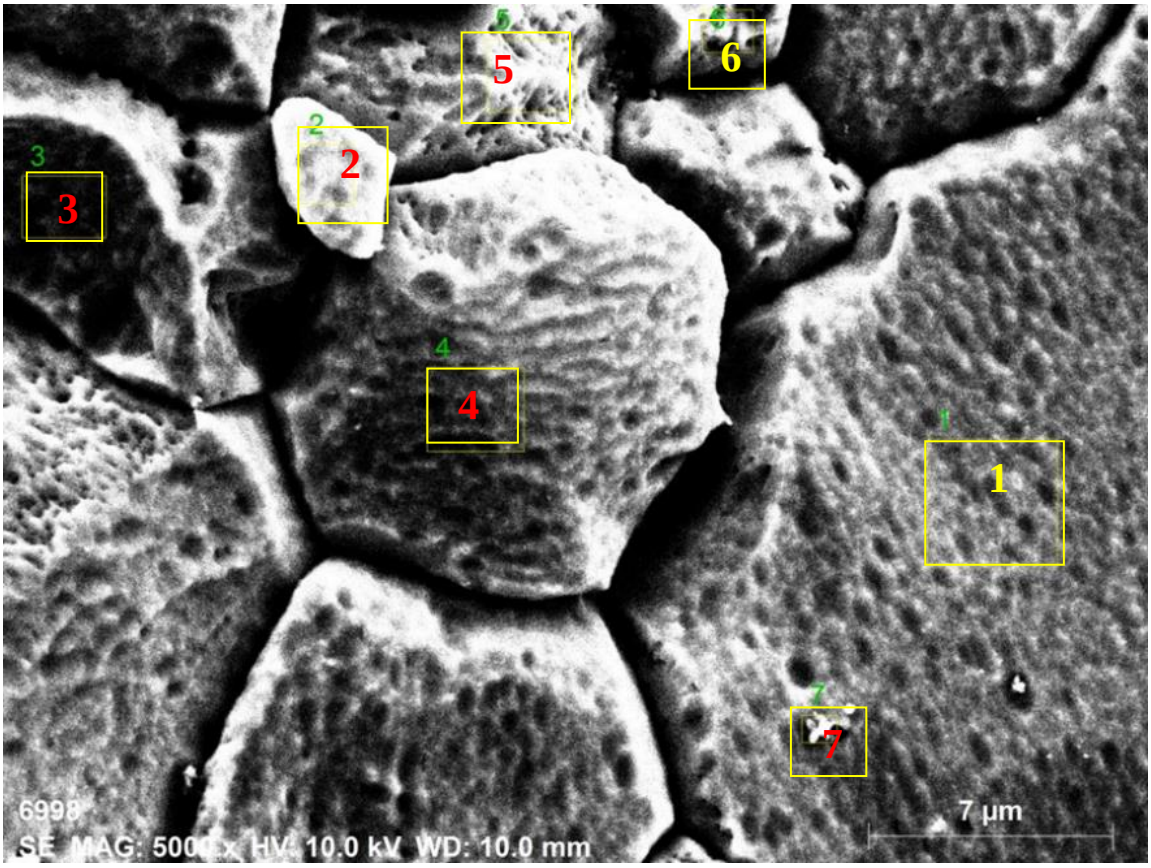

(a)

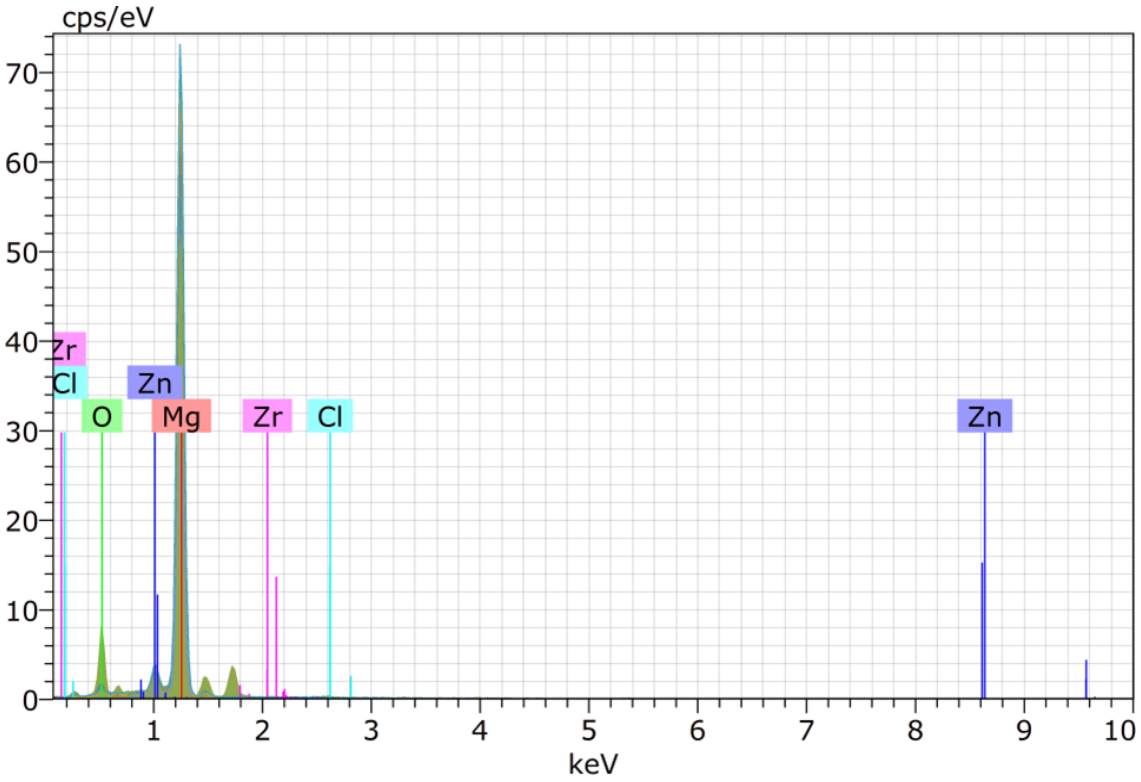

(b)

Figure 0.15. Showcases: a) Visual representations of the corroded surface of ZK60 at 5 KX magnification, and b) the graphical presentation of the elemental spectrum response for ZK60.

Table 6.4. Presents comprehensive energy-dispersive X-ray (EDX) analyses corresponding to the image depicted in Figure 6.15a.

Aspects of	O	Mg	Cl	Zn	Zr
1	2.33	89.67	0.01	7.81	0.17
2	2.76	89.05	0.10	8.01	0.09
3	0.35	92.44	0.03	7.07	0.10
4	2.01	89.95	0.06	7.99	0.00
5	3.86	87.98	0.06	8.01	0.10
6	2.71	88.99	0.09	8.06	0.15
7	18.92	72.20	0.50	8.38	0.00
Average	4.71	87.17	0.11	7.91	0.08
Sigma	6.35	6.76	0.16	0.41	0.06
Sigma value	2.41	2.56	0.05	0.16	0.02

Figure 6.16a displays a magnified view (1 KX) of the corroded surface of the ZK60III composite, while Figure 6.16b exhibits the overall graphical representation of the elemental spectrum response for the identical composite.

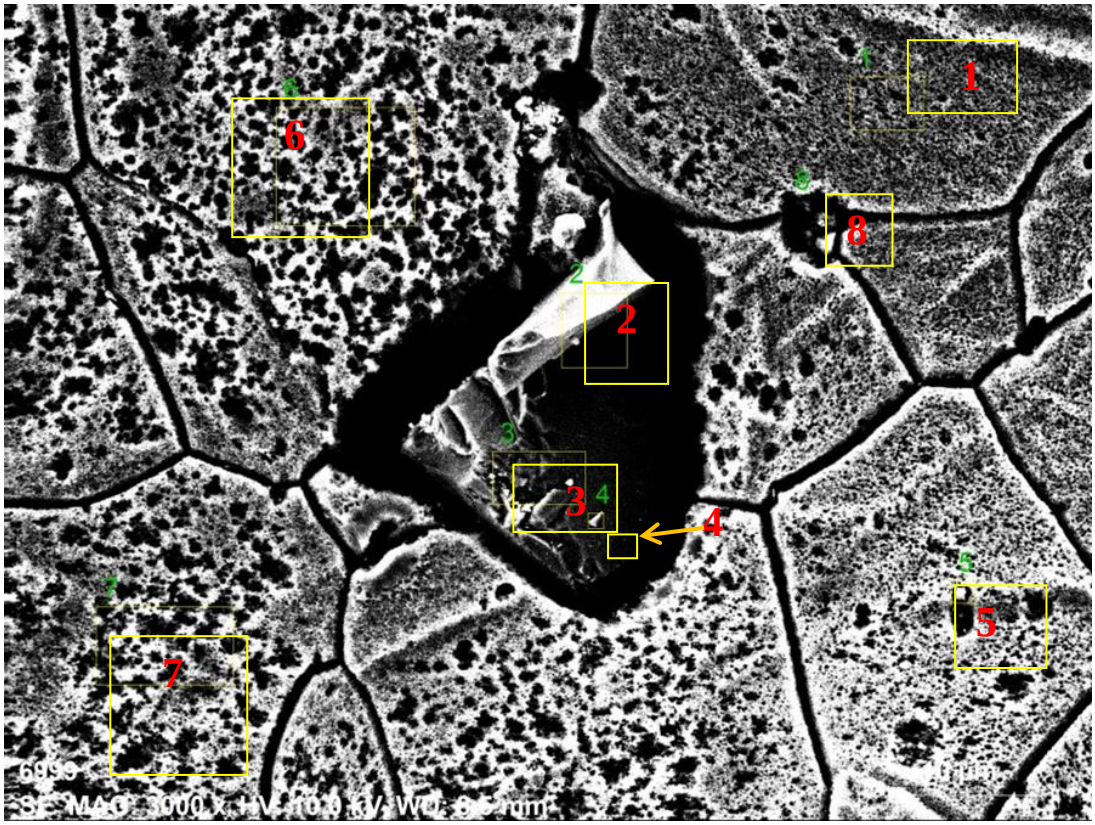

(a)

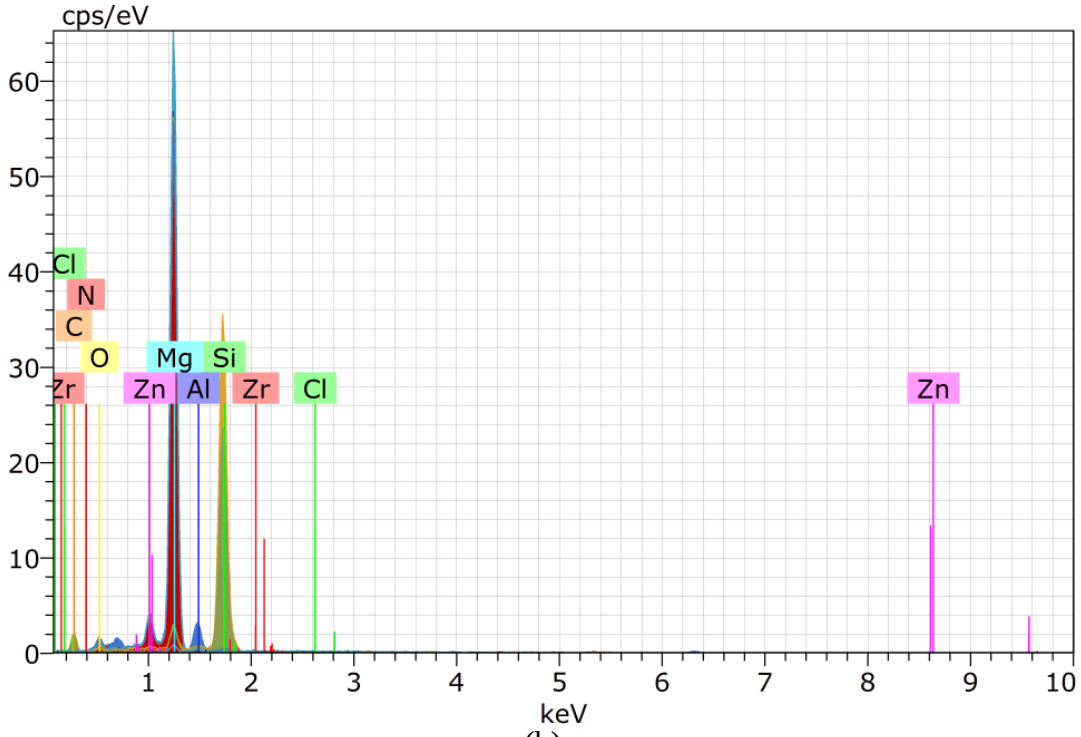

(b)

Figure 6.16. Demonstrates: a) At a 5 KX magnification, visual representations of the corroded surface of ZK60III; and b) A graphical depiction of the elemental spectrum response specific to ZK60III.

Table 0.5. Provides comprehensive energy-dispersive X-ray (EDX) analyses corresponding to the visual content displayed in Figure 6.16a.

Aspects of	C	N	O	Mg	Al	Si	Cl	Zn	Zr
1	2.14	0.95	2.33	85.04	0.48	0.00	0.00	8.93	0.12
2	27.18	1.55	2.20	4.15	0.98	63.39	0.01	0.52	0.02
3	1.64	0.00	0.54	1.48	0.75	94.88	0.00	0.42	0.30
4	22.45	1.27	2.56	3.17	0.61	69.27	0.00	0.68	0.00
5	2.90	1.12	3.67	76.37	6.61	0.51	0.00	8.75	0.08
6	1.81	0.90	3.13	84.08	0.16	0.31	0.06	9.57	0.00
7	2.17	1.06	4.31	82.23	0.29	0.22	0.00	9.59	0.15
8	2.39	0.94	3.68	82.73	0.40	0.05	0.00	9.69	0.13
Average	7.82	0.96	2.82	52.40	1.27	28.57	0.02	6.01	0.11
Sigma	10.55	0.44	1.18	41.06	2.18	40.16	0.03	4.54	0.11
Sigma value	3.74	0.15	0.41	14.50	0.76	14.21	0.02	1.62	0.03

The initiation of corrosion, as observed in Figure 6.15, was predominantly attributed to galvanic cells formed between the $MgZn_2$ phase and the Mg grains. This led to the formation of voids at the grain boundaries. Upon the removal of ZK60 alloy grains from the matrix, the corrosion process proceeds further. The disintegration of the intermetallics at the grain boundary in back of the detached grains can be accelerated by corrosive ions. As shown in Figure 6.16, the ZK60III hybrid composite exhibits improved corrosion resistance due to the significantly more refined and uniform MgZn2 intermetallics and larger grain boundaries, which function as corrosion barriers due to the reduced ratio of anode to cathode area. There is a belief that the incorporation of SiC+AlN to the investigated composite reduced the grain boundary corrosion. Corrosion resistance is increased when a surface film rich in Si+O components forms on the corroded surface, as seen in Figure 6.16 and Table 6.5. SiC and AlN were added, and Mg2Si, SiC, and AlN peaks were produced as a result. Mg2Si intermetallics more efficiently limit corrosion due to their polygonal shape [229,230].

6.5.2. Potentiodynamic Polarization Test Results

Figures 6.17 and 6.18 illustrate the outcomes of potentiodynamic polarization experiments conducted on the composites. The measurements of corrosion potential (Ecorr) and corrosion current density (Icorr) are plotted on a graph to facilitate the application of the Tafel extrapolation method for analysis. The corrosion potential

readings are shown in Volts and the corrosion current density is shown in A/dm^2 . The extruded samples' potentiodynamic characteristics are evaluated both parallel to and perpndicular to the extrusion direction. In comparison to measurement conducted from a parallel section, Measurements done from a segment perpendicular to the direction of extrusion provide more precise findings. Results acquired from the region orthogonal to the direction of extrusion surpassed those gathered from the parallel segment in terms of performance. In general, a high rate of corrosion is indicated by elevated icorr measurements and reduced Ecorr values (more negative). The composites consist of ZK60III. shown greater corrosion resistance when the composites are compared. The corrosion resistances of all composite materials are compared using values for corrosion current density (icorr), and the findings are as follows: ZK60III is superior to ZK60II and ZK60I. The corrosion current density (I_{corr}) values for ZK60, ZK60I, ZK60II, and ZK60III are 245 $\mu A/cm^2$, 151 $\mu A/cm^2$, 136 $\mu A/cm^2$, and 53.70 $\mu A/cm^2$, respectively, As per the corrosion test results acquired from the section perpendicular to the extrusion direction. ZK60 has a corrosion potential of 1.370 volts, ZK60I of 1.410 volts, ZK60II of 1.390 volts, and ZK60III of 1.140 volts. According to the findings of the corrosion tests performed on the segment aligned with the extrusion direction, the density of corrosion current (I_{corr}) values for ZK60, ZK60I , 200 A/cm2, and 152 A/cm2 for ZK60III are 377 $\mu A/cm^2$, 242 $\mu A/cm^2$, 200 $\mu A/cm^2$, and 152 $\mu A/cm^2$ respectively. ZK60, ZK60I, ZK60II, and ZK60III have respective corrosion potentials of -1.420 V, -1.480 V, 1.410 V, and -1.360 V. I_{corr} and E_{corr} values in ZK60 alloy have a tendency to diminish, when SiC and AlN reinforcements are added. Silicon dioxide (SiO_2), which is produced atop the material's surfaceas a result of the addition of SiC, offers protection against corrosion.

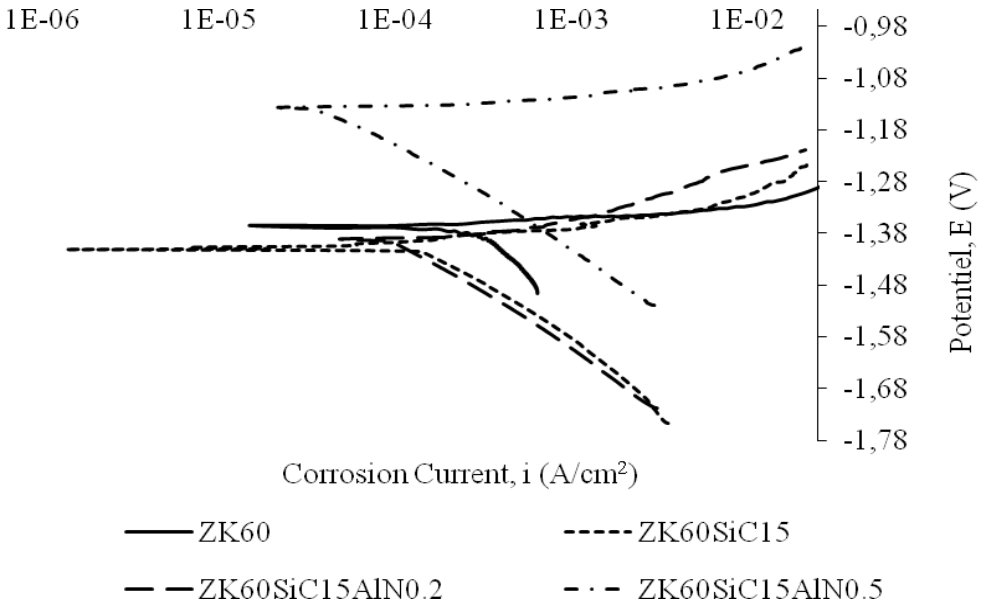

a)

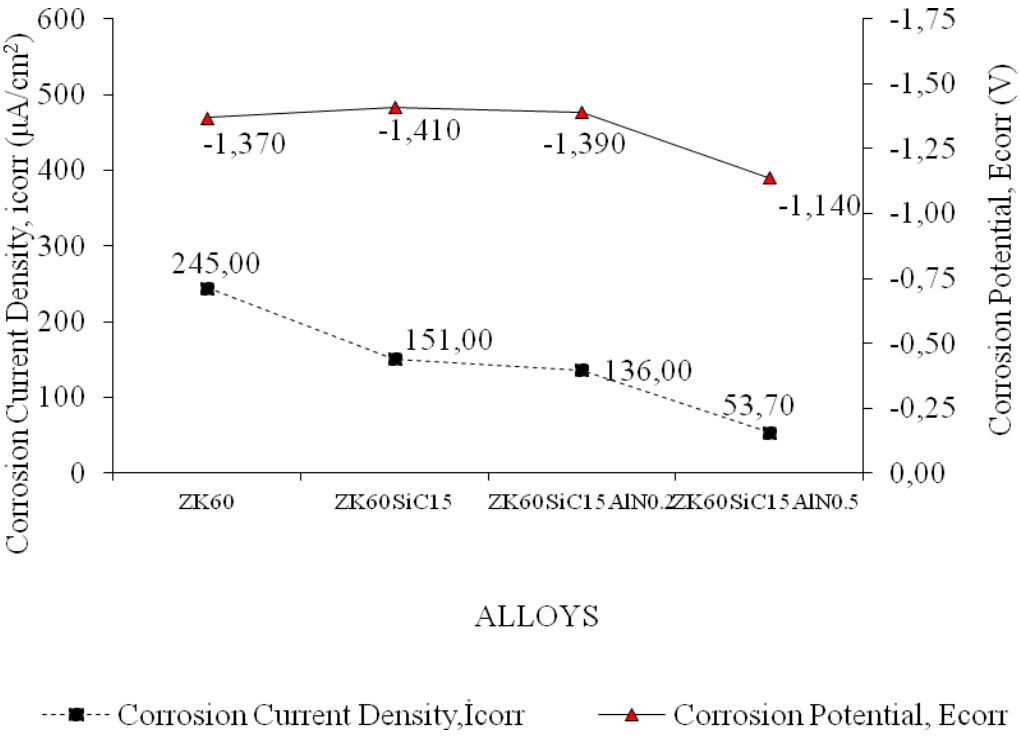

b)

Figure 6.17. Presents the outcomes of corrosion tests obtained from the cross-sectional analysis of the specimens perpendicular to the extrusion direction. This is depicted in: a) the potentiodynamic polarization graph, and b) the values of i_{corr} (corrosion current) and E_{corr} (corrosion potential).

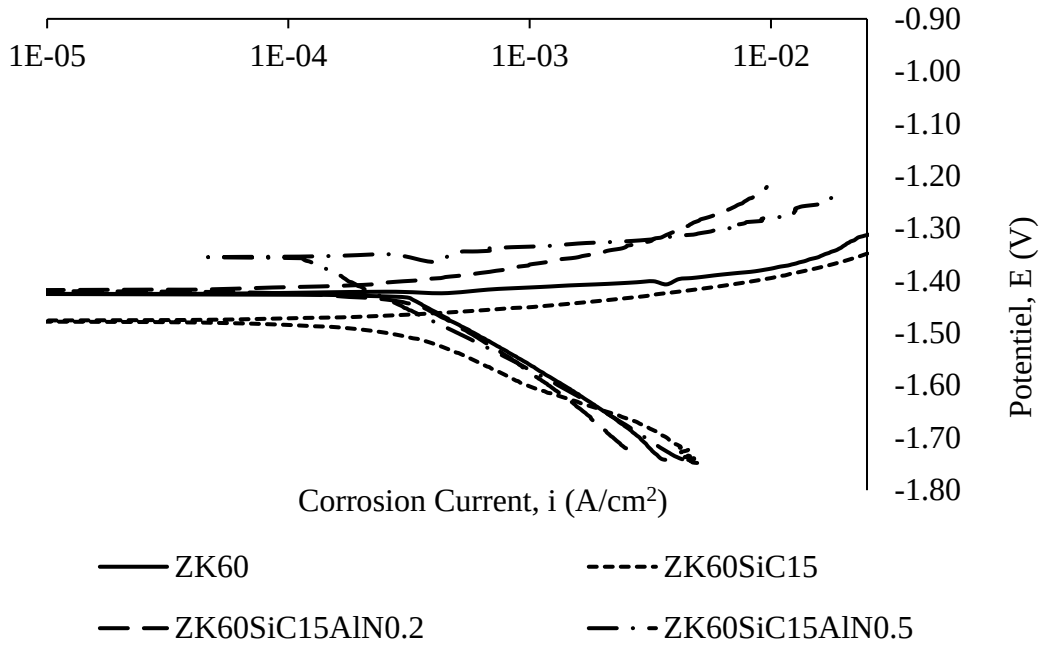

a)

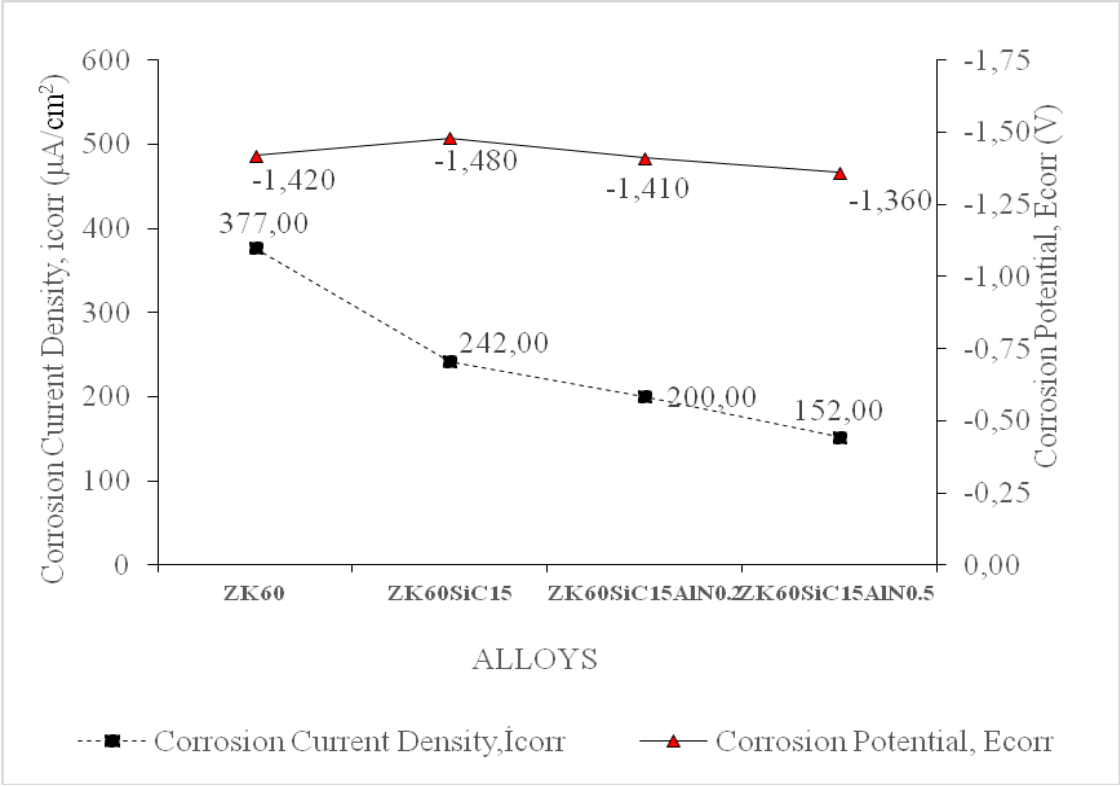

b)

Figure 6.18. showcases the results obtained from corrosion tests performed on the segment aligned parallel to the direction of sample extrusion. This is demonstrated by: a) the potentiodynamic polarization graph, and b) the values of i_{corr} (corrosion current) and E_{corr} (corrosion potential).

6.6. WEAR TEST RESULTS

Figure 6.19 displays the weight loss of the samples as a function of sliding distance after a reciprocating wear test was conducted on the extruded materials under a 20 N load, at a speed of 0.1 mm/s, and over 1000 m. Volume losses per meter are used to determine wear rates. The weight loss of the ZK60 is 0.0359 gram after the 1000m sliding test. A weight drop of 0.03287 gram is experienced by the ZK60I reinforced composite, 0.03203 gram is experienced by the ZK60III reinforced composite, and 0.0301 gram is experienced by the ZK60III reinforced composite. In comparison to the quantity of addition, the wear resistance has thereby improved due to the reinforcing parts.

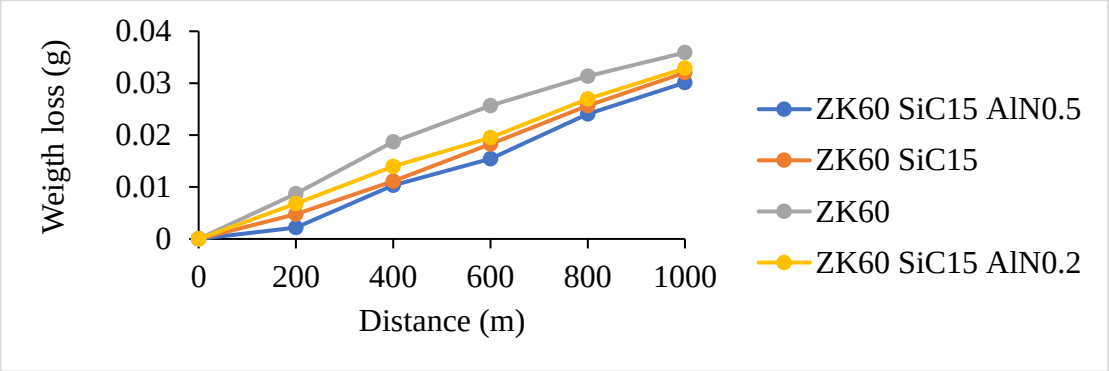

Figure 6.19. illustrates the outcomes of the dry wear test conducted on both the unreinforced ZK60 and the reinforced composite materials.

The wear rates (g/m) depicted in Figure 6.20 are derived from Figure 6.19. Specifically, under a 20 N load, the wear rates for ZK60, ZK60I, ZK60II, and ZK60III were 4e-5, 3.5e-5, 2.8e-5, and 2.5e-5 g/m respectively.

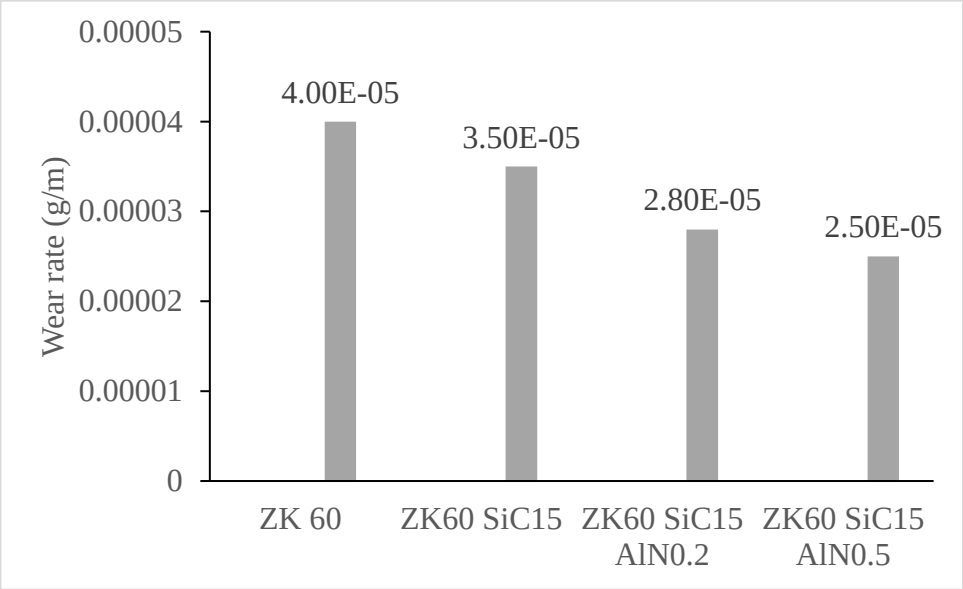

Figure 0.20. displays the computed wear rates of all composite materials (g/m).

Figure 6.21 presents the comparisons of how the friction coefficient varies with sliding distance. The average friction coefficients for the samples, including ZK60 alloy, ZK60I, ZK60II, and ZK60III composites, are 0.1268, 0.1262, 0.0994, and 0.0684, respectively.

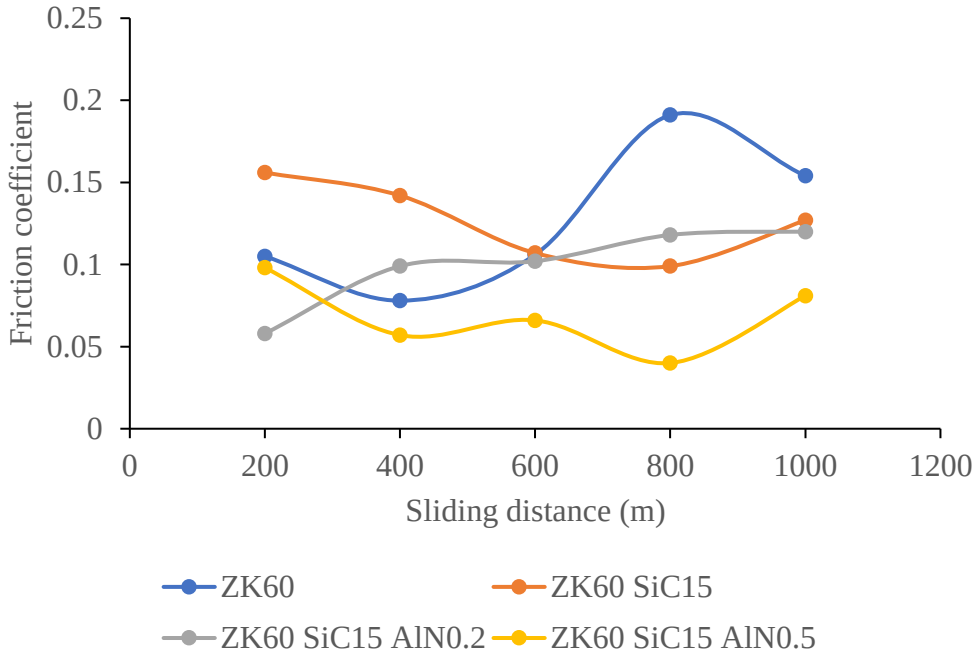

Figure 6.21. illustrates the variations in the friction coefficient concerning the sliding distance across all samples.

Figures 6.22 and 6.23 depict the scanning electron microscope (SEM) images illustrating the surfaces of the utilized samples. The SEM photos of the extruded ZK60 alloy at 1kX the illustration is presented in the figure 6.22a, and Figure 6.22b shows the overall elemental spectrum response graph of the ZK60 without reinforcement. The adhesive and abrasive wear processes are identified on the SEM images in Figure 6.22a , they are denoted by the letters A and B, respectively. The counter surface and other alloying components listed in Table 6.6 are richer in Mg, Zn, and a trace amount of Fe and Cr elements, which are added to the adhesion wear mechanism (A).

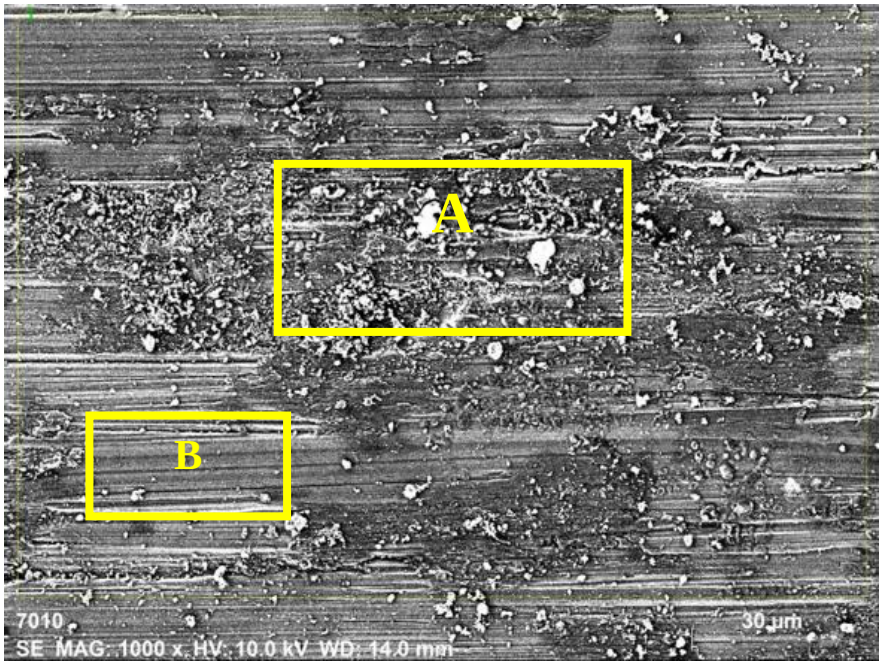

(a)

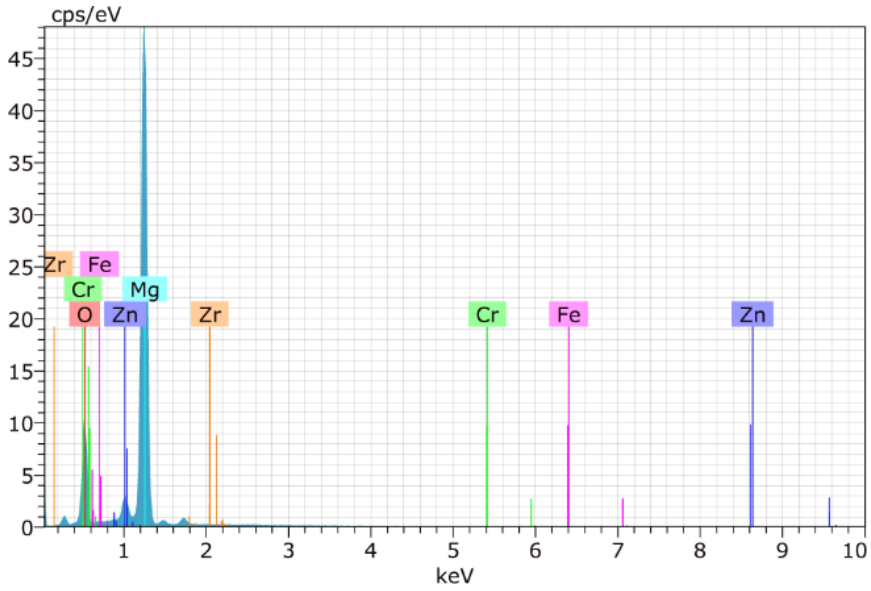

(b)

Figure 6.22. Worn ZK60 exhibit surfaces : (a) SEM image at 1 kX; (b) The graph displaying the elemental spectrum response of the ZK60.

Table 0.6. General EDX analyses of the image shown in Figure 6.22a.

The Parts	Compound with Atoms[%]
O	32.54
Mg	64.72
Cr	0.03
Fe	0.02
Zn	2.65
Zr	0.04
Total	100.00

Figure 6.23a shows a SEM image at 1kX of a surface that has been worn down for ZK60 SiC15 AIN0.5. As illustrated in Figure 6.23a, the adhesive, abrasive, and wear mechanism sections are labeled A and B, respectively. The adhesion wear mechanism layer (A) is enriched in Al element and a trace quantity of Fe and Cr elements from the counter surface, according to the elemental EDX map picture (Figure 6.23b). Other alloying elements are listed in Table 6.7. Figure 6.22a's SEM pictures of the ZK60 alloy and the reinforced composite of ZK60III show that the latter exhibits degreased adhesive wear.

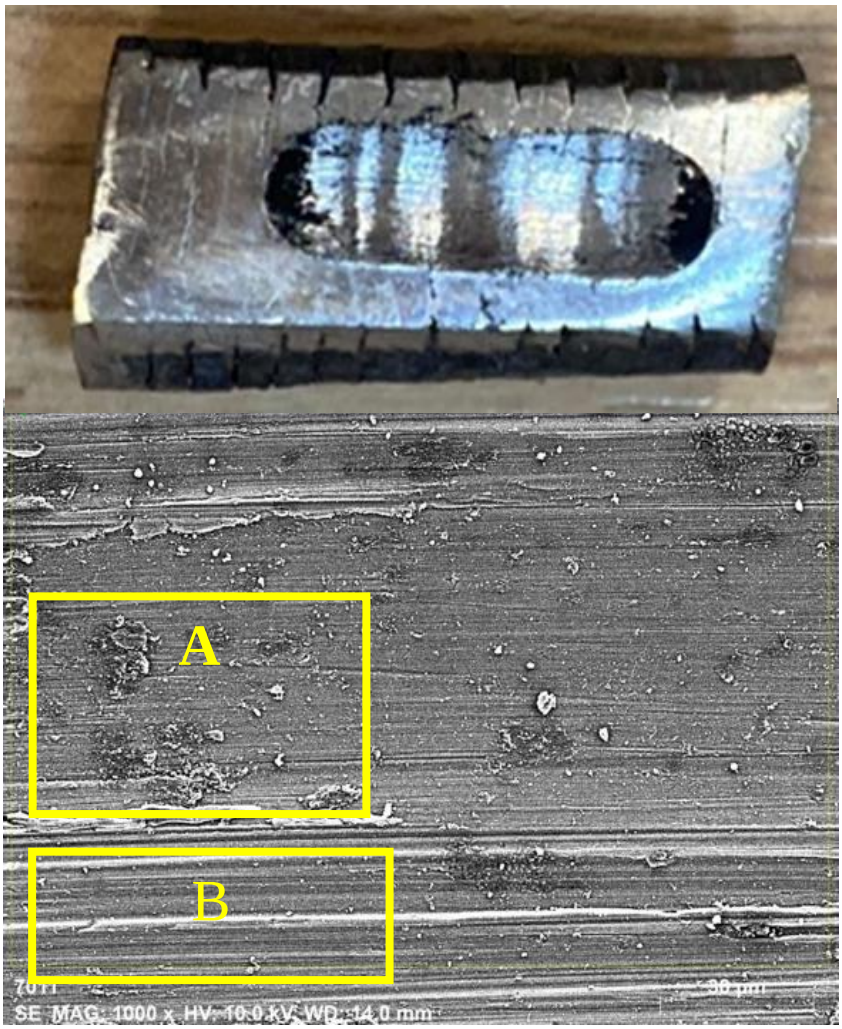

(a)

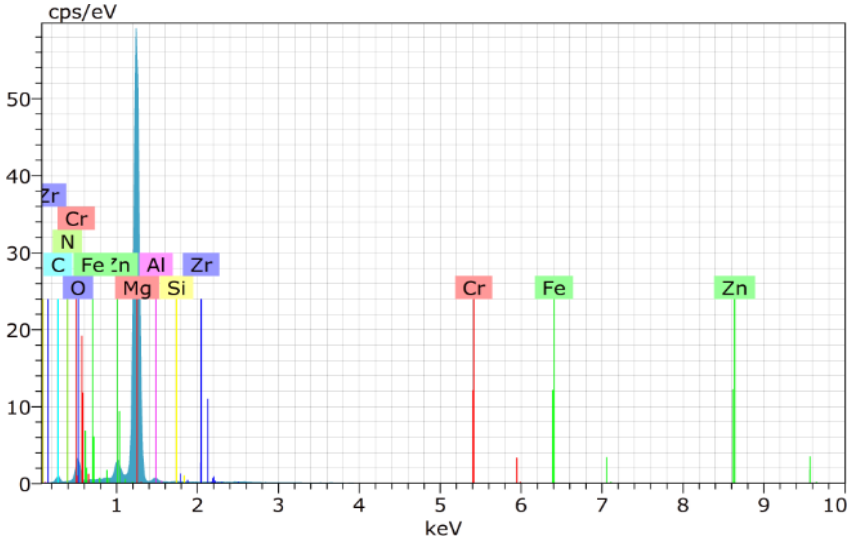

(b)

Figure 6.23. Worn ZK60III exhibit surfaces : (a) SEM image at 1 kX; (b) The graph displaying the elemental spectrum response of the ZK60III.

Table 0.7. General EDX analyses of the image shown in Figure 6.23a.

The parts	Compound with Atoms[%]
C	12.11
N	1.84
O	10.90
Mg	71.68
Al	0.86
Si	0.09
Cr	0.04
Fe	0.07
Zn	2.38
Zr	0.01
Total	100.00

PART 7

GENERAL CONCLUSIONS AND RECOMMENDATIONS

After conducting an analysis of the microstructure and the study of corrosion characteristics of numerous new hybrid composites formed by incorporating 15% SiC and varying proportions of 0.2% to 0.5% AlN into ZK60 magnesium alloy, the subsequent findings have been established.

- The coarse primary -Mg dendritic grains and distinct intermetallic phases that resemble spheres make up the ZK60 alloy's casting microstructure. The images clearly display the uniform distribution of the black particles, which are commonly found in microstructures and are thought to represent SiC. Mg2Si and SiC phases were produced with the addition of SiC, according to the findings of the XRD investigation. AlN was added, and as a result, peaks of both MgSi and AlN were produced.
- • The as-cast microstructure of ZK60 alloy is mostly coarse-Mg. ZK60, ZK60I, ZK60II, and ZK60III samples had average grain sizes of 65 µm, 60 µm, 62 µm, and 48 µm. Extruded ZK60, ZK60I, ZK60II, and ZK60III samples have average grain sizes of 32 µm, 28 µm, 25 µm, and 23 µm.
- The hardness test results for the as-cast unreinforced ZK60, ZK60I, ZK60II, and ZK60III are 60.23, 73.33, 78.29, and 81.61 HB, respectively. The hardness values of ZK60, ZK60I, ZK60II, and ZK60III were measured as 85.65, 96.86, 101.23, and 103.94, respectively, after the extrusion process.
- The unreinforced ZK60's compression test result was 340 MPa; with ZK60I reinforcement, it increased to 355 MPa; and ZK60II reinforcement, it increased to 370 MPa. Finally, it increased to 410 MPa for ZK60III.
- The corrosion rates from the immersion test showed a decrease in corrosion rate of 1.13, 1.41, and 1.49, respectively, for the samples containing ZK60I, ZK60II reinforced , and ZK60III.This was related to the creation of surface coatings wit h a high Si-O content.

- • The potentiodynamic polarization test findings showed that measurements done perpendicular to the extrusion direction demonstrated better performance than those taken parallel to the extrusion direction. The corrosion resistances of the composites are assessed by comparing their corrosion current density (icorr) values. The ranking of corrosion resistances is as follows: ZK60III> ZK60II > ZK60I > ZK60.
- The ZK60, ZK60I, ZK60II, and ZK60III have respective wear test values of 4e-5, 3.5e-5, 2.8e-5, and 2.5e-5 gram/m. The samples' average friction coefficients for ZK60, ZK60I, ZK60II, and ZK60III, respectively, are 0.1268, 0.1262, 0.0994, and 0.0684.

  In recent years, the utilization of magnesium alloys with high specific strength has increased due to the need for weight gain, which has emerged with the increasing developments in the automotive and aerospace industry. For this reason, composite technology will soon see an increase in interest in this topic. By using these ceramic micro and nanoparticles, it will be able to increase the utilization of magnesium and its alloys in industries such as automotive, aerospace and electrical products. In this study, the focus is on evaluating both the mechanical and corrosion properties of the ZK60 alloy. which is a common extrusion alloy, were investigated with different alloying and shaping processes, and significant improvements were obtained in mechanical properties, while a decrease in corrosion resistance occurred. In this study, It is thought that the amount of nano reinforcement should be 0.5% for best results. The desired amount of hardness increase could not be achieved with the addition of 15% SiC. For this reason, it is recommended to evaluate the results by adding higher rates of SiC.

REFERENCES

[1] Atrens A, Shi Z, Mehreen SU, Johnston S, Song GL, Chen X, et al. Review of Mg alloy corrosion rates. J Magnes Alloy 2020;8:989–98. https://doi.org/10.1016/j.jma.2020.08.002.

[2] Li Y, Lu X, Wu K, Yang L, Zhang T, Wang F. Exploration the inhibition mechanism of sodium dodecyl sulfate on Mg alloy. Corros Sci 2020;168:108559. https://doi.org/10.1016/j.corsci.2020.108559.

[3] Fakhar N, Sabbaghian M. A good combination of ductility, strength, and corrosion resistance of fine-grained ZK60 magnesium alloy produced by repeated upsetting process for biodegradable applications. J Alloys Compd 2021;862:158334. https://doi.org/10.1016/j.jallcom.2020.158334.

[4] Xiong Y, Yu Y, Hu X. Fatigue behavior of modified ZK60 magnesium alloy after pre-corrosion under stress-controlled loading. Eng Fract Mech 2022;260. https://doi.org/10.1016/j.engfracmech.2021.108187.

[5] Wei X, Liu P, Ma S, Li Z, Peng X, Deng R, et al. Improvement on corrosion resistance and biocompability of ZK60 magnesium alloy by carboxyl ion implantation. Corros Sci 2020;173:108729. https://doi.org/10.1016/j.corsci.2020.108729.

[6] Wei X, Ma J, Ma S, Liu P, Qing H, Zhao Q. Enhanced anti-corrosion and biocompatibility of a functionalized layer formed on ZK60 Mg alloy via hydroxyl (OH-) ion implantation. Colloids Surfaces B Biointerfaces 2022;216:112533. https://doi.org/10.1016/j.colsurfb.2022.112533.

[7] Ma H, Wang J, Wang H, Dong N, Zhang J, Jin P, et al. Influence of nano-diamond content on the microstructure, mechanical and thermal properties of the ZK60 composites. J Magnes Alloy 2022;10:440–8. https://doi.org/10.1016/j.jma.2021.03.034.

[8] Zengin H, Turen Y, Turan ME. Tensile and wear properties of as-cast and as-extruded ZK60 magnesium alloys containing minor Nd additions. Mater Res Express 2019;6:086528. https://doi.org/10.1088/2053-1591/aaf99a.

[9] Yu H, Hyuk Park S, Sun You B, Min Kim Y, Shun Yu H, Soo Park S. Effects of extrusion speed on the microstructure and mechanical properties of ZK60 alloys with and without 1wt% cerium addition. Mater Sci Eng A 2013;583:25–35. https://doi.org/10.1016/j.msea.2013.06.073.

[10] Liang J, Lei Z, Chen Y, Fu W, Wu S, Chen X, et al. Microstructure evolution of laser powder bed fusion ZK60 Mg alloy after different heat treatment. J Alloys Compd 2022;898:163046. https://doi.org/10.1016/j.jallcom.2021.163046.

[11] YIN D song, ZHANG E lin, ZENG S yan. Effect of Zn on mechanical property

and corrosion property of extruded Mg-Zn-Mn alloy. Trans Nonferrous Met Soc China (English Ed 2008;18:763–8. https://doi.org/10.1016/S1003-6326(08)60131-4.

[12] Tayebi M, Nategh S, Najafi H, Khodabandeh A. Tensile properties and microstructure of ZK60/SiCw composite after extrusion and aging. J Alloys Compd 2020;830. https://doi.org/10.1016/j.jallcom.2020.154709.

[13] Cho JH, Han SH, Jeong HT, Choi SH. The effect of aging on mechanical properties and texture evolution of ZK60 alloys during warm compression. J Alloys Compd 2018;743:553–63. https://doi.org/10.1016/j.jallcom.2017.12.275.

[14] Xu Y, Liang Y, Peng G. Effect of a compound modification process on the microstructure and mechanical properties of ZK60 magnesium alloys. Mater Sci Eng A 2020;778:139117. https://doi.org/10.1016/j.msea.2020.139117.

[15] Park SH, Yu H, Bae JH, Yim CD, You BS. Microstructural evolution of indirect-extruded ZK60 alloy by adding Ce. J Alloys Compd 2012;545:139–43. https://doi.org/10.1016/j.jallcom.2012.08.025.

[16] Yu H, Kim YM, You BS, Yu HS, Park SH. Effects of cerium addition on the microstructure, mechanical properties and hot workability of ZK60 alloy. Mater Sci Eng A 2013;559:798–807. https://doi.org/10.1016/j.msea.2012.09.026.

[17] Silva EP, Marques F, Nossa TS, Alfaro U, Pinto HC. Impact of Ce-base mischmetal on the microstructure and mechanical behavior of ZK60 magnesium casting alloys. Mater Sci Eng A 2018;723:306–13. https://doi.org/10.1016/j.msea.2018.02.024.

[18] Banijamali SM, Palizdar Y, Najafi S, Sheikhani A, Soltan Ali Nezhad M, Valizadeh Moghaddam P, et al. Effect of Ce Addition on the Tribological Behavior of ZK60 Mg-Alloy. Met Mater Int 2021;27:2732–42. https://doi.org/10.1007/s12540-020-00832-4.

[19] Wu H, Yan T, Wang L, Li X, Wei Y, Li S, et al. Effect of Yb addition on the microstructure and mechanical properties of ZK60 alloy during extrusion. Mater Sci Eng A 2020;777:139033. https://doi.org/10.1016/j.msea.2020.139033.

[20] Zhang T, Cui H, Cui X, Chen H, Zhao E, Chang L, et al. Effect of addition of small amounts of samarium on microstructural evolution and mechanical properties enhancement of an as-extruded ZK60 magnesium alloy sheet. J Mater Res Technol 2020;9:133–41. https://doi.org/10.1016/j.jmrt.2019.10.038.

[21] Abbas A, Hu KC, Lin HC, Lin KM. Influence of severe plastic deformation and some additives on hydrogenation of ZK60 alloy. J Phys Chem Solids 2021;151:109927. https://doi.org/10.1016/j.jpcs.2020.109927.

[22] Huang Z, Liu W, Qi W, Xu J, Zhou N. Effects of Bi on the microstructure and mechanical property of ZK60 alloy. J Magnes Alloy 2015;3:29–35.

https://doi.org/10.1016/j.jma.2014.12.005.

[23] Labib F, Ghasemi HM, Mahmudi R. Dry tribological behavior of Mg/SiCp composites at room and elevated temperatures. Wear 2016;348–349:69–79. https://doi.org/10.1016/j.wear.2015.11.021.

[24] Sabbaghian M, Fakhar N, Nagy P, Fekete K, Gubicza J. Investigation of shear and tensile mechanical properties of ZK60 Mg alloy sheet processed by rolling and sheet extrusion. Mater Sci Eng A 2021;828:142098. https://doi.org/10.1016/j.msea.2021.142098.

[25] Banijamali SM, Shariat Razavi M, Palizdar Y, Najafi S, Sheikhani A, Torkamani H. Experimental and Simulation Study on Wear Behavior of ZK60 Alloy with 3 wt.% Yttrium Addition. J Mater Eng Perform 2022;31:4721–34. https://doi.org/10.1007/s11665-022-06585-y.

[26] Behnamian Y, Serate D, Aghaie E, Zahiri R, Tolentino Z, Niazi H, et al. Tribological behavior of ZK60 magnesium matrix composite reinforced by hybrid MWCNTs/B4C prepared by stir casting method. Tribol Int 2022;165:107299. https://doi.org/10.1016/j.triboint.2021.107299.

[27] Cai S, Lei T, Li N, Feng F. Effects of Zn on microstructure, mechanical properties and corrosion behavior of Mg-Zn alloys. Mater Sci Eng C 2012;32:2570–7. https://doi.org/10.1016/j.msec.2012.07.042.

[28] Wu CL, Zai W, Man HC. Additive manufacturing of ZK60 magnesium alloy by selective laser melting: Parameter optimization, microstructure and biodegradability. Mater Today Commun 2021;26. https://doi.org/10.1016/j.mtcomm.2020.101922.

[29] Silva EP, Buzolin RH, Marques F, Soldera F, Alfaro U, Pinto HC. Effect of Ce-base mischmetal addition on the microstructure and mechanical properties of hot-rolled ZK60 alloy. J Magnes Alloy 2021;9:995–1006. https://doi.org/10.1016/j.jma.2020.09.018.

[30] Liu DB, Wu B, Wang X, Chen MF. Corrosion and wear behavior of an Mg–2Zn–0.2Mn alloy in simulated body fluid. Rare Met 2015;34:553–9. https://doi.org/10.1007/s12598-013-0052-y.

[31] Li Q, Yan Y, Gao H. Improving the corrosion resistance and osteogenic differentiation of ZK60 magnesium alloys by hydroxyapatite/graphene/graphene oxide composite coating. Ceram Int 2022;48:16131–41. https://doi.org/10.1016/j.ceramint.2022.02.161.

[32] Tang J, Chen L, Li Z, Zhao G, Zhang C, Lin J, et al. Microstructure characterization and corrosion behavior of hollow ZK60 Mg profile containing longitudinal welds. Corros Sci 2021;193:109875. https://doi.org/10.1016/j.corsci.2021.109875.

[33] Li Z, Peng Z, Qiu Y, Qi K, Chen Z, Guo X. Study on heat treatment to improve the microstructure and corrosion behavior of ZK60 magnesium alloy. J Mater

Res Technol 2020;9:11201–19. https://doi.org/10.1016/j.jmrt.2020.08.004.

[34] Song Y, Han EH, Dong K, Shan D, Yim CD, You BS. Effect of hydrogen on the corrosion behavior of the Mg-xZn alloys. J Magnes Alloy 2014;2:208–13. https://doi.org/10.1016/j.jma.2014.10.002.

[35] Zhang S, Bi Y, Li J, Wang Z, Yan J, Song J, et al. Biodegradation behavior of magnesium and ZK60 alloy in artificial urine and rat models. Bioact Mater 2017;2:53–62. https://doi.org/10.1016/j.bioactmat.2017.03.004.

[36] Gao C, Li S, Liu L, Bin S, Yang Y, Peng S, et al. Dual alloying improves the corrosion resistance of biodegradable Mg alloys prepared by selective laser melting. J Magnes Alloy 2021;9:305–16. https://doi.org/10.1016/j.jma.2020.03.016.

[37] Shuai C, Wang B, Yang Y, Peng S, Gao C. 3D honeycomb nanostructure-encapsulated magnesium alloys with superior corrosion resistance and mechanical properties. Compos Part B Eng 2019;162:611–20. https://doi.org/10.1016/j.compositesb.2019.01.031.

[38] Wang ZX, Xu L, Zhang JW, Ye F, Lv WG, Xu C, et al. Preparation and Degradation Behavior of Composite Bio-Coating on ZK60 Magnesium Alloy Using Combined Micro-Arc Oxidation and Electrophoresis Deposition. Front Mater 2020;7:1–14. https://doi.org/10.3389/fmats.2020.00190.

[39] Yang Y, Lu C, Shen L, Zhao Z, Peng S, Shuai C. In-situ deposition of apatite layer to protect Mg-based composite fabricated via laser additive manufacturing. J Magnes Alloy 2021. https://doi.org/10.1016/j.jma.2021.04.009.

[40] Yang Y, Lu C, Peng S, Shen L, Wang D, Qi F, et al. Laser additive manufacturing of Mg-based composite with improved degradation behaviour. Virtual Phys Prototyp 2020;15:278–93. https://doi.org/10.1080/17452759.2020.1748381.

[41] Zengin H, Turen Y. Effect of Y addition on microstructure and corrosion behavior of extruded Mg–Zn–Nd–Zr alloy. J Magnes Alloy 2020;8:640–53. https://doi.org/10.1016/j.jma.2020.06.004.

[42] Huan ZG, Leeflang MA, Zhou J, Fratila-Apachitei LE, Duszczyk J. In vitro degradation behavior and cytocompatibility of Mg-Zn-Zr alloys. J Mater Sci Mater Med 2010;21:2623–35. https://doi.org/10.1007/s10856-010-4111-8.

[43] Li H, Zhang R, Zheng Y, Fu K. Study on Ultrasonic Nondestructive Evaluation Method for Grain Size of Magnesium Alloy Components With Complex Profile. J Phys Conf Ser 2023. https://doi.org/10.1088/1742-6596/2499/1/012014.

[44] Zhang D, Liu Y, Liu Z, Wang Q. Advances in Antibacterial Functionalized Coatings on Mg and Its Alloys for Medical Use—A Review. Coatings 2020. https://doi.org/10.3390/coatings10090828.

[45] Figueiredo RB, Langdon TG. Record Superplastic Ductility in a Magnesium Alloy Processed by Equal-Channel Angular Pressing. Adv Eng Mater 2008. https://doi.org/10.1002/adem.200700315.

[46] Silva CLP, Soares RB, Pereira PHR, Figueiredo RB, de Freitas Cunha Lins V, Langdon TG. The Effect of High-Pressure Torsion on Microstructure, Hardness and Corrosion Behavior for Pure Magnesium and Different Magnesium Alloys. Adv Eng Mater 2019. https://doi.org/10.1002/adem.201801081.

[47] Liang H, Dong Z, Zhang Y, Bai Y. Homogenization Treatment and Heat Deformation Behavior of Cast ZK60 Magnesium Alloy. J Phys Conf Ser 2023. https://doi.org/10.1088/1742-6596/2459/1/012038.

[48] Feng X, Sun Y, Wan S, Chen G, He J. Effects of Aging Process on the Damping Performance of ZK60 Magnesium Alloys Prepared by Large Strain Rolling. Materials (Basel) 2020. https://doi.org/10.3390/ma13235574.

[49] Li Q, Yang J, Liu WJ, Luo SQ, Cheng RJ, Li C, et al. Effect of Y and Heat Treatment on Microstructure and Deformation Performance of ZK60 Alloy. Adv Mater Res 2014. https://doi.org/10.4028/www.scientific.net/amr.1015.207.

[50] Linderov M, Vasilev E, Merson D, Markushev M, Vinogradov A. Corrosion Fatigue of Fine Grain Mg-Zn-Zr and Mg-Y-Zn Alloys. Metals (Basel) 2017. https://doi.org/10.3390/met8010020.

[51] Xue Y, Pang X, Jiang B, Jahed H, Wang D. Characterization of the Corrosion Performances of As-cast Mg–Al and Mg–Zn Magnesium Alloys With Microarc Oxidation Coatings. Mater Corros 2019. https://doi.org/10.1002/maco.201911384.

[52] Gao B, Huang P, Ou C, Li K, Yan B, Lu W. In Vitro Corrosion and Cytocompatibility of ZK60 Magnesium Alloy Coated With Hydroxyapatite by a Simple Chemical Conversion Process for Orthopedic Applications. Int J Mol Sci 2013. https://doi.org/10.3390/ijms141223614.

[53] Zheng Y, Li Y, Chen J, Zou Z. Surface Characteristics and Corrosion Resistance of Biodegradable Magnesium Alloy ZK60 Modified by Fe Ion Implantation and Deposition. Prog Nat Sci Mater Int 2014. https://doi.org/10.1016/j.pnsc.2014.08.011.

[54] Su J, Teng J, Xu Z, Li Y. Corrosion-Wear Behavior of a Biocompatible Magnesium Matrix Composite in Simulated Body Fluid. Friction 2020. https://doi.org/10.1007/s40544-020-0361-8.

[55] Fu Y, Yin Y, Guan J-W, Ji Q-B, Wang Y, Singh VP. The Evaluation of a Degradable Magnesium Alloy Bio-Transfix Nail System Compounded With Bone Morphogenetic Protein-2 in a Beagle Anterior Cruciate Ligament Reconstruction Model. J Biomater Appl 2019. https://doi.org/10.1177/0885328219865069.

[56] Chen J, Tan L, Yang K. Effect of Heat Treatment on Mechanical and Biodegradable Properties of an Extruded ZK60 Alloy. Bioact Mater 2017. https://doi.org/10.1016/j.bioactmat.2016.12.002.

[57] Liu CL, Jiang J, Wang M, Wang YJ, Chu PK, Huang WJ. \≪i\>In Vitro\</I\> Degradation and Biocompatibility of WE43, ZK60, and AZ91 Biodegradable Magnesium Alloys. Adv Mater Res 2011. https://doi.org/10.4028/www.scientific.net/amr.287-290.2008.

[58] Zhang W, Feng Z, Li X, Chen Y. Effect of Zr Content on the Distribution Characteristic of the 14H and 18R LPSO Phases. Mater Res 2020. https://doi.org/10.1590/1980-5373-mr-2019-0539.

[59] Makkar P, Kang H-J, Padalhin AR, Park I, Moon BH, Lee B-T. Development and Properties of Duplex MgF2/PCL Coatings on Biodegradable Magnesium Alloy for Biomedical Applications. PLoS One 2018. https://doi.org/10.1371/journal.pone.0193927.

[60] Grill A, Horky J, Panigrahi A, Krexner G, Zehetbauer MJ. Long-Term Hydrogen Storage in Mg and ZK60 After Severe Plastic Deformation. Int J Hydrogen Energy 2015. https://doi.org/10.1016/j.ijhydene.2015.05.145.

[61] Sager A, Esen I, Ahlatci H, Turen Y. Dry Wear Behaviour of the New ZK60/AlN/SiC Particle Reinforced Composites. Materials (Basel) 2022. https://doi.org/10.3390/ma15238582.

[62] Xie G, Luo Z, Ma ZY, Xue P, Wang G. Superplastic Behavior of Friction Stir Processed ZK60 Magnesium Alloy. Mater Trans 2011. https://doi.org/10.2320/matertrans.m2011231.

[63] Subramani M, Huang S-J, Borodianskiy K. Effect of SiC Nanoparticles on AZ31 Magnesium Alloy. Materials (Basel) 2022. https://doi.org/10.3390/ma15031004.

[64] Aravindan S, Rao PRV, Ponappa K. Evaluation of Physical and Mechanical Properties of AZ91D/SiC Composites by Two Step Stir Casting Process. J Magnes Alloy 2015. https://doi.org/10.1016/j.jma.2014.12.008.

[65] Dieringa H. Properties of Magnesium Alloys Reinforced With Nanoparticles and Carbon Nanotubes: A Review. J Mater Sci 2010. https://doi.org/10.1007/s10853-010-5010-6.

[66] Kumar A, Kumar S, Mukhopadhyay NK, Yadav A, Kumar V, Winczek J. Effect of Variation of SiC Reinforcement on Wear Behaviour of AZ91 Alloy Composites. Materials (Basel) 2021. https://doi.org/10.3390/ma14040990.

[67] Veeranjaneyulu I, das Vemulapalli C, Krishna MG. Fabrication, Microstructure, and Mechanical Properties of AZ31/Silicon Carbide/Graphite Teinforced Hybrid Composites. Adv Sci Technol – Res J 2022. https://doi.org/10.12913/22998624/156915.

[68] Wang X, La P, Chao H, Nan H. Electroless Ni-P-TiO2/Ni-P-SiC Composite Coatings Corrosion Resistances on Mg2B2O5w/Az91d Magnesium Matrix Composites 2015. https://doi.org/10.2991/ic3me-15.2015.7.

[69] Akbar HI, Surojo E, Ariawan D, Prabowo AR. Technical Investigation of Sea Sand Reinforcement for Novel Al6061- Sea Sand Composites: Identification of Performance and Mechanical Properties. Periódico Tchê Química 2020. https://doi.org/10.52571/ptq.v17.n36.2020.63_periodico36_pgs_47_57.pdf.

[70] Li J, Ren X, Zhang Y, Hou H. Effect of Annealing Process on Microstructure of SiC-Mg Mixture Powder. J Min Mech Eng 2019. https://doi.org/10.32474/jomme.2019.01.000106.

[71] Shen M, Jia J. Microstructure Evolution Mechanism and Fracture Characteristic of Bimodal Size SiC_p/Mg Composite. Ieee Access 2019. https://doi.org/10.1109/access.2019.2925842.

[72] Kumar A, Kumar S, Mukhopadhyay NK, Yadav A, Winczek J. Effect of SiC Reinforcement and Its Variation on the Mechanical Characteristics of AZ91 Composites. Materials (Basel) 2020. https://doi.org/10.3390/ma13214913.

[73] Peng GG, Liang YL, Li W. The Microstructure and Corrosion Resistance of SiC Reinforced Magnesium Matrix Composites With Laminated Gradient Structure. Mater Res Express 2021. https://doi.org/10.1088/2053-1591/ac3a42.

[74] Shen J-L, Liu KJR, Zhai D, Wang D, Xu N, Jiang CJ. Effects of SiC Ceramic Particles on Microstructures and Mechanical Properties of Gas Tungsten Arc Welded AZ31magnesium Alloy With Cr₂O₃flux Coating. Sci Technol Weld \& Join 2013. https://doi.org/10.1179/1362171812y.0000000063.

[75] Song JF, Dieringa H, Huang Y, Gan WM, Kainer KU, Hort N. Mechanical Properties and Microstructures of Nano SiC Reinforced ZE10 Composites Prepared With Ultrasonic Vibration. Adv Mater Res 2014. https://doi.org/10.4028/www.scientific.net/amr.1019.169.

[76] Khrustalyov AP, Zhukov I, Nikitin P, Kolarik V, Klein F, Akhmadieva AA, et al. Study of Influence of Aluminum Nitride Nanoparticles on the Structure, Phase Composition and Mechanical Properties of AZ91 Alloy. Metals (Basel) 2022. https://doi.org/10.3390/met12020277.

[77] Meignanamoorthy M, Velmurugan PGS, Ravichandran M, Alonazi WB, Sivakumar S, Gebrekidan AM. Effect of Nanoaluminium Nitride Ceramic Particles on Microstructure, Mechanical Wear, and Machining Behavior of Al-Si-Mg Alloy Matrix Composites Produced by Bottom Pouring Type Stir Casting Route. J Nanomater 2022. https://doi.org/10.1155/2022/5013914.

[78] Sankaranarayanan S, Habibi MK, Jayalakshmi S, Jia Ai K, Almajid A, Gupta M. Nano-AlN particle reinforced Mg composites: Microstructural and mechanical properties. Mater Sci Technol (United Kingdom) 2015;31:1122–30.

https://doi.org/10.1179/1743284714Y.0000000686.

[79] Garrido M, Davoust L, Daudin R, Salvo L, Sillekens WH, Fautrelle Y. Reinforcement of Magnesium Elektron 21 With Aluminium Nitride (AlN) Nanoparticles Dispersed Using a Travelling Magnetic Field. Metall Res \& Technol 2020. https://doi.org/10.1051/metal/2020016.

[80] Paramsothy M, Chan JYW, Kwok RK, Gupta M. TiC Nanoparticle Addition to Enhance the Mechanical Response of Hybrid Magnesium Alloy. J Nanotechnol 2012. https://doi.org/10.1155/2012/401574.

[81] Paramsothy M, Chan JYW, Kwok RK, Gupta M. Al2O3 Nanoparticle Addition to Commercial Magnesium Alloys: Multiple Beneficial Effects. Nanomaterials 2012. https://doi.org/10.3390/nano2020147.

[82] Shimizu Y, Miki S, Soga T, Itoh I, Todoroki H, Hosono T, et al. Multi-Walled Carbon Nanotube-Reinforced Magnesium Alloy Composites. Scr Mater 2008. https://doi.org/10.1016/j.scriptamat.2007.10.014.

[83] Lakavat M. Investigations on Surface Behavior of Electro-Less Nickel Phosphorus Coatings With Nano Additives on Magnesium Alloy Used in Automotive Applications. Psychol Educ J 2021. https://doi.org/10.17762/pae.v58i3.4609.

[84] Giannopoulou D, Bohlen J, Khalifa N Ben, Dieringa H. Influence of Extrusion Rate on Microstructure and Mechanical Properties of Magnesium Alloy AM60 and an AM60-Based Metal Matrix Nanocomposite. Nanomaterials 2022. https://doi.org/10.3390/nano12152682.

[85] Baril G, Blanc C, Pébère N. AC Impedance Spectroscopy in Characterizing Time-Dependent Corrosion of AZ91 and AM50 Magnesium Alloys Characterization With Respect to Their Microstructures. J Electrochem Soc 2001. https://doi.org/10.1149/1.1415722.

[86] Ishizaki T, Masuda Y, Sakamoto M. Corrosion Resistance and Durability of Superhydrophobic Surface Formed on Magnesium Alloy Coated With Nanostructured Cerium Oxide Film and Fluoroalkylsilane Molecules in Corrosive NaCl Aqueous Solution. Langmuir 2011. https://doi.org/10.1021/la2002783.

[87] Bagherifard S, Hickey DT, Fintová S, Pastorek F, Fernández-Pariente I, Bandini M, et al. Effects of Nanofeatures Induced by Severe Shot Peening (SSP) on Mechanical, Corrosion and Cytocompatibility Properties of Magnesium Alloy AZ31. Acta Biomater 2018. https://doi.org/10.1016/j.actbio.2017.11.032.

[88] Mostaed E, Vedani M, Hashempour M, Bestetti M. Influence of ECAP Process on Mechanical and Corrosion Properties of Pure Mg and ZK60 Magnesium Alloy for Biodegradable Stent Applications. Biomatter 2014. https://doi.org/10.4161/biom.28283.

[89] Lee H, Lin D, Yeh MCP. Phenolic Modified Ceramic Coating on Biodegradable

Mg Alloy: The Improved Corrosion Resistance and Osteoblast-Like Cell Activity. Materials (Basel) 2017. https://doi.org/10.3390/ma10070696.

[90] Trang LT, Le H Van, Hiromoto S, O M, Kobayashi E, Nguyen NV, et al. In Vitro Cellular Biocompatibility and in Vivo Degradation Behavior of Calcium Phosphate-Coated ZK60 Magnesium Alloy. Biomed Mater 2023. https://doi.org/10.1088/1748-605x/acbf16.

[91] Myagkikh P. Strain Rate Sensitivity of Mechanical Properties of the ZK60 Alloy With the High Degree of Corrosion Damage. Front Mater \& Technol 2023. https://doi.org/10.18323/2782-4039-2023-1-45-55.

[92] Li Z, Peng Z, Qi K, Li H, Qiu Y, Guo X. Microstructure and corrosion of cast magnesium alloy ZK60 in NaCl solution. Materials (Basel) 2020;13. https://doi.org/10.3390/ma13173833.

[93] Dou Z, Jiang H, Ao R, Luo T, Zhang D. Improving the Surface Friction and Corrosion Resistance of Magnesium Alloy AZ31 by Ion Implantation and Ultrasonic Rolling. Coatings 2022. https://doi.org/10.3390/coatings12070899.

[94] Gao J, Qiao L, Xin R. Effect of Mg2+ Concentration on Biocompatibility of Pure Magnesium. Front Mater Sci China 2010. https://doi.org/10.1007/s11706-010-0030-3.

[95] Xue Y, Pang X, Karparvarfard SMH, Jahed H, Luo S, Shen Y. Corrosion Protection of ZK60 Wrought Magnesium Alloys by Micro-Arc Oxidation. Metals (Basel) 2022. https://doi.org/10.3390/met12030449.

[96] Zhao X, Dong T, Fu B, Li G, Liu Q, Li Y. Microstructure and Properties of Cold Sprayed NiCrAl Coating on AZ91D Magnesium Alloy. Coatings 2021. https://doi.org/10.3390/coatings11020193.

[97] da Silva Rodrigues J, Antonini LM, Bastos AC, Zhou J, de Fraga Malfatti C. Corrosion Resistance and Tribological Behavior of ZK30 Magnesium Alloy Coated by Plasma Electrolytic Oxidation. Surf Coatings Technol 2021. https://doi.org/10.1016/j.surfcoat.2021.126983.

[98] Merson D, Vasiliev E, Markushev M, Vinogradov A. On the Corrosion of ZK60 Magnesium Alloy After Severe Plastic Deformation. Lett Mater 2017. https://doi.org/10.22226/2410-3535-2017-4-421-427.

[99] Jian S-Y, Lin C-F, Tsai T-L, Wang P-H, Chen C-H, Lin S-Y, et al. In Vivo Degradation Behavior of Magnesium Alloy for Bone Implants With Improving Biological Activity, Mechanical Properties, and Corrosion Resistance. Int J Mol Sci 2023. https://doi.org/10.3390/ijms24021602.

[100] Fahad M, Bavanish B. Tribological and Ageing Behavior of Az91D Magnesium Alloy Fortified With Nano Lanthanum and Nanoceria by Stir Casting for Aviation Application. Ind Lubr Tribol 2021. https://doi.org/10.1108/ilt-12-2020-0475.

[101] Crivello J-C, Dam B, Denys R V, Dornheim M, Grant D, Huot J, et al. Review of Magnesium Hydride-Based Materials: Development and Optimisation. Appl Phys A 2016. https://doi.org/10.1007/s00339-016-9602-0.

[102] Li D, Wang Q, Ding W. Effects of Ho on the Microstructure and Mechanical Properties of Mg-Zn-Ho-Zr Magnesium Alloys. Rare Met 2011. https://doi.org/10.1007/s12598-011-0211-y.

[103] Liu C, Ren Z, Xu Y, Pang S, Zhao X, Zhao Y. Biodegradable Magnesium Alloys Developed as Bone Repair Materials: A Review. Scanning 2018. https://doi.org/10.1155/2018/9216314.

[104] Linderov M, Afanasyev M, Asmolov AN, Danilov VI, Merson D. Regulation of Corrosion Damage of Magnesium Alloys Through the Use of Vacuum Zirconium Coatings. Lett Mater 2021. https://doi.org/10.22226/2410-3535-2021-3-357-362.

[105] Karparvarfard SMH, Roostaei AA, Behravesh SB, Jahed H. Multiaxial Fatigue Behavior of Low-temperature Closed-die Forged ZK60 Extrusion Under Proportional and Non-proportional Loading. Fatigue \& Fract Eng Mater \& Struct 2022. https://doi.org/10.1111/ffe.13706.

[106] Cai J, Wang H, Qiu C-W, Cao G, Zhang D. Excellent High-Strain-Rate Superplasticity of Fine-Grained ZK60 Magnesium Alloy Produced by Submerged Friction Stir Processing. Adv Eng Mater 2022. https://doi.org/10.1002/adem.202101268.

[107] Meng S, Zhang M, Xiao H, Luo Z, Yu W, Jiang R, et al. A Superior High-Strength Dilute Mg-Bi-Ca Extrusion Alloy With a Bimodal Microstructure. Metals (Basel) 2022. https://doi.org/10.3390/met12071162.

[108] Maier P, Steinacker A, Clausius B, Hort N. Influence of Solution Heat Treatment on the Microstructure, Hardness and Stress Corrosion Behavior of Extruded Resoloy®. Jom 2020. https://doi.org/10.1007/s11837-020-04077-9.

[109] Rahman M, Balu R, Dutta NK, Choudhury NR. In Vitro Corrosion Resistance of a Layer-by-Layer Engineered Hybrid Coating on ZK60 Magnesium Alloy. Sustainability 2022. https://doi.org/10.3390/su14042459.

[110] Pacheco M, Silva JM, Aroso IM, Lima E, Barros AA, Reis RL. Biomaterials for Ureteral Stents: Advances and Future Perspectives 2022. https://doi.org/10.1007/978-3-031-04484-7_17.

[111] Huan Z, Leeflang MA, Zhou J, Fratila-Apachitei LE, Duszczyk J. In Vitro Degradation Behavior and Cytocompatibility of Mg–Zn–Zr Alloys. J Mater Sci Mater Med 2010. https://doi.org/10.1007/s10856-010-4111-8.

[112] Wang T, Lin C, Batalu D, Hu J, Lu W. Tunable Microstructure and Morphology of the Self-Assembly Hydroxyapatite Coatings on ZK60 Magnesium Alloy Substrates Using Hydrothermal Methods. Coatings 2020. https://doi.org/10.3390/coatings11010008.

[113] Merson D, Brilevsky A, Myagkikh P, Tarkova A, Prokhorikhin A, Kretov E, et al. The Functional Properties of Mg–Zn–X Biodegradable Magnesium Alloys. Materials (Basel) 2020. https://doi.org/10.3390/ma13030544.

[114] Pan YB, Chen C, Wang D, Yu X. Microstructure and Biological Properties of Micro-Arc Oxidation Coatings on ZK60 Magnesium Alloy. J Biomed Mater Res Part B Appl Biomater 2012. https://doi.org/10.1002/jbm.b.32726.

[115] Yang H, Yan X, Ling M, Xiong Z, Ou C, Lu W. In Vitro Corrosion and Cytocompatibility Properties of Nano-Whisker Hydroxyapatite Coating on Magnesium Alloy for Bone Tissue Engineering Applications. Int J Mol Sci 2015. https://doi.org/10.3390/ijms16036113.

[116] Lin DJ, Hung FY, Yeh ML, Lui T-S. Microstructure-Modified Biodegradable Magnesium Alloy for Promoting Cytocompatibility and Wound Healing in Vitro. J Mater Sci Mater Med 2015. https://doi.org/10.1007/s10856-015-5572-6.

[117] Qi Z-R, Singh VP, Tan L, Lin X, Yin Y, Wang X-L, et al. Comparison of Degradation Behavior and the Associated Bone Response of ZK60 and PLLA in Vivo. J Biomed Mater Res Part A 2013. https://doi.org/10.1002/jbm.a.34795.

[118] Yang Y, Guo X-Y, He C, Gao C, Shuai C. Regulating Degradation Behavior by Incorporating Mesoporous Silica for Mg Bone Implants. Acs Biomater Sci \& Eng 2018. https://doi.org/10.1021/acsbiomaterials.8b00020.

[119] Zhang S, Bi Y, Li J, Wang Z, Yan J, Song J, et al. Biodegradation Behavior of Magnesium and ZK60 Alloy in Artificial Urine and Rat Models. Bioact Mater 2017. https://doi.org/10.1016/j.bioactmat.2017.03.004.

[120] Liang T, Zeng L, Shi Y, Pan H, Chu PK, Yeung KWK, et al. In Vitro and in Vivo Antibacterial Performance of Zr \&Amp; O PIII Magnesium Alloys With High Concentration of Oxygen Vacancies. Bioact Mater 2021. https://doi.org/10.1016/j.bioactmat.2021.02.025.

[121] Xue Y, Pang X, Jiang B, Jahed H. Corrosion Performances of Micro-Arc Oxidation Coatings on Az31B, Az80 and Zk60 Cast Mg Alloys 2018. https://doi.org/10.25071/10315/35419.

[122] Yue TM, Wang AH, Man HC. Corrosion resistance enhancement of magnesium ZK60/SiC composite by Nd:YAG laser cladding. Scr Mater 1999;40:303–11. https://doi.org/10.1016/S1359-6462(98)00416-3.

[123] Dong N, Li M, Sun L, Wang J, Jin P, Wei Y, et al. Effect of nanodiamond content on the hot deformation behaviors of ND/ZK60 composites. Diam Relat Mater 2022;125:108983. https://doi.org/10.1016/j.diamond.2022.108983.

[124] Chen J, Bao C, Chen W, Zhang L, Liu J. Mechanical Properties and Fracture Behavior of Mg-Al/AlN Composites with Different Particle Contents. J Mater Sci Technol 2017;33:668–74. https://doi.org/10.1016/j.jmst.2016.07.010.

[125] Gu SW, Hao H, Fang CF, Ji SH, Zhang XG. Effects of AlN particles and electromagnetic stirring on as-cast structure of AZ31 alloys. Mater Sci Forum 2011;675 677:771–4. https://doi.org/10.4028/www.scientific.net/MSF.675-677.771.

[126] Li Z, Gao T, Xu Q, Yang H, Han M, Liu X. Microstructure and Mechanical Properties of an AlN/Mg–Al Composite Synthesized by Al–AlN Master Alloy. Int J Met 2019;13:384–91. https://doi.org/10.1007/s40962-018-0261-0.

[127] METALURJİ VE MALZEME MÜHENDİSLİĞİ 2018.

[128] Kiani M, Gandikota I, Rais-Rohani M, Motoyama K. Design of lightweight magnesium car body structure under crash and vibration constraints. J Magnes Alloy 2014;2:99–108. https://doi.org/10.1016/j.jma.2014.05.005.

[129] Dahle AK, Lee YC, Nave MD, Schaffer PL, StJohn DH. Development of the as-cast microstructure in magnesium-aluminium alloys. J Light Met 2001;1:61–72. https://doi.org/10.1016/S1471-5317(00)00007-9.

[130] Wu RZ, Qu ZK, Zhang ML. Reviews on the influences of alloying elements on the microstructure and mechanical properties of Mg-Li base alloys. Rev Adv Mater Sci 2010;24:35–43.

[131] Manuscript A. 可注射水凝胶作为糖尿病创面修复的动态黏附敷料 Materials Chemistry B 2021.

[132] Vojtěch D, Kubásek J, Šerák J, Novák P. Mechanical and corrosion properties of newly developed biodegradable Zn-based alloys for bone fixation. Acta Biomater 2011;7:3515–22. https://doi.org/10.1016/j.actbio.2011.05.008.

[133] Kulekci MK. Magnesium and its alloys applications in automotive industry. Int J Adv Manuf Technol 2008;39:851–65. https://doi.org/10.1007/s00170-007-1279-2.

[134] Aravindan S, Rao P V., Ponappa K. Evaluation of physical and mechanical properties of AZ91D/SiC composites by two step stir casting process. J Magnes Alloy 2015;3:52–62. https://doi.org/10.1016/j.jma.2014.12.008.

[135] Rzychoń T, Szala J, Kiełbus A. Microstructure, castability, microstructural stability and mechanical properties of ZRE1 magnesium alloy. Arch Metall Mater 2012;57:245–52. https://doi.org/10.2478/v10172-012-0018-3.

[136] Bettles CJ, Gibson MA. Current wrought magnesium alloys: Strengths and weaknesses. Jom 2005;57:46–9. https://doi.org/10.1007/s11837-005-0095-0.

[137] Hutchinson CR, Nie JF, Gorsse S. Modeling the precipitation processes and strengthening mechanisms in a Mg-Al-(Zn) AZ91 alloy. Metall Mater Trans A Phys Metall Mater Sci 2005;36:2093–105. https://doi.org/10.1007/s11661-005-0330-x.

[138] Lee YC, Dahle AK, St John DH. Grain Refinement of Magnesium. Essent

Readings Magnes Technol 2014;9781118858:247–54. https://doi.org/10.1002/9781118859803.ch41.

[139] Caceres CH, Mann GE, Griffiths JR. Grain size hardening in Mg and Mg-Zn solid solutions. Metall Mater Trans A Phys Metall Mater Sci 2011;42:1950–9. https://doi.org/10.1007/s11661-010-0599-2.

[140] 6. 1-s2.0-S0928493112003608-main.pdf n.d.

[141] Wei LY, Dunlop GL, Westengen H. Precipitation Hardening of Mg-Zn and Mg-Zn-RE alloys. Metall Mater Trans A 1995;26:1705–16. https://doi.org/10.1007/BF02670757.

[142] Gao X, Nie JF. Characterization of strengthening precipitate phases in a Mg-Zn alloy. Scr Mater 2007;56:645–8. https://doi.org/10.1016/j.scriptamat.2007.01.006.

[143] Cáceres CH, Blake A. The strength of concentrated Mg-Zn solid solutions. Phys Status Solidi Appl Res 2002;194:147–58. https://doi.org/10.1002/1521-396X(200211)194:1<147::AID-PSSA147>3.0.CO;2-L.

[144] Blake AH, Cáceres CH. Solid-solution hardening and softening in Mg-Zn alloys. Mater Sci Eng A 2008;483–484:161–3. https://doi.org/10.1016/j.msea.2006.10.205.

[145] Robson JD, Paa-Rai C. The interaction of grain refinement and ageing in magnesium-zinc-zirconium (ZK) alloys. Acta Mater 2015;95:10–9. https://doi.org/10.1016/j.actamat.2015.05.012.

[146] Bohlen J, Letzig D, Kainer KU. New Perspectives for Wrought Magnesium Alloys. Mater Sci Forum 2007;546–549:1–10. https://doi.org/10.4028/www.scientific.net/msf.546-549.1.

[147] Bhan S, Lal A. The Mg-Zn-Zr system (magnesium-zinc-zirconium). J Phase Equilibria 1993;14:634–7. https://doi.org/10.1007/BF02669156.

[148] He ML, Luo TJ, Zhou JX, Yang YS. Microstructure and mechanical properties of as-cast Mg-4Zn-0.5Zr-0.2Cu-0.2Ce alloy. Mater Sci Technol (United Kingdom) 2018;34:1370–8. https://doi.org/10.1080/02670836.2018.1457288.

[149] Ren YP, Guo Y, Chen D, Li S, Pei WL, Qin GW. Isothermal section of MgZnZr ternary system at 345 ° C. Calphad Comput Coupling Phase Diagrams Thermochem 2011;35:411–5. https://doi.org/10.1016/j.calphad.2011.05.009.

[150] Liu P, Jiang H, Cai Z, Kang Q, Zhang Y. The effect of Y, Ce and Gd on texture, recrystallization and mechanical property of Mg–Zn alloys. J Magnes Alloy 2016;4:188–96. https://doi.org/10.1016/j.jma.2016.07.001.

[151] Lim, D. S., Morse, E. A., Mitchell, R. K., & Seawright, K. K. Ins 34(3) 491-516. https://doi.org/10.1111%2Fj.1540-6520.2010.00384.x. No 主観的健康感を中心とした在宅高齢者における 健康関連指標に関する共分散構造分

析Title. Titutional Environ Entrep Cogn A Comp Bus Syst Perspect Entrep Theory Pract 2010:1–73.

[152] Downloaded from: http://sure.sunderland.ac.uk/id/eprint/5458/ 2015.

[153] Mueller WD, Lucia Nascimento M, Lorenzo De Mele MF. Critical discussion of the results from different corrosion studies of Mg and Mg alloys for biomaterial applications. Acta Biomater 2010;6:1749–55. https://doi.org/10.1016/j.actbio.2009.12.048.

[154] Mordike BL, Ebert T. Magnesium Properties - applications - potential. Mater Sci Eng A 2001;302:37–45. https://doi.org/10.1016/S0921-5093(00)01351-4.

[155] Luo AA. Magnesium casting technology for structural applications. J Magnes Alloy 2013;1:2–22. https://doi.org/10.1016/j.jma.2013.02.002.

[156] Sillekens WH, Kaufmann> H, Sillekens W, Van Hout M, Pravdic F. Extrusion technology for magnesium: Avenues for improving performance 2005.

[157] Musfirah AH, Jaharah AG. Magnesium and aluminum alloys in automotive industry. J Appl Sci Res 2012;8:4865–75.

[158] Mishra RR, Sharma AK. Structure-property correlation in Al–Zn–Mg alloy cast developed through in-situ microwave casting. Mater Sci Eng A 2017;688:532–44. https://doi.org/10.1016/j.msea.2017.02.021.

[159] Mert F, Özdemir A, Kainer KU, Hort N. Influence of Ce addition on microstructure and mechanical properties of high pressure die cast AM50 magnesium alloy. Trans Nonferrous Met Soc China (English Ed 2013;23:66–72. https://doi.org/10.1016/S1003-6326(13)62430-9.

[160] Fu P, Luo AA, Jiang H, Peng L, Yu Y, Zhai C, et al. Low-pressure die casting of magnesium alloy AM50: Response to process parameters. J Mater Process Technol 2008;205:224–34. https://doi.org/10.1016/j.jmatprotec.2007.11.111.

[161] Gertsman VY, Li J, Xu S, Thomson JP, Sahoo M. Microstructure and second-phase particles in low- and high-pressure die-cast magnesium alloy AM50. Metall Mater Trans A Phys Metall Mater Sci 2005;36:1989–97. https://doi.org/10.1007/s11661-005-0319-5.

[162] Transactions of the ASME Copyright © 1977 by ASME 2017:26850.

[163] Fan H, El-Awady JA. Molecular Dynamics Simulations of Orientation Effects during Tension, Compression, and Bending Deformations of Magnesium Nanocrystals. J Appl Mech Trans ASME 2015;82. https://doi.org/10.1115/1.4030930.

[164] Barnett MR. Twinning and the ductility of magnesium alloys. Part II. “Contraction” twins. Mater Sci Eng A 2007;464:8–16. https://doi.org/10.1016/j.msea.2007.02.109.

[165] ERDEM A. Magnezyum-Kalay Esasli Magnezyum Alaşimlarinin Döküm Ve Ekstrüzyon SonraÖzelliklerinİncelenmesi 2019.

[166] Kainer KU, Bohlen J, Letzig D. New Developments in Extruded Magnesium Alloys for Structural Applications. Mater Sci Forum 2007;561–565:1545–8. https://doi.org/10.4028/www.scientific.net/msf.561-565.1545.

[167] Zeng Z, Stanford N, Davies CHJ, Nie JF, Birbilis N. Magnesium extrusion alloys: a review of developments and prospects. Int Mater Rev 2019;64:27–62. https://doi.org/10.1080/09506608.2017.1421439.

[168] Sun HF, Li CJ, Fang W Bin. Evolution of microstructure and mechanical properties of Mg-3.0Zn-0.2Ca-0.5Y alloy by extrusion at various temperatures. J Mater Process Technol 2016;229:633–40. https://doi.org/10.1016/j.jmatprotec.2015.10.021.

[169] Chen Y, Wang Q, Peng J, Zhai C, Ding W. Effects of extrusion ratio on the microstructure and mechanical properties of AZ31 Mg alloy. J Mater Process Technol 2007;182:281–5. https://doi.org/10.1016/j.jmatprotec.2006.08.012.

[170] Ishihara S, Shibata H, Komano K, Goshima T, Nan ZY. Effect of Extrusion Ratio on Fatigue Properties of Hot-Extruded Magnesium Alloys. Key Eng Mater 2007;353–358:291–4. https://doi.org/10.4028/www.scientific.net/kem.353-358.291.

[171] Uematsu Y, Tokaji K, Kamakura M, Uchida K, Shibata H, Bekku N. Effect of extrusion conditions on grain refinement and fatigue behaviour in magnesium alloys. Mater Sci Eng A 2006;434:131–40. https://doi.org/10.1016/j.msea.2006.06.117.

[172] Gupta M, Lai MO, Saravanaranganathan D. Synthesis, microstructure and properties characterization of disintegrated melt deposited Mg/SiC composites. J Mater Sci 2000;35:2155–65. https://doi.org/10.1023/A:1004706321731.

[173] Soorya Prakash K, Balasundar P, Nagaraja S, Gopal PM, Kavimani V. Mechanical and wear behaviour of Mg–SiC–Gr hybrid composites. J Magnes Alloy 2016;4:197–206. https://doi.org/10.1016/j.jma.2016.08.001.

[174] Hübler D, Winkler K, Riedel R, Kamrani S, Fleck C. Cyclic deformation behavior of Mg–SiC nanocomposites on the macroscale and nanoscale. Fatigue Fract Eng Mater Struct 2022;45:386–99. https://doi.org/10.1111/ffe.13600.

[175] Matin A, Saniee FF, Abedi HR. Microstructure and mechanical properties of Mg/SiC and AZ80/SiC nano-composites fabricated through stir casting method. Mater Sci Eng A 2015;625:81–8. https://doi.org/10.1016/j.msea.2014.11.050.

[176] Choi H, Alba-Baena N, Nimityongskul S, Jones M, Wood T, Sahoo M, et al. Characterization of hot extruded Mg/SiC nanocomposites fabricated by casting. J Mater Sci 2011;46:2991–7. https://doi.org/10.1007/s10853-010-5176-y.

[177] Penther D, Ghasemi A, Riedel R, Fleck C, Kamrani S. Effect of SiC

nanoparticles on manufacturing process, microstructure and hardness of Mg-SiC nanocomposites produced by mechanical milling and hot extrusion. Mater Sci Eng A 2018;738:264–72. https://doi.org/10.1016/j.msea.2018.09.106.

[178] Ponhan K, Tassenberg K, Weston D, Nicholls KGM, Thornton R. Effect of SiC nanoparticle content and milling time on the microstructural characteristics and properties of Mg-SiC nanocomposites synthesized with powder metallurgy incorporating high-energy ball milling. Ceram Int 2020;46:26956–69. https://doi.org/10.1016/j.ceramint.2020.07.173.

[179] Zhang L, Luo X, Liu J, Leng Y, An L. Dry sliding wear behavior of Mg-SiC nanocomposites with high volume fractions of reinforcement. Mater Lett 2018;228:112–5. https://doi.org/10.1016/j.matlet.2018.05.114.

[180] Ghasali E, Bordbar-Khiabani A, Alizadeh M, Mozafari M, Niazmand M, Kazemzadeh H, et al. Corrosion behavior and in-vitro bioactivity of porous Mg/Al 2 O 3 and Mg/Si 3 N 4 metal matrix composites fabricated using microwave sintering process. Mater Chem Phys 2019;225:331–9. https://doi.org/10.1016/j.matchemphys.2019.01.007.

[181] Singh A, Bala N. Synthesis and comparative sliding wear behavior of stir cast Mg and Mg/Al2O3 metal matrix composites. Mater Res Express 2019;6. https://doi.org/10.1088/2053-1591/ab10d3.

[182] Aydin F, Sun Y, Emre Turan M. Influence of TiC content on mechanical, wear and corrosion properties of hot-pressed AZ91/TiC composites. J Compos Mater 2020;54:141–52. https://doi.org/10.1177/0021998319860570.

[183] Anasori B, Caspi EN, Barsoum MW. Fabrication and mechanical properties of pressureless melt infiltrated magnesium alloy composites reinforced with TiC and Ti2AlC particles. Mater Sci Eng A 2014;618:511–22. https://doi.org/10.1016/j.msea.2014.09.039.

[184] Dash D, Samanta S, Rai RN. Flexural, Dry Sliding Wear and Machinability (EDM) Characteristics of AZ91D/TiC (0, 5, 10, 15, & 20 wt%) MMCs. Adv Mater Process Technol 2022;8:3344–62. https://doi.org/10.1080/2374068X.2021.1949537.

[185] Falcon LA, Bedolla B. E, Lemus J, Leon C, Rosales I, Gonzalez-Rodriguez JG. Corrosion behavior of Mg-Al/TiC composites in NaCl solution. Int J Corros 2011;2011. https://doi.org/10.1155/2011/896845.

[186] Meenashisundaram GK, Gupta M. Synthesis and characterization of high performance low volume fraction TiC reinforced Mg nanocomposites targeting biocompatible/structural applications. Mater Sci Eng A 2015;627:306–15. https://doi.org/10.1016/j.msea.2015.01.007.

[187] Narayanasamy P, Selvakumar N, Balasundar P. Effect of hybridizing MoS2 on the tribological behaviour of Mg–TiC composites. Trans Indian Inst Met 2015;68:911–25. https://doi.org/10.1007/s12666-015-0530-z.

[188] Narayanasamy P, Selvakumar N, Balasundar P. Effect of weight percentage of TiC on their tribological properties of magnesium composites. Mater Today Proc 2018;5:6570–8. https://doi.org/10.1016/j.matpr.2017.11.312.

[189] Reyes A, Bedolla E, Perez R, Contreras A. Effect of heat treatment on the mechanical and microstructural characterization of Mg-AZ91E/TiC composites. Compos Interfaces 2017;24:593–609. https://doi.org/10.1080/09276440.2017.1248201.

[190] Selvakumar N, Narayanasamy P. Optimization and Effect of Weight Fraction of MoS2 on the Tribological Behavior of Mg-TiC-MoS2 Hybrid Composites. Tribol Trans 2016;59:733–47. https://doi.org/10.1080/10402004.2015.1110866.

[191] Venkit H. Investigation of mechanical properties and wear behavior of magnesium alloy AZ91D reinforced with TiC. 2012 Int Conf Green Technol ICGT 2012 2012:335–9. https://doi.org/10.1109/ICGT.2012.6477996.

[192] Chen J, Bao C, Chen W, Zhang L, Liu J. Mechanical Properties and Fracture Behavior of Mg-Al/AlN Composites with Different Particle Contents. J Mater Sci Technol 2017;33:668–74. https://doi.org/10.1016/j.jmst.2016.07.010.

[193] Metal Matrix Composite Fabricated from Electrospun PAN , EGNS / PAN Nanofibers and AL 5049 Alloy by Using Friction Stir Processing 2023:1–23.

[194] Yusof N, Ismail AF. Post spinning and pyrolysis processes of polyacrylonitrile (PAN)-based carbon fiber and activated carbon fiber: A review. J Anal Appl Pyrolysis 2012;93:1–13. https://doi.org/10.1016/j.jaap.2011.10.001.

[195] Lindsay B, Abel ML, Watts JF. A study of electrochemically treated PAN based carbon fibres by IGC and XPS. Carbon N Y 2007;45:2433–44. https://doi.org/10.1016/j.carbon.2007.04.017.

[196] Liu J, Chen X, Liang D, Xie Q. Development of pitch-based carbon fibers: a review. Energy Sources, Part A Recover Util Environ Eff 2020;00:1–21. https://doi.org/10.1080/15567036.2020.1806952.

[197] Viala JC, Fortier P, Claveyrolas G, Vincent H, Bouix J. Effect of magnesium on the composition, microstructure and mechanical properties of carbon fibres. J Mater Sci 1991;26:4977–84. https://doi.org/10.1007/BF00549880.

[198] Xiao H, Lu Y, Zhao W, Qin X. A comparison of the effect of hot stretching on microstructures and properties of polyacrylonitrile and rayon-based carbon fibers. J Mater Sci 2014;49:5017–29. https://doi.org/10.1007/s10853-014-8206-3.

[199] Shi H, Wang X, Hu X, Meng L, Leng X, Wu K. Interfacial Modification Using Matrix Alloying in Mg/CNT Composites for Improved Mechanical Performance. J Mater Eng Perform 2019;28:3041–7. https://doi.org/10.1007/s11665-019-04068-1.

[200] Aung NN, Zhou W, Goh CS, Nai SML, Wei J. Effect of carbon nanotubes on corrosion of Mg-CNT composites. Corros Sci 2010;52:1551–3. https://doi.org/10.1016/j.corsci.2010.02.025.

[201] Habibi MK, Paramsothy M, Hamouda AMS, Gupta M. Enhanced compressive response of hybrid Mg-CNT nano-composites. J Mater Sci 2011;46:4588–97. https://doi.org/10.1007/s10853-011-5358-2.

[202] Kumar N, Gautam A, Singh RS, Manoj MK. Study of B4C/Al–Mg–Si Composites as Highly Hard and Corrosion-Resistant Materials for Industrial Applications. Trans Indian Inst Met 2019;72:2495–501. https://doi.org/10.1007/s12666-019-01717-w.

[203] Navaneetha Krishnan M, Suresh S, Vettivel SC. Effects on Micro-Surface Texturing of Mg/B4C Matrix Composites Under Dry Sliding Wear Condition. Trans Indian Inst Met 2020;73:897–912. https://doi.org/10.1007/s12666-020-01913-z.

[204] Majzoobi GH, Rahmani K. Mechanical characterization of Mg-B4C nanocomposite fabricated at different strain rates. Int J Miner Metall Mater 2020;27:252–63. https://doi.org/10.1007/s12613-019-1902-x.

[205] Paulo Hang Jutanaiman S, Zulfia Syahrial A. Characteristics of Magnesium/B4C Reinforced Composite Fabricated by Stir Casting Method. IOP Conf Ser Mater Sci Eng 2020;924. https://doi.org/10.1088/1757-899X/924/1/012020.

[206] Rahmani K, Majzoobi GH. The effect of compaction loading rate on hardness and wear resistance of Mg-B4C nanocomposite. Mater Res Express 2019;6. https://doi.org/10.1088/2053-1591/ab5abd.

[207] Rahmani K, Majzoobi GH, Bakhtiari H, Sadooghi A. On the effect of compaction velocity, size, and content of reinforcing particles on corrosion resistance of Mg–B4C composites. Mater Chem Phys 2021;271:124946. https://doi.org/10.1016/j.matchemphys.2021.124946.

[208] Singh A, Bala N. Fabrication and Tribological Behavior of Stir Cast Mg/B4C Metal Matrix Composites. Metall Mater Trans A Phys Metall Mater Sci 2017;48:5031–45. https://doi.org/10.1007/s11661-017-4203-x.

[209] Yao YT, Jiang L, Fu GF, Chen LQ. Wear behavior and mechanism of B4C reinforced Mg-matrix composites fabricated by metal-assisted pressureless infiltration technique. Trans Nonferrous Met Soc China (English Ed 2015;25:2543–8. https://doi.org/10.1016/S1003-6326(15)63873-0.

[210] Bhooloka Rao B, Reddy NK, Mulay VN, Jaleel MA. Synthesis and characterization of silicon carbide whiskers. Met Mater Process 1996;7:275–8.

[211] Wang Z, Wu Q, Wang L, Qi Q, Cui N, Li T, et al. Effect of magnesium oxide in multiphase additive on the formation process and morphology of β-Si3N4 whisker. J Asian Ceram Soc 2023;00:1–11.

https://doi.org/10.1080/21870764.2023.2217606.

[212] Bikiaris D. Microstructure and properties of polypropylene/carbon nanotube nanocomposites. Materials (Basel) 2010;3:2884–946. https://doi.org/10.3390/ma3042884.

[213] Han Z, Fina A. Thermal conductivity of carbon nanotubes and their polymer nanocomposites: A review. Prog Polym Sci 2011;36:914–44. https://doi.org/10.1016/j.progpolymsci.2010.11.004.

[214] Selvam B, Marimuthu P, Narayanasamy R, Anandakrishnan V, Tun KS, Gupta M, et al. Dry sliding wear behaviour of zinc oxide reinforced magnesium matrix nano-composites. Mater Des 2014;58:475–81. https://doi.org/10.1016/j.matdes.2014.02.006.

[215] Lim CYH, Lim SC, Gupta M. Wear behaviour of SiCp-reinforced magnesium matrix composites. Wear 2003;255:629–37. https://doi.org/10.1016/S0043-1648(03)00121-2.

[216] Nguyen QB, Sim YHM, Gupta M, Lim CYH. Tribology characteristics of magnesium alloy AZ31B and its composites. Tribol Int 2015;82:464–71. https://doi.org/10.1016/j.triboint.2014.02.024.

[217] NANO AlN İLAVELİ AZ91 /% 15 SiC KOMPOZİT MALZEMELERİN EKSTRÜZYONU , KOROZYON METALURJİ VE MALZEME MÜHENDİSLİĞİ Tez Danışmanı Prof . Dr . Hayrettin AHLATCI 2022.

[218] Oranlarda F, Grafen T, İle T, Az Ü. DAVRANIŞLARININ İNCELENMESİ Murat GÜNDOĞAN Tez Danışmanı Dr . Öğr . Üyesi Engin ÇEVİK 2020.

[219] Song GL, Atrens A. Corrosion mechanisms of magnesium alloys. Adv Eng Mater 1999;1:11–33. https://doi.org/10.1002/(SICI)1527-2648(199909)1:1<11::AID-ADEM11>3.0.CO;2-N.

[220] Song G, Atrens A. Understanding magnesium corrosion. A framework for improved alloy performance. Adv Eng Mater 2003;5:837–58. https://doi.org/10.1002/adem.200310405.

[221] Roll T, Cast S, Sheet M-A. Effect of Reheating and Warm Rolling on Microstructure and Mechanical 2017.

[222] Ghali E, Dietzel W, Kainer KU. General and Localized Corrosion of Magnesium Alloys: A Critical Review. J Mater Eng Perform 2004;13:7–23. https://doi.org/10.1361/10599490417533.

[223] Dong Z. No TitleФормирование парадигмальной теории региональной экономики. Экономика Региона 2012:49–56.

[224] Mino T, Asakawa M, Lee D, Fujiwara T, Matsuzaki K, Kobayashi M. Twin-roll strip casting of AZ61 magnesium alloy and improvement of formability by structure-control rolling. J Mater Process Technol 2006;177:534–8.

https://doi.org/10.1016/j.jmatprotec.2006.04.112.

[225] Nakaura Y, Ohori K. Properties of AZ31 Magnesium Alloy Sheet Produced by Twin Roll Casting. Mater Sci Forum 2005;488–489:419–26. https://doi.org/10.4028/www.scientific.net/msf.488-489.419.

[226] Song GL, Xu ZQ. The surface, microstructure and corrosion of magnesium alloy AZ31 sheet. Electrochim Acta 2010;55:4148–61. https://doi.org/10.1016/j.electacta.2010.02.068.

[227] Stanford N, Sha G, Xia JH, Ringer SP, Barnett MR. Solute segregation and texture modification in an extruded magnesium alloy containing gadolinium. Scr Mater 2011;65:919–21. https://doi.org/10.1016/j.scriptamat.2011.08.012.

[228] Sandlöbes S, Zaefferer S, Schestakow I, Yi S, Gonzalez-Martinez R. On the role of non-basal deformation mechanisms for the ductility of Mg and Mg-Y alloys. Acta Mater 2011;59:429–39. https://doi.org/10.1016/j.actamat.2010.08.031.

[229] Ben-Hamu G, Eliezer D, Shin KS. The role of Mg2Si on the corrosion behavior of wrought Mg-Zn-Mn alloy. Intermetallics 2008;16:860–7. https://doi.org/10.1016/j.intermet.2008.03.003.

[230] Tiwari S, Balasubramaniam R, Gupta M. Corrosion behavior of SiC reinforced magnesium composites. Corros Sci 2007;49:711–25. https://doi.org/10.1016/j.corsci.2006.05.047.

RESUME

Abdulmuaen M. M. SAGER in 2012 Abdulmuaen obtained him bachelor degree in mechanical engineering field from university of Elmergib, Libya. he began working as assistant at Elmergib university between 2012 and 2015.